(12)

DNA 3827T

COLLISIONAL MOMENTUM AND ENERGY TRANSFER RATES FOR TWO-FLUID NUCLEAR-BURST SIMULATIONS

Mission Research Corporation
735 State Street
Santa Barbara, California 93101

25 July 1975

Topical Report for Period October 1974—July 1975

CONTRACT No. DNA 001-74-C-0144

THIS WORK SPONSORED BY THE DEFENSE NUCLEAR AGENCY
UNDER SUBTASK S99QAXHC065-05.

Prepared for
Director
DEFENSE NUCLEAR AGENCY
Washington, D. C. 20305

Destroy this report when it is no longer needed. Do not return to sender.

UCRL PRINTING PLANT

UNCLASSIFIED

SECURITY CLASSIFICATION OF THIS PAGE (When Data Entered)

REPORT DOCUMENTATION PAGE

READ INSTRUCTIONS BEFORE COMPLETING FORM

1 REPORT NUMBER: DNA 3827T

2 GOVT ACCESSION NO.

3 RECIPIENT'S CATALOG NUMBER

4 TITLE (and Subtitle): COLLISIONAL MOMENTUM AND ENERGY TRANSFER RATES FOR TWO-FLUID NUCLEAR-BURST SIMULATIONS.

5 TYPE OF REPORT & PERIOD COVERED: Topical Report for Period October 1974—July 1975

6 PERFORMING ORG. REPORT NUMBER: MRC-R-181

7 AUTHOR(s): Robert E. Stoeckly, Robert W. Stagat, Ralph W. Kilb

8 CONTRACT OR GRANT NUMBER(s): DNA 001-74-C-0144

9 PERFORMING ORGANIZATION NAME AND ADDRESS: Mission Research Corporation, 735 State Street, Santa Barbara, California 93101

10 PROGRAM ELEMENT, PROJECT, TASK AREA & WORK UNIT NUMBERS: NWED Subtask S99QAXHC065-05

11 CONTROLLING OFFICE NAME AND ADDRESS: Director, Defense Nuclear Agency, Washington, D.C. 20305

12 REPORT DATE: 25 July 1975

13 NUMBER OF PAGES: 122

14 MONITORING AGENCY NAME & ADDRESS (if different from Controlling Office)

15 SECURITY CLASS (of this report): UNCLASSIFIED

15a DECLASSIFICATION/DOWNGRADING SCHEDULE

16 DISTRIBUTION STATEMENT (of this Report)

Approved for public release; distribution unlimited.

DA9-NWED-QAXH

17 DISTRIBUTION STATEMENT (of the abstract entered in Block 20, if different from Report)

C465

18 SUPPLEMENTARY NOTES

This work sponsored by the Defense Nuclear Agency under Subtask S99QAXHC065-05.

19 KEY WORDS (Continue on reverse side if necessary and identify by block number)

Atomic Collisions
High-altitude Nuclear Bursts
Two-fluid Magnetohydrodynamic Simulations
Momentum Coupling Coefficients
Charge-transfer Cross Section
Elastic Scattering Cross Section
Inelastic Scattering Cross Section
Heat-transfer Coefficients

20 ABSTRACT (Continue on reverse side if necessary and identify by block number)

A compendium of cross sections is given for atomic collision processes relevant to high-altitude nuclear bursts. Experimental or theoretical cross sections for elastic scattering, inelastic scattering, and charge exchange in ion-neutral and neutral-neutral collisions and for elastic scattering in electron-neutral and electron-ion collisions are given for atmospheric species in the velocity range of 10^4 to 10^9 cm/sec. The electrical resistivity and the rates of momentum and heat transfer between the ion fluid

DD FORM 1473 EDITION OF 1 NOV 65 IS OBSOLETE

UNCLASSIFIED

SECURITY CLASSIFICATION OF THIS PAGE (When Data Entered)

H 30 544

20. ABSTRACT (Continued)

and the neutral fluid are obtained from these cross sections for the case that the particle velocity distribution of each species is Maxwell-Boltzmann. The coefficients for these quantities are given graphically and numerically for temperatures in the range 0.01 to 500 eV. A summary shows how to use these data in two-fluid magnetohydrodynamic simulations of high-altitude nuclear bursts at times subsequent to one second.

PREFACE

We are indebted to Drs. N. G. Utterback and M. Scheibe of Mission Research Corporation and Drs. D. A. Vroom, J. A. Rutherford, and R. H. Neynaber of Intelcom Rad Tech for helpful information on this work.

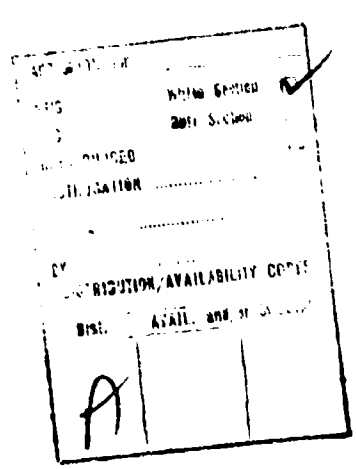

CONTENTS

LIST OF ILLUSTRATIONS

LIST OF TABLES

SECTION I
INTRODUCTION AND SUMMARY

Analysis of the effect of high-altitude nuclear bursts on communication, radar, optical, and infrared systems requires reliable computations of:

(1) the interaction of the high-velocity weapon debris with the surrounding air;

(2) the subsequent motion of the heated and ionized air;

(3) the late-time formation, drift, and decay of striations in the high-altitude ion-electron plasma.

For high-altitude nuclear bursts such phenomena depend strongly on the rates of collisions between ions and neutrals, electrons and neutrals, and electrons and ions. For bursts below 100 km altitude collisions are sufficiently rapid that the one-fluid hydrodynamic equations describe most phenomena adequately. For bursts above 100 km altitude, however, the lower densities cause the collision mean free paths to be quite long, and so the details of the collision processes become important. This report presents a survey of the collision cross sections relevant to high-altitude bursts and describes how to use this data in two-fluid magnetohydrodynamic (MHD) simulations for prediction of burst phenomena.

The relevant types of collisions are elastic scattering, inelastic scattering, and charge exchange. A reliable analysis of burst phenomena requires these cross sections over the velocity range of 10^{-1} to 10^{9} cm/sec. During the first second, much of the burst debris kinetic energy is transferred to the surrounding air, creating air ions with velocities as large as $\sim 10^{9}$ cm/sec. The subsequent expansion and rise of these fireball ions launch a neutral-fluid shock from the burst area that involves particle velocities as low as $\sim 10^{-1}$ cm/sec. The sources of these cross-section data and relevant

theoretical computations are described in Sections 3, 4 and Appendix C. Figures 4-1 through 4-8 summarize the cross-section data for the particle species important in high altitude bursts.

To use the cross-section data, one must define the phenomena to be analyzed and then do the appropriate integrals over the particle velocity distributions. During the first second, when the particle velocities are extremely high ($\sim 10^7$ cm/sec), these phenomena tend to involve very specialized applications (for example CHEX losses and collisional pickup), which we do not attempt to analyze here. Subsequent to one second the main application is a two fluid MHD simulation of nuclear burst phenomena. This requires a detailed knowledge of the rates of mass, momentum, and energy transfer between the ion-electron fluid and the neutral fluid. The resistivity of the medium is also required in order to determine the decay of currents, perturbed magnetic fields, and striations; the resistivity is directly related to the rate of electron momentum loss. Very late-time nuclear burst simulations require an average collision frequency of ions with neutrals, and this collision frequency can be expressed in terms of the rate of ion momentum loss.

One major approximation that we have made in calculating the transfer rates due to collisions is that we have considered the particle velocity distributions of each species to be Maxwell-Boltzmann in the frame moving at the mean velocity of that species. This approximation is a compromise: it is simple enough so that we can treat many cases, while at the same time it gives sufficiently accurate results for use in high-altitude simulations.

Section 2 derives the integrals needed to compute the collisional rates of momentum transfer (Eq. 2-36), of total energy transfer (Eq. 2-37) and of internal energy transfer (Eq. 2-40), and the rate of energy loss due to inelastic collisions (Eq. 2-41). These transfer rates are expressed in terms of the momentum-coupling coefficient ν_s (Eq. 2-35), the heat-transfer coefficient h (Eq. 2-34) and the inelastic energy loss integral νk_s (Eq. 2-38).

Section 3 summarizes the momentum and internal energy transfer rates needed in two-fluid MHD simulations subsequent to the first few seconds after a nuclear burst. This section is self-contained, so readers who are primarily interested in results can skip the analysis in Sections 2, 5, and 6. Equations 3-24 through 3-29 show the simplest version of the momentum-coupling and heat-transfer coefficients that we believe to be adequate for nuclear burst simulations. Eq. 3-30 shows the simplest form of the electrical resistivity adequate over the electron temperature range of 0.01 to 10 eV. Eqs. 3-31 show the simplified form of the collision frequencies for collisions of ions with neutrals, of electrons with neutrals, and of electrons with ions that are needed for very late-time simulations.

During the initial debris-air interaction when the particle velocities exceed 10^8 cm/sec, inelastic collisions are more important than elastic collisions. Appendix C summarizes the relevant experimental stopping cross sections (Table C-1) and shows how to relate these to the momentum-transfer cross section q (Eq. C-8) and the total scattering cross section σ_t (Eq. C-9) which are needed to compute the collisional momentum and energy transfer rates from Eqs. 2-33 through 2-41.

Two fluid MHD simulations are essential for realistic simulations of late-time nuclear burst phenomena. Unfortunately, they are extremely complex and therefore cannot be redone easily. Thus, it is important that the momentum and energy transfer coefficients be reasonably accurate (e.g., to within 50%). We believe the following analysis and cross-section data do provide a reliable set of coefficients. If the reader notes any errors in this analysis or is aware of better cross section data, we would appreciate hearing from him so that improvements can be made as soon as possible.

To help the reader keep track of the mathematical notation, a Glossary of Symbols is given in Appendix A.

SECTION 2

THEORY OF MOMENTUM AND ENERGY TRANSFER BY COLLISIONS

2.1 SCATTERING COLLISIONS

(a) Statement of the Problem

We consider two-body (inelastic or elastic) collisions characterized by an arbitrary differential scattering cross section. The colliding particles may be atoms, molecules, ions, or electrons. The particles of the first species are characterized by mass m_1, uniform number density n_1, mean velocity $\vec{V}_1$, and temperature T_1 (the particle velocity distribution is Maxwell-Boltzmann in the frame moving at velocity $\vec{V}_1$); the particles of the second species are characterized by m_2, n_2, $\vec{V}_2$, and T_2. In a collision between two particles of different species moving initially at relative speed v, each particle is scattered through an angle θ measured in their center-of-mass frame, and in inelastic collisions the pair loses an amount of kinetic energy ε due to ionization, excitation followed by radiation, etc. The collisions are described by a differential scattering cross section $d\sigma(v,\theta)/d\Omega$ in the center-of-mass frame (Reference 1). The interaction potential is assumed to be spherically symmetric, so the azimuthal angle ϕ is not needed.

The scattering cross section and the inelastic energy loss ε depend on the initial and final states of the particles. For elastic collisions (Section 3) these are all ground states. For inelastic collisions (Appendix C) we must do sums over states.

Let the colliding particles have incoming velocities $\vec{v}_1$, $\vec{v}_2$ and outgoing velocities $\vec{v}_1'$, $\vec{v}_2'$ in the laboratory frame. (We use lower case v's to denote particle velocities and capital V's to denote macroscopic velocities of gases.) The density of particles of the first species in velocity space is Maxwell-Boltzmann in the frame moving at velocity $\vec{V}_1$; we denote these Maxwell-Boltzmann distributions by

$$f_1\left(\vec{v}_1;\vec{V}_1,\frac{T_1}{m_1}\right) = \begin{cases} n_1\left(\frac{m_1}{2\pi kT_1}\right)^{3/2} \exp\left[-\frac{m_1(\vec{v}_1-\vec{V}_1)^2}{2kT_1}\right] & \text{if } T_1 > 0, \\ n_1\delta(\vec{v}_1-\vec{V}_1) & \text{if } T_1 = 0, \end{cases} \tag{2-1}$$

and likewise for the second species. Here δ is the Dirac delta function.

We take the rate of change due to collisions of the density of momentum of the first gas to be

$$\frac{\Delta(\rho_1\vec{V}_1)}{\Delta t} = \int m_1\left[\vec{v}_1'-\vec{v}_1\right] f_1(\vec{v}_1) f_2(\vec{v}_2) |\vec{v}_1-\vec{v}_2| \frac{d\sigma(|\vec{v}_1-\vec{v}_2|,\theta)}{d\Omega}\, d\Omega d^3v_1 d^3v_2 \quad . \tag{2-2}$$

and that of the total kinetic energy of particles of the first species to be

$$\frac{\Delta\left(\frac{1}{2}\rho_1\overline{v_1^2}\right)}{\Delta t} = \int \frac{1}{2}\, m_1\left[v_1'^2-v_1^2\right] f_1(\vec{v}_1) f_2(\vec{v}_2) |\vec{v}_1-\vec{v}_2| \frac{d\sigma(|\vec{v}_1-\vec{v}_2|,\theta)}{d\Omega}\, d\Omega d^3v_1 d^3v_2 \quad , \tag{2-3}$$

where $\rho_1 = n_1 m_1$. These quantities derive from the collision term in the Boltzmann transport equation, $(\partial f_1(\vec{v}_1)/\partial t)_{col}$; for example, the first one is $m_1\vec{v}_1$ times this collision term, integrated over all velocities $\vec{v}_1$.

Our terminology concerning the forms of energy of a gas follows a scheme used by some workers in high-altitude phenomenology. The internal energy of a gas is the translational kinetic energy of its particles in the frame moving with the mean velocity $\vec{V}_1$ plus the energy of rotational excitation. (In this scheme, the ionization energy and the energies of electronic and vibrational excitation must be treated separately.) This internal energy density is denoted by $\rho_1 I_1$. The "total energy" of a gas is the sum of its internal energy plus its macroscopic kinetic energy $\frac{1}{2}\rho_1 V_1^2$. We assume unless otherwise noted that changes in rotational energy are negligible, and so we refer to $\Delta\left(\frac{1}{2}\rho_1 \overline{v_1^2}\right)$ simply as the change of total energy density of the first gas.

In the integrals in Eqs. 2-2 and 2-3 the final velocity $\vec{v}_1'$ is a function of $\vec{v}_1$, $\vec{v}_2$, ε, and θ. We will change the independent variables to $\vec{v}_1$, $\vec{v} \equiv \vec{v}_1 - \vec{v}_2$, ε, and θ because the differential scattering cross section is most easily expressed in terms of these variables.

(b) Change of Momentum and Kinetic Energy in a Collision

First we seek to express the final particle velocity $\vec{v}_1'$ in terms of the (new) independent variables. We denote the reduced mass of these species by

$$\mu = m_1 m_2/(m_1+m_2) \quad , \tag{2-4}$$

the center-of-mass velocity by

$$\vec{v}_{cm} \equiv \frac{m_1\vec{v}_1 + m_2\vec{v}_2}{m_1 + m_2} \quad , \tag{2-5}$$

and the initial relative velocity by

$$\vec{v} = \vec{v}_1 - \vec{v}_2 \quad . \tag{2-6}$$

The initial velocities are related by

$$\vec{v}_1 = \vec{v}_{cm} + \frac{\mu}{m_1}\vec{v} \; ; \tag{2-7}$$

the final velocities, denoted by primes, have relations just like Eqs. 2-5 to 2-7.

The initial kinetic energy of the pair of particles in terms of $\vec{v}_{cm}$ and $\vec{v}$ is

$$\frac{1}{2} m_1 v_1^2 + \frac{1}{2} m_2 v_2^2 = \frac{1}{2}(m_1+m_2) v_{cm}^2 + \frac{1}{2} \mu v^2 \quad . \tag{2-7a}$$

Conservation of momentum and conservation of energy give

$$\vec{v}_{cm} = \vec{v}'_{cm} \tag{2-8}$$

and

$$\frac{1}{2} \mu v^2 = \frac{1}{2} \mu v'^2 + \varepsilon \quad . \tag{2-9}$$

where ε is the loss of kinetic energy during an inelastic collision.

We define $\Delta\vec{v}_1 \equiv \vec{v}_1' - \vec{v}_1$ and $\Delta\vec{v} \equiv \vec{v}' - \vec{v}$; from above these are related by

$$\Delta\vec{v}_1 = \frac{\mu}{m_1} \Delta\vec{v} \; . \tag{2-10}$$

The change in kinetic energy of the first particle can be written

$$\frac{1}{2} m_1 v_1'^2 - \frac{1}{2} m_1 v_1^2 = m_1 \vec{v}_1 \cdot \Delta\vec{v}_1 + \frac{1}{2} m_1 (\Delta v_1)^2$$

$$= \mu \vec{v}_1 \cdot \Delta\vec{v} + \frac{1}{2} \frac{\mu^2}{m_1} (\Delta v)^2 \quad . \tag{2-11}$$

The scattering angle θ in the center-of-mass frame is defined by the diagram.

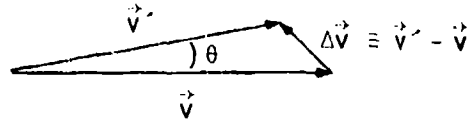

The azimuthal angle ϕ measures the angle around the $\vec{v}$ axis. We assume that the differential cross section is independent of ϕ, so we can average $\Delta\vec{v}_1$ and $\frac{1}{2} m_1 (v_1'^2 - v_1^2)$ over ϕ. The component of $\Delta\vec{v}$ perpendicular to $\vec{v}$ therefore averages to zero, while the parallel component averages to

$$\left\langle \Delta\vec{v} \right\rangle_\phi = \frac{\vec{v} \cdot \Delta\vec{v}}{v^2} \vec{v}$$

$$= \frac{(\vec{v} \cdot \vec{v}' - v^2)}{v^2} \vec{v}$$

$$= -\left(1 - \frac{v'}{v} \cos\theta\right) \vec{v} \quad , \tag{2-11a}$$

or by the conservation relation Eq. 2-9,

$$\left\langle \Delta\vec{v} \right\rangle_\phi = -\left(1 - \sqrt{1 - \frac{2\varepsilon}{\mu v^2}} \cos\theta\right) \vec{v} \quad . \tag{2-12}$$

The quantity $(\Delta v)^2$ is independent of ϕ and is given by

$$(\Delta v)^2 = v^2 + v'^2 - 2vv'\cos\theta$$

$$= v^2 \left(2 - \frac{2\varepsilon}{\mu v^2} - 2\sqrt{1 - \frac{2\varepsilon}{\mu v^2}} \cos\theta\right) \quad . \tag{2-13}$$

Using these in relations 2-10 and 2-11 gives the two desired averages,

$$\left\langle \Delta\vec{v}_1 \right\rangle_\phi = -\frac{\mu}{m_1}\left(1 - \sqrt{1 - \frac{2\varepsilon}{\mu v^2}}\cos\theta\right)\vec{v} \tag{2-14}$$

and

$$\left\langle \frac{1}{2} m_1 (v_1'^2 - v_1^2) \right\rangle_\phi = -\mu\vec{v}_1 \cdot \vec{v}\left(1 - \sqrt{1 - \frac{2\varepsilon}{\mu v^2}}\cos\theta\right) + \frac{\mu^2}{m_1} v^2\left(1 - \sqrt{1 - \frac{2\varepsilon}{\mu v^2}}\cos\theta\right) - \frac{\mu}{m_1}\varepsilon. \tag{2-15}$$

(c) Evaluation of Integrals

Having expressed the final velocity in terms of the initial velocities and θ and ε, we are ready to integrate Eqs. 2-2 and 2-3. First we express the product $f_1 f_2$ of the velocity distributions in terms of the variables $\vec{v}_1$ and $\vec{v}$. We define the abbreviations

$$\hat{f}_1(\vec{v}_1) \equiv \begin{cases} f_1\left(\vec{v}_1;\ \dfrac{m_1\vec{V}_1 + m_2(\vec{V}_2+\vec{v})}{(m_1+m_2)} + \dfrac{\mu(T_2-T_1)(\vec{V}_1-\vec{V}_2-\vec{v})}{(m_1T_2+m_2T_1)},\ \dfrac{T_1T_2}{(m_1T_2+m_2T_1)}\right) & \text{if } T_1 > 0 \text{ or } T_2 > 0, \\ n_1\delta(\vec{v}_1-\vec{V}_1) & \text{if } T_1 = 0 \text{ and } T_2 = 0, \end{cases} \tag{2-16}$$

$$\hat{f}_2(\vec{v}) \equiv f_2\left(\vec{v};\ \vec{V}_1-\vec{V}_2, \frac{m_1T_2+m_2T_1}{m_1m_2}\right). \tag{2-17}$$

$\hat{f}_2(\vec{v})/n_2$ is the normalized distribution of relative velocities of pairs of particles of different species. Some algebra then shows that

$$f_1\left(\vec{v}_1;\ \vec{V}_1,\ \frac{T_1}{m_1}\right) f_2\left(\vec{v}_2;\ \vec{V}_2,\ \frac{T_2}{m_2}\right) = \hat{f}_1(\vec{v}_1)\hat{f}_2(\vec{v}), \tag{2-18}$$

and the Jacobian of the transformation has an absolute value

$$\left|\frac{\partial(\vec{v}_1,\vec{v})}{\partial(\vec{v}_1,\vec{v}_2)}\right| = 1 \tag{2-19}$$

so that $d^3v_1 d^3v_2 = d^3v_1 d^3v$.

In treating $\hat{f}_2(\vec{v})$ it is convenient to denote the macroscopic velocity of the first gas with respect to the second by

$$\vec{V} \equiv \vec{V}_1 - \vec{V}_2 \tag{2-20}$$

and the temperature characterizing the distribution of relative velocities by

$$T_m \equiv \frac{(m_1T_2+m_2T_1)}{(m_1+m_2)} \quad . \tag{2-21}$$

The subscript m denotes a weighted mean. We also define the total scattering cross section (Reference 1)

$$\sigma_t(v) = \int_{4\pi} \frac{d\sigma(v,\theta)}{d\Omega}\, d\Omega \quad . \tag{2-22}$$

and the momentum-transfer cross section

$$q(v) = \int_{4\pi} \left(1 - \sqrt{1 - \frac{2\varepsilon}{\mu v^2}}\cos\theta\right) \frac{d\sigma(v,\theta)}{d\Omega}\, d\Omega \quad . \tag{2-23}$$

This cross section is called $Q_{ab}^{(1)cd}$ by McDaniel and Mason (Reference 2, p 158). For elastic collisions ($\varepsilon = 0$) we denote this cross section by $q_D(v)$; it is also known as the diffusion cross section.

Equations 2-2 and 2-3 then become

$$\frac{\Delta(\rho_1 \vec{V}_1)}{\Delta t} = -\int \hat{f}_1(\vec{v}_1)\hat{f}_2(\vec{v})vq(v)\mu\vec{v}d^3v_1 d^3v \quad , \tag{2-24}$$

$$\frac{\Delta\left(\frac{1}{2}\rho_1\overline{v_1^2}\right)}{\Delta t} = \int \hat{f}_1(\vec{v}_1)\hat{f}_2(\vec{v})v\left[\mu\left(\frac{\mu}{m_1}v^2 - \vec{v}\cdot\vec{v}_1\right)q(v) - \frac{\mu}{m_1}\varepsilon\sigma_t(v)\right] d^3v_1 d^3v \quad . \tag{2-25}$$

The integrals over d^3v_1 are done next, and after some algebra on the energy equation we have

$$\frac{\Delta(\rho_1 \vec{V}_1)}{\Delta t} = -\mu n_1 \int \hat{f}_2(\vec{v})q(v)v\vec{v}d^3v \quad , \tag{2-26}$$

$$\frac{\Delta\left(\frac{1}{2}\rho_1\overline{v_1^2}\right)}{\Delta t} = \begin{cases} n_1\mu\int\left[-\frac{(m_1\vec{V}_1+m_2\vec{V}_2)}{(m_1+m_2)}\cdot\vec{v} + \frac{\mu(T_2-T_1)}{(m_1T_2+m_2T_1)}(v^2-\vec{v}\cdot\vec{V})\right]\hat{f}_2(\vec{v})vq(v)d^3v \\ \qquad - n_1\frac{\mu}{m_1}\varepsilon\int\hat{f}_2(\vec{v})\sigma_t(v)vd^3v \\ \qquad\qquad \text{if } T_1 > 0 \text{ or } T_2 > 0 \quad , \\ n_1\mu\int\left[-\frac{(m_1\vec{V}_1+m_2\vec{V}_2)}{(m_1+m_2)}\cdot\vec{v} + \frac{\mu}{m_1}(v^2-\vec{v}\cdot\vec{V})\right]\hat{f}_2(\vec{v})vq(v)d^3v \\ \qquad - n_1\frac{\mu}{m_1}\varepsilon\int\hat{f}_2(\vec{v})\sigma_t(v)vd^3v \\ \qquad\qquad \text{if } T_1 = 0 \text{ and } T_2 = 0 \quad . \end{cases} \tag{2-27}$$

The last integral in Eq. 2-27, $\int \hat{f}_2(\vec{v})\sigma_t(v)v d^3v$, is the mean frequency of scattering collisions of a particle of the first species. We will use the closely related rate coefficient for scattering collisions (of inelastic energy loss ε),

$$k_s(T_m,V) \equiv \frac{1}{n_2}\int \hat{f}_2(\vec{v})\sigma_t(v)v d^3v \quad . \tag{2-28}$$

We need two other integrals, for which we use the closely related rate coefficients s and h:

$$s(T_m,V)\,\vec{V} \equiv \frac{1}{n_2}\mu\int \hat{f}_2(\vec{v})q(v)v\vec{v}d^3v \quad , \tag{2-29}$$

$$h(T_m,V) \equiv \frac{1}{n_2}\frac{\mu^2}{k(m_1T_2+m_2T_1)}\int \hat{f}_2(\vec{v})q(v)v(v^2-\vec{v}\cdot\vec{V})d^3v \quad . \tag{2-30}$$

Note that k_s and h are in cm^3/sec, while s in in $gm\text{-}cm^3/sec$. We will show in Section 2.1d that s can be interpreted as the rate coefficient for momentum transfer or "coupling coefficient" and h as the rate coefficient for heat transfer.

We do the angular integrals using spherical coordinates about the $\vec{V}$ axis. Integrating first over the azimuthal angle, we note that in the integral of Eq. 2-29, the components perpendicular to $\vec{V}$ integrate to zero. This result occurs because the particle velocity distributions of each species are considered to be Maxwell-Boltzmann in some frame. We then integrate over the cosine of the zenithal angle and change the remaining integration variable to

$$\xi \equiv \sqrt{\frac{m_1m_2}{2k(m_1T_2+m_2T_1)}}\;v \quad . \tag{2-31}$$

For brevity we eliminate the mean temperature T_m in favor of the related thermal speed parameter

$$U \equiv \sqrt{\frac{2kT_1}{m_1}+\frac{2kT_2}{m_2}} \quad . \tag{2-32}$$

The results for the three rate coefficients are

$$s(T_m,V) = \begin{cases} \dfrac{1}{\sqrt{\pi}} \dfrac{m_1 m_2}{(m_1+m_2)} \dfrac{U^4}{V^5} \displaystyle\int_0^\infty q(U\xi)\left[\left(\frac{V}{U}\xi^3 - \frac{1}{2}\xi^2\right) e^{-(\xi-V/U)^2} + \left(\frac{V}{U}\xi^3 + \frac{1}{2}\xi^2\right) e^{-(\xi+V/U)^2}\right] d\xi \\ \qquad\qquad \text{if } T_m > 0 \text{ and } V > 0 \ , \\ \dfrac{8}{3\sqrt{\pi}} \dfrac{m_1 m_2}{(m_1+m_2)} U \displaystyle\int_0^\infty q(U\xi)\xi^5 e^{-\xi^2} d\xi \qquad \text{if } V = 0 \ , \\ \dfrac{m_1 m_2}{(m_1+m_2)} Vq(V) \qquad \text{if } T_m = 0 \ , \end{cases} \qquad (2\text{-}33)^{***}$$

$$h(T_m,V) = \begin{cases} \dfrac{2}{\sqrt{\pi}} \dfrac{m_1 m_2}{(m_1+m_2)^2} \dfrac{U^2}{V} \displaystyle\int_0^\infty q(U\xi)\left[\left(\xi^4 - \frac{V}{U}\xi^3 + \frac{1}{2}\xi^2\right) e^{-(\xi-V/U)^2} + \left(-\xi^4 - \frac{V}{U}\xi^3 - \frac{1}{2}\xi^2\right) e^{-(\xi+V/U)^2}\right] d\xi \\ \qquad\qquad \text{if } T_m > 0 \text{ and } V > 0 \ , \\ \dfrac{3}{(m_1+m_2)} s(T_m,0) \qquad \text{if } V = 0 \ , \\ \dfrac{m_1 m_2}{(m_1+m_2)^2} V\left(4q(V) + V \dfrac{dq}{dv}(V)\right) \qquad \text{if } T_m = 0 \ , \end{cases} \qquad (2\text{-}34)^{***}$$

$$ck_s(T_m,V) = \begin{cases} \dfrac{1}{\sqrt{\pi}}\dfrac{U^2}{V}\displaystyle\int_0^\infty \varepsilon\sigma_t(U\xi)\xi^2\left[e^{-(\xi-V/U)^2} - e^{-(\xi+V/U)^2}\right]d\xi & \\ & \text{if } T_m > 0 \text{ and } V > 0, \\ \dfrac{4}{\sqrt{\pi}}U\displaystyle\int_0^\infty \varepsilon\sigma_t(U\xi)\xi^3 e^{-\xi^2}d\xi & \text{if } V = 0 \ , \\ V\varepsilon\sigma_t(V) & \text{if } T_m = 0 \ . \end{cases} \qquad (2\text{-}35)$$

These rate coefficients are continuous functions of T_m (or U) and V. The cross sections q needed to evaluate the integrals (2-33) to (2-35) are shown in Figs. 4-1 to 4-8. The quantity $\varepsilon\sigma_t$ can be related to the cross section q by $\varepsilon\sigma_t = v^2 q_{inel}\, m_1 m_2/(m_1+m_2)$ (Eq. C-7 of Appendix C).

(d) General Results

The time rate of change due to collisions of the density of momentum of the first gas is

$$\frac{\Delta(\rho_1 \vec{V}_1)}{\Delta t} = -n_1 n_2 s(T_m,V)\,(\vec{V}_1-\vec{V}_2), \qquad (2\text{-}36)$$

and that of the total energy of the first gas is

$$\frac{\Delta\left(\frac{1}{2}\rho_1 \overline{V_1^2}\right)}{\Delta t} = n_1 n_2\left[-\frac{(m_1\vec{V}_1+m_2\vec{V}_2)\cdot(\vec{V}_1-\vec{V}_2)}{(m_1+m_2)}s(T_m,V) + h(T_m,V)k(T_2-T_1) - \frac{m_2}{(m_1+m_2)}ck_s(T_m,V)\right]. \qquad (2\text{-}37)$$

The total energy of each gas can always be split into its macroscopic kinetic energy and its internal energy:

$$\frac{\Delta\left(\frac{1}{2}\rho_1\overline{v_1^2}\right)}{\Delta t} = \frac{\Delta\left(\frac{1}{2}\rho_1 v_1^2\right)}{\Delta t} + \frac{\Delta(\rho_1 I_1)}{\Delta t} \quad . \tag{2-38}$$

The rate of change of the macroscopic kinetic energy of the first gas due to collisions is

$$\frac{\Delta\left(\frac{1}{2}\rho_1 v_1^2\right)}{\Delta t} = \frac{\Delta(\rho_1\vec{v}_1)}{\Delta t}\cdot\vec{v}_1 \quad . \tag{2-39}$$

so we have for the rate of change of the internal energy density due to collisions

$$\frac{\Delta(\rho_1 I_1)}{\Delta t} = n_1 n_2\left[\frac{m_2}{(m_1+m_2)}\, s(T_m,V)V^2 + h(T_m,V)k(T_2-T_1) - \frac{m_2}{(m_1+m_2)}\,\varepsilon k_s(T_m,V)\right] \quad . \tag{2-40}$$

The first term on the right side of Eq. 2-40 is the part of the macroscopic kinetic energy of the gases that is converted to internal energy of the first gas; this is the rate of internal or resistive heating. The second term is the heat transfer between the gases, and the third term is the energy diverted to excitation and ionization. We refer to h as the rate coefficient for heat transfer and to s as the rate coefficient for momentum transfer or simply as the coupling coefficient.

Rates for the second gas can be found from symmetry by interchanging subscripts 1 and 2. The total power per unit volume transferred by collisions from the total energy of both gases to other forms of energy is

$$-\left(\frac{\Delta\left(\frac{1}{2}\rho_1\overline{v_1^2}\right)}{\Delta t} + \frac{\Delta\left(\frac{1}{2}\rho_2\overline{v_2^2}\right)}{\Delta t}\right) = n_1 n_2 \varepsilon k_s(T_m,V) \quad . \tag{2-41}$$

For the special case of elastic collisions between two gases having no relative velocity ($c = 0$, $V = 0$), Eq. 2-37 agrees with Desloge's result (Reference 5, Eq. 20).

2.2 CHARGE-EXCHANGE REACTIONS

(a) Introduction

While elastic scattering is the most important means of transferring momentum and energy between ions and neutrals at low speeds, charge exchange is also important at relative particle speeds above 10^5 cm/sec. In this report we concentrate on symmetric charge exchange, in which the products are the same as the reactants:

$$X^+ + X \rightarrow X + X^+ \quad . \tag{2-42}$$

If each reactant and product is in its ground state, this reaction has zero energy defect and is called resonant (or elastic) charge exchange. Such resonant reactions can have unusually large cross sections (see Figures 4-1 to 4-4) and are among the most important reactions at times after a few seconds after a high-altitude nuclear burst. Symmetric charge exchange is much like a scattering process, and we will treat it by a minor modification of the scattering theory of Section 2.1.

Asymmetric charge transfer is a chemical reaction in our view and is treated differently. A treatment comparable to Section 2.1 is given in Appendix B, subsections (a) to (d), and a simplified treatment is given in subsection (e). Experimental cross sections for some asymmetric charge-exchange reactions are plotted in Section 4 for comparison with the others. We do not want to become enmeshed here in choosing which chemical reactions are important, though, so we have not evaluated rate coefficients for asymmetric charge exchange in Section 5.

(b) Symmetric Charge Exchange

Symmetric charge exchange can be treated within the framework of Section 2.1. We simplify this slightly by assuming that such reactions are forward scattering and have no inelastic loss or gain of kinetic energy (that is, $d\sigma/d\Omega$ is negligible unless $\theta \ll 1$ and $\varepsilon = 0$).

Symmetric charge exchange can be considered an ordinary scattering collision by relabeling the particles after the encounter. An encounter that is forward scattering in the center-of-mass frame is backscattering in this alternate description. The effective momentum-transfer cross section in this alternate description, denoted by an asterisk, is given by Eqs. 2-25 and 2-22 with $\theta \to \pi$ and $\varepsilon = 0$:

$$q^*(v) = 2\sigma_X(v) \quad . \tag{2-43}$$

This point is elaborated in Reference 2, Section 5-7-A. Given $\sigma_X(v)$ one can use this relation in Eqs. 2-33 and 2-34 to get a coupling coefficient s^* and heat-transfer coefficient h^* due to symmetric charge exchange; these must be added to the coupling coefficient s and heat-transfer coefficient h due to scattering collisions (see Eq. 2-48).

2.3 RELATION TO THE EQUATIONS OF FLUID DYNAMICS

(a) Momentum Balance Equations

We show here how our results for elastic scattering and symmetric charge exchange relate to the momentum and energy balance equations of a two-fluid treatment. Inelastic scattering is not considered here; at times after 1 sec following a nuclear burst when the two-fluid equations are a good approximation, inelastic scattering is unimportant except for the energy transfer between electrons and the vibrational excitation of N_2 molecules.

The neutral fluid, indicated by subscript n, is composed of species X_j^o, $j = 1,2,\ldots$, so that

$$n_n = \sum_j n(X_j^o); \tag{2-44}$$

similarly the ions are composed of singly charged species X_k^+, k = 1,2,..., so that

$$n_i = \sum_k n(X_k^+) \quad . \tag{2-45}$$

We assume that all neutral species have the same temperature T_n and gas velocity $\vec{V}_n$ and all ions have the same temperature T_i and velocity $\vec{V}_i$. The electrons have density $n_e = n_i$, temperature T_e, and velocity

$$\vec{V}_e = \vec{V}_i - c\vec{J}/en_i \quad . \tag{2-46}$$

For each pair of a neutral species j and an ion species k, Eq. 2-21 defines a weighted mean temperature

$$T_{jk} = \frac{(m_j T_i + m_k T_n)}{(m_j + m_k)} \quad . \tag{2-47}$$

If either species is an electron the weighted temperature is simply $T_m \approx T_e$.

The rate of momentum transfer due to ion-neutral collisions is a sum of terms of the form of the right side of Eq. 2-36. For each pair of a neutral species j and an ion species k, Eq. 2-33 defines a coupling coefficient $s_{jk}(T_{jk}, |\vec{V}_n - \vec{V}_i|)$ due to scattering. The ion-neutral coupling coefficient s_{ni} is given by

$$n_n n_i s_{ni} \equiv \sum_j \sum_k n(X_j^o) n(X_k^+) s_{jk}(T_{jk}, |\vec{V}_n - \vec{V}_i|) + \sum_k n(X_k^o) n(X_k^+) s_k^*((T_n + T_j)/2, |\vec{V}_n - \vec{V}_i|) \quad , \tag{2-48}$$

where the s_k^* are coupling coefficients due to symmetric charge exchange of ions of species k with their parent atoms or molecules (Section 2.2b).

Similarly the electron-neutral coupling coefficient s_{ne} is

$$n_n s_{ne} \equiv \sum_j n(X_j^o) s_{je}(T_e, |\vec{V}_n - \vec{V}_e|) \ , \tag{2-49}$$

where we have assumed that the neutral temperature is small compared to $(m_j/m_e)T_e$. The ion-electron coupling coefficient is

$$n_i s_{ie} \equiv \sum_k n(X_k^+) s_{ke}(T_e, cJ/en_i); \tag{2-50}$$

s_{ie} and s_{ne} are closely related to the electrical resistivity (Eq. 5-22).

The momentum balance equations for the neutral fluid, for the ion-electron plasma, and for the electrons can be written as (see Glossary of Symbols in Appendix A)

$$\frac{\partial(\rho_n \vec{V}_n)}{\partial t} + \nabla\cdot(\rho_n \vec{V}_n \vec{V}_n) = -\nabla P_n + \rho_n \vec{g} - n_n n_i s_{ni}(\vec{V}_n - \vec{V}_i) - n_n n_e s_{ne}(\vec{V}_n - \vec{V}_e) \ , \tag{2-51}$$

$$\frac{\partial(\rho_i \vec{V}_i)}{\partial t} + \nabla\cdot(\rho_i \vec{V}_i \vec{V}_i) = -\nabla(P_i + P_e) + \vec{J} \times \vec{B} + (\rho_i + \rho_e)\vec{g} + n_n n_i s_{ni}(\vec{V}_n - \vec{V}_i) + n_n n_e s_{ne}(\vec{V}_n - \vec{V}_e) \ , \tag{2-52}$$

$$0 = -\nabla P_e - en_e\left(\vec{E} + \frac{\vec{V}_e \times \vec{B}}{c}\right) + \rho_e \vec{g} + n_n n_e s_{ne}(\vec{V}_n - \vec{V}_e) + n_i n_e s_{ie}(\vec{V}_i - \vec{V}_e). \tag{2-53}$$

We have ignored viscosity and electron inertia. One can eliminate $\vec{V}_e$ in terms of $\vec{V}_i$ and $\vec{J}$ by Eq. 2-46.

(b) Energy Balance Equations

For the energy balance equations, Eq. 2-34 defines a heat-transfer coefficient $h_{jk}(T_{jk}, |\vec{V}_n - \vec{V}_i|)$ for each pair of a neutral species j and an ion species k. The ion-neutral, electron-neutral, and ion-electron heat-transfer coefficients h_{ni}, h_{ne}, and h_{ie} are defined as in Eqs. 2-48 to 2-50.

The energy balance equations also include frictional or resistive heating, which is the sum over all pairs of species of the first term on the right side of Eq. 2-40. For each pair of species the rate at which collisions between species 1 and 2 convert their total macroscopic kinetic energy into internal energy is $n_1 n_2 s(T_m,V)V^2$, and each species receives a fraction of this that is inversely proportional to its particle mass. The fraction $d_{ni}^{(n)}$ of the ion-neutral frictional heating that goes into internal energy of neutrals is given by

$$n_n n_i s_{ni} d_{ni}^{(n)} \equiv \sum_j \sum_k n(X_j^o) n(X_k^+) \frac{m_k}{(m_j+m_k)} s_{jk}(T_{jk}, |\vec{V}_n - \vec{V}_i|) + \sum_k n(X_k^o) n(X_k^+) \frac{1}{2} s_k^* \left(\frac{1}{2} T_n + \frac{1}{2} T_i, |\vec{V}_n - \vec{V}_i| \right) ; \quad (2\text{-}53a)$$

recall that j and k specify neutral and ion species, respectively. The corresponding fraction that goes to ions is $1 - d_{ni}^{(n)}$. For atmospheric ions and neutrals considered in Sections 3 to 5 this fraction is in the range $0.3 < d_{ni}^{(n)} < 0.7$. We also define a "fractional coupling coefficient" for electron-neutral collisions $d_{ne}^{(n)}$ by

$$n_n s_{ne} d_{ne}^{(n)} \equiv \sum_j n(X_j^o) \frac{m_e}{(m_j+m_e)} s_{je}(T_e, |\vec{V}_n - \vec{V}_e|) , \quad (2\text{-}54)$$

and similarly for $d_{ie}^{(i)}$. The fractions $d_{ne}^{(n)}$ and $d_{ie}^{(i)}$ are of the order of the electron mass divided by the mean mass of neutrals or ions (see Eqs. 2-63 and 2-65).

With the collisional terms expressed by means of Eq. 2-40 with $\varepsilon = 0$, the energy balance equations for the neutral fluid, for the ions, and for the electrons are

$$\frac{\partial(\rho_n I_n)}{\partial t} + \nabla \cdot (\rho_n I_n \vec{V}_n) = - P_n \nabla \cdot \vec{V}_n + n_n n_i s_{ni} d_{ni}^{(n)} (\vec{V}_n - \vec{V}_i)^2 + n_n n_e s_{ne} d_{ne}^{(n)} (\vec{V}_n - \vec{V}_e)^2 + n_n n_i h_{ni} k (T_i - T_n) + n_n n_e h_{ne} k (T_e - T_n) , \quad (2\text{-}55)$$

$$\frac{\partial(\rho_i I_i)}{\partial t} + \nabla\cdot(\rho_i I_i \vec{V}_i) = - P_i \nabla\cdot\vec{V}_i + n_n n_i s_{ni} (1-d_{ni}^{(n)}) (\vec{V}_n-\vec{V}_i)^2$$

$$+ n_i n_e s_{ie} d_{ie}^{(i)} (\vec{V}_i-\vec{V}_e)^2 - n_n n_i h_{ni} k(T_i-T_n) - n_i n_e h_{ie} k(T_i-T_e) \quad , \tag{2-56}$$

$$\frac{\partial(n_e \frac{3}{2} kT_e)}{\partial t} + \nabla\cdot(n_e \frac{3}{2} kT_e \vec{V}_e) = - P_e \nabla\cdot\vec{V}_e + n_n n_e s_{ne} (\vec{V}_n-\vec{V}_e)^2$$

$$+ n_i n_e s_{ie} (\vec{V}_i-\vec{V}_e)^2 - n_n n_e h_{ne} k(T_e-T_n) + n_i n_e h_{ie} k(T_i-T_e) \quad . \tag{2-57}$$

We have ignored thermal conductivity and viscosity, which are not treated in this paper although they are important processes above 300 km altitude. In Eq. 2-57 we have assumed that $1 - d_{ne}^{(n)} \approx 1$ and $1 - d_{ie}^{(i)} \approx 1$. In the approximation that $\vec{V}_i \approx \vec{V}_n$, the second and third terms on the right side of this equation are the rate of resistive heating ηJ^2, where η is the electrical resistivity (Eq. 5-22). For nuclear burst simulations that include an N_2 vibrational temperature T_v, Eq. 2-57 should also include heat transfer proportional to (T_v-T_e).

A special case provides several simplifications to the rate coefficients. Our numerical results in Section 5 are for the special case of low relative velocities:

$$|\vec{V}_n-\vec{V}_j|^2 << \frac{2kT_n}{m_j} + \frac{2kT_i}{m_k} \quad , \tag{2-58}$$

$|\vec{V}_n-\vec{V}_e|^2 << 2kT_e/m_e$, and similarly for the ion-electron velocity. From Eq. 2-34b the heat-transfer coefficients become

$$n_n n_i h_{ni} \approx \sum_j \sum_k n(X_j^o) n(X_k^+) \frac{3s_{jk}}{(m_j+m_k)} + \sum_k n(X_k^o) n(X_k^+) \frac{3s_k^*}{2m_k} \quad , \tag{2-59}$$

$$n_n h_{ne} \approx \sum_j n(X_j^o) 3 s_{je}/m_j \quad , \tag{2-60}$$

$$n_i h_{ie} \approx \sum_k n(X_k^+) 3 s_{ke}/m_k \quad . \tag{2-61}$$

Electron-neutral scattering is important mainly at altitudes below 150 km, where the neutrals are primarily N_2. From Eqs. 2-60, 2-49, and 2-54 one finds

$$h_{ne} \approx 3\, s_{ne}/m(N_2) \quad , \tag{2-62}$$

$$d_{ne}^{(n)} \approx m_e/m(N_2) = 2.0 \times 10^{-5} \quad . \tag{2-63}$$

Similarly if most ions have a mass near that of O^+, one finds from Eqs. 2-61 and 2-50

$$h_{ie} \approx 3\, s_{ie}/m(O^+) \quad , \tag{2-64}$$

$$d_{ie}^{(i)} \approx m_e/m(O^+) = 3.4 \times 10^{-5} \quad . \tag{2-65}$$

Under the above assumptions the ion-neutral fractional coupling coefficient defined in Eq. 2-53a can be approximated as

$$d_{ni}^{(n)} \approx 0.4 \quad , \tag{2-66}$$

accurate to ± 20 percent.

SECTION 3
SCATTERING CROSS SECTIONS FOR ATMOSPHERIC SPECIES

To use the preceding theory in two-fluid simulations of high-altitude nuclear explosions, one needs momentum-transfer cross sections for scattering collisions as a function of relative speed or of energy. One needs to consider ion-neutral, electron-neutral, and electron-ion scattering for principal atmospheric species. Also one needs charge-exchange cross sections, which will be presented in Section 4.

We consider the species N, O, N_2, O_2, NO, He, N^+, O^+, N_2^+, O_2^+, NO^+, He^+, and electrons. We concentrate on elastic collisions ($\varepsilon = 0$) in the energy range from 0.005 eV to roughly 30 eV for electrons or tens of keV for ion-neutral collisions. At higher energies, inelastic collisions dominate; ion-neutral inelastic collisions are considered in Appendix C. We consider electron-neutral scattering using experimental data, electron-ion scattering using theory, and ion-neutral scattering using mainly theory or semi-empirical methods.

3.1 ELECTRON-NEUTRAL SCATTERING BELOW 100 eV

For scattering of electrons from N, O, N_2, O_2, and NO, we have used the momentum-transfer cross sections recommended by Phelps (Reference 4). For the molecules his cross sections extend over electron energies from 0.005 to 100 eV. He tabulates the frequency of momentum-transfer collisions per unit density of molecules (cm^3/sec); we have divided by the electron speed to obtain a cross section. Figs. 4-2 to 4-4 show these cross sections.

The cross sections come from various types of experiments. The e + N_2 cross section comes from an analysis of dc swarm experiments, and Phelps estimates ±20 percent accuracy or better. The e + NO cross section* is based on an analysis of dc mobility data and, for energies below 0.02 eV, on theory for a polar molecule; the accuracy is a factor two. The e + O_2 cross section below 0.1 eV is from microwave measurements and is considered accurate only to order of magnitude; at higher energies it is from beam and swarm experiments and is good generally to ±20 percent. The e + N and e + O cross sections are order-of-magnitude estimates based on total scattering cross sections from electron beam experiments; these cover a more restricted range of electron energy.

For e + He scattering we have used the momentum-transfer cross section recommended by Itikawa (Reference 5), which covers electron energies from 0.01 to 10 eV. This is based on dc swarm experiments and should be accurate to better than 20 percent (Reference 6). This is plotted in Fig. 4-1.

3.2 ELECTRON-ION ELASTIC SCATTERING

We consider electron-ion collisions at low energies, where inelastic processes are not yet important. For electron energies up to 10 eV, we need consider only elastic (coulomb) scattering. For a coulomb force between a singly-charged ion and an electron we use the Rutherford differential scattering cross section (Reference 1)

$$\frac{d\sigma}{d\Omega}(v,\theta) = \frac{e^4}{4\mu^2 v^2} \frac{1}{\sin^4(\theta/2)} \quad . \tag{3-1}$$

---

* For e + NO at 20 eV energy we use 2.95×10^{-7} cm^3/sec instead of Phelps' tabulated value.

The reduced mass is $\mu \approx m_e$, but we have not used this in order to retain the strong advantage of having the results symmetric between ions and electrons. In the Debye approximation the force is assumed zero beyond one Debye shielding length λ_D because the ion charge is shielded by free electrons.

The minimum center-of-mass scattering angle is then (Reference 7, Eqs. 8-34, 8-35)

$$\theta_m = \text{maximum} \left(\frac{2e^2}{\lambda_D \mu v^2} , \frac{h/2\pi}{\lambda_D \mu v} \right) , \tag{3-2}$$

which gives a finite momentum-transfer cross section (from Eq. 2-23),

$$q_D(v) = \frac{4\pi e^4}{\mu^2 v^4} \ln \frac{2}{\theta_m} . \tag{3-3}$$

The weak v-dependence of $\ln(2/\theta_m)$ is ignored by substituting in Eq. 3-2 a typical relative speed,

$$v_t = \sqrt{\frac{3kT_e}{m_e} + \frac{3kT_i}{m_i} + V^2} , \tag{3-4}$$

where T_e and T_i are the electron and ion temperatures and V is the ion-electron macroscopic relative speed, given by Eq. 3-10. We abbreviate the coefficient in the cross section by

$$A = \frac{4\pi e^4}{\mu^2} \ln \frac{2}{\theta_m} , \tag{3-5}$$

$$= 8.06 \times 10^{17} \ln(2/\theta_m) \quad \text{cm}^6/\text{sec}^4 .$$

The factor $\ln(2/\theta_m)$ depends weakly on n_e, T, and V and is plotted for V = 0 in Reference 7, Figure 8-6. In Section 5 we use $\ln(2/\theta_m) = 12$.

This Debye analysis is valid only when a sphere of radius equal to the Debye shielding length contains a statistically large number of electrons (Reference 7, Eq. 8-18).

The coupling coefficient $s_{ie}(T_m,V)$ and heat-transfer coefficient $h_{ie}(T_m,V)$ due to elastic scattering of electrons on ions are calculated by integration from Eqs. 2-33 and 2-34. The integrands involved have removable singularities at $\xi = 0$ and can be integrated by parts. The results can be expressed in terms of the error function,

$$\mathrm{erf}(x) = (2/\sqrt{\pi}) \int_0^x e^{-t^2}\, dt \quad . \tag{3-6}$$

The results are

$$s_{ie}(T_m,V) = \begin{cases} \dfrac{m_i m_e}{(m_i+m_e)} \dfrac{\Lambda}{V^3} \left[\mathrm{erf}\left(\dfrac{V}{U}\right) - \dfrac{2}{\sqrt{\pi}} \dfrac{V}{U} e^{-V^2/U^2} \right] & \text{if } V > 0 \ , \\ \dfrac{4}{3\sqrt{\pi}} \dfrac{m_i m_e}{(m_i+m_e)} \dfrac{\Lambda}{U^3} \ , & \text{if } V = 0 \ , \end{cases} \tag{3-7}$$

$$h_{ie}(T_m,V) = \frac{4}{\sqrt{\pi}} \frac{m_i m_e}{(m_i+m_e)^2} \frac{\Lambda}{U^3} e^{-V^2/U^2} \quad , \tag{3-8}$$

where we have again eliminated the mean temperature T_m in favor of the related thermal speed parameter (Eq. 2-32)

$$U = \sqrt{\frac{2kT_e}{m_e} + \frac{2kT_i}{m_i}} \quad . \tag{3-9}$$

Usually the ion temperature is small compared to $(m_i/m_e)T_e$, so $U \approx (2kT_e/m_e)^{\frac{1}{2}}$. The ion-electron relative velocity is related to the current density by

$$\vec{V} \equiv \vec{V}_i - \vec{V}_e = c\vec{J}/en_e \quad . \tag{3-10}$$

The rates of change due to ion-electron collisions of the momentum and internal energy densities of the ions are given by Eqs. 2-36 and 2-40:

$$\frac{\Delta(\rho_i \vec{V}_i)}{\Delta t} = - n_i n_e \, (\vec{V}_i - \vec{V}_e) \, s_{ie}(T_m, |\vec{V}_i - \vec{V}_e|) \quad , \tag{3-11}$$

$$\frac{\Delta(\rho_i I_i)}{\Delta t} = n_i n_e \left[\frac{m_e}{(m_i + m_e)} \, |\vec{V}_i - V_e|^2 \, s_{ie}(T_m, |\vec{V}_i - \vec{V}_e|) \right.$$
$$\left. + \, k(T_e - T_i) h_{ie}(T_m, |\vec{V}_i - \vec{V}_e|) \right] \quad . \tag{3-12}$$

The rates for electrons are found by interchanging subscripts i and e.

In the static case ($|\vec{V}_i - \vec{V}_e| = 0$), the second term on the right side of Eq. 3-12 is the rate of ion-electron heat transfer; when Eq. 3-8 with 3-5 and 3-9 is substituted this term agrees with the long-known form (Reference 7, Eq. 9-60; Reference 8, Eqs. 5-30, 5-31).

The first term on the right side of Eq. 3-12 is also familiar. In the relation for electron temperature change, which is found from Eq. 3-12 by interchanging subscripts i and e, this term can be considered in the case of a fully ionized plasma with equal temperatures as the electron-ion resistive heating ηJ^2. If $V \ll U$ so that Eq. 3-7b can be substituted, this electron-ion resistivity agrees with the resistivity

η_{lei} in a weak electric field and a strong perpendicular magnetic field, given by Spitzer (Reference 8, Eq. 5-42) and Longmire (Reference 7, Eq. 10-68).

The electron-ion coupling coefficient of Eq. 3-7 is essentially independent of ion mass. It can be identified with the above electron-ion resistivity by

$$s_{ie}(T_e,0) = (e/c)^2 \eta_{lei} \tag{3-13}$$

and has a temperature dependence of $T_e^{-3/2}$. For relative ion-electron speeds $V \ll U$ the heat-transfer coefficient h_{ie} varies as $m_i^{-1} T_e^{-3/2}$. At higher speeds both s_{ie} and h_{ie} decrease; the function in Table 3-1 is useful here.

We have checked one other special case. For a beam of ions impinging on stationary electrons ($T_i = 0$ and $V_e = 0$), Eq. 2-38 with substitutions 2-39, 3-11, 3-12, 3-7a, and 3-8 agrees with Reference 7, Eq. 9-55.

Table 3-1. The function $f(x) = \mathrm{erf}(x) - (2/\sqrt{\pi})xe^{-x^2}$.

x	small	0.2	0.4	0.6	0.8	1.0
f(x)	$(4/3\sqrt{\pi})x^3$	0.00586	0.0438	0.132	0.266	0.428
x	1.2	1.4	1.6	1.8	2.0	2.5
f(x)	0.590	0.730	0.837	0.910	0.954	0.994

3.3 ION-NEUTRAL AND NEUTRAL-NEUTRAL ELASTIC SCATTERING

(a) Low-Energy Limit — the Polarization Force

We consider elastic collisions of singly charged ions with atoms or nonpolar molecules at low energies, below about 0.1 eV in the center-of-mass frame. The dominant long-range force between these particles is the attractive force between the ionic charge +e (or -e) and the electric dipole moment induced by it in the molecule. As long as the separation r between the ion and molecule exceeds 5×10^{-8} cm, their potential energy is that due to this polarization force,

$$\Phi(r) = - \frac{e^2 \alpha}{2r^4} \quad , \tag{3-14}$$

where α is the polarizability of the molecule.

We use a classical theory of this interaction, for the errors caused by a classical treatment seem to be mild (Reference 9). The momentum-transfer cross section is given by (Reference 2, Eq. 5-7-48; Reference 11, pp. 457-458)

$$q_{jj}(v) = 2.210 \pi e \sqrt{\frac{\alpha (m_j + m_k)}{m_j m_k}} \frac{1}{v} \quad . \tag{3-15}$$

This is the polarizability limit of the classical Langevin theory (Reference 12). Table 3-2 gives the polarizabilities of some atmospheric gases, and Figures 4-1 to 4-8 show the related cross sections.

The coupling coefficient $s_{jk}(T_m,V)$ and heat-transfer coefficient $h_{jk}(T_m,V)$ for elastic scattering of ions on molecules by the polarization force are known to be independent of temperature when the gases are static

Table 3-2. Angle-averaged dipole polarizability and electric dipole and quadrupole moments of some atmospheric atoms and molecules in their ground states (Reference 2, Appendix II).

Neutral Molecule	Polarizability α, 10^{-24} cm^3	Dipole moment, 10^{-18} statcoul-cm	Quadrupole moment, 10^{-26} statcoul-cm^2
He	0.205	0	0
N	1.13	0	0
O	0.77	0	0
N_2	1.76	0	-1.52
O_2	1.60	0	-0.39
NO	1.70	0.153	-1.8

(V = 0); this result remains true when the gases are moving. From Eqs. 2-53 and 2-54 the rate coefficients become

$$s_{jk}(T_m,V) = 2.210\,\pi c \sqrt{\frac{\alpha m_j m_k}{(m_j+m_k)}} \quad , \tag{3-16}$$

$$h_{jk}(T_m,V) = \frac{6.631\,\pi e}{(m_1+m_2)} \sqrt{\frac{\alpha m_j m_k}{(m_j+m_k)}} \quad . \tag{3-17}$$

Table 3-3 lists values of these rate coefficients for various ion-molecule pairs.

The NO molecule has a small intrinsic electric dipole moment (see Table 3-2). This dipole moment is essential to e + NO scattering at low energy, as noted in Section 3.1. For scattering of an atomic ion from NO, this dipole moment presumably causes a long-range force whose potential varies

Table 3-3. Coupling coefficient and heat-transfer coefficient due to polarization force for various atmospheric ion-neutral pairs. These are calculated from Equations 3-16 and 3-17.

Ion and neutral	Coupling coefficient, s_{jk}, 10^{-32} gm-cm^3/sec	Heat-transfer coefficient, h_{jk}, 10^{-10} cm^3/sec
$N^+ + N$	1.21	7.80
$O^+ + N$	1.25	7.52
$N_2^+ + N$	1.40	6.00
$NO^+ + N$	1.41	5.80
$N^+ + O$	1.03	6.20
$O^+ + O$	1.07	6.02
$O_2^+ + O$	1.23	4.63
$NO^+ + O$	1.22	4.78
$N^+ + N_2$	1.74	7.49
$O^+ + N_2$	1.82	7.47
$N_2^+ + N_2$	2.13	6.88
$NO^+ + N_2$	2.17	6.75
$N^+ + O_2$	1.70	6.66
$O^+ + O_2$	1.78	6.68
$NO^+ + O_2$	2.14	6.23
$O_2^+ + O_2$	2.17	6.14
$N^+ + NO$	1.73[a]	7.11[a]
$O^+ + NO$	1.81[a]	7.11[a]
$NO^+ + NO$	2.17[a]	6.53[a]
$He^+ + He$	0.275	6.21

[a] Less accurate, because of the intrinsic dipole moment of NO. See text.

with separation like r^{-2}; this potential-energy term also depends on the orientation of the NO molecule. For the polar gas CO, however, measurements of the mobility of alkali ions in CO unexpectedly agree with the prediction based on the polarization force (Reference 13; Reference 10, Section 9-9-F). This agreement may be because the dipole moment of CO is very small (0.11×10^{-18} statcoul-cm) or because the r^{-2} potential energy vanishes when averaged over all orientations (Reference 10, p.446). We will therefore use the polarization-force cross section and rate coefficients for NO, as shown in Figure 4-8 and Table 3-3. We similarly ignore the electric-quadrupole interaction potential (which varies as r^{-3}) between an ion and an N_2 or O_2 molecule.

(b) Scattering Below 20 eV

We consider elastic atom-atom or ion-molecule collisions for center-of-mass kinetic energies below 20 eV. For atmospheric species this implies a relative speed less than 2×10^6 cm/sec and a distance of closest approach of about 1×10^{-8} cm or more.

For two atoms or nonpolar molecules, the interaction potential energy $\Phi(r)$ has an attractive r^{-6} dependence at long range (the London dispersion or induced-dipole-induced-dipole interaction) and a repulsive, approximately exponential dependence on r at short range. We use the Lennard-Jones (12-6) potential, the r^{-12} term being a convenient power-law approximation to the short-range repulsion. For an ion and an atom or nonpolar molecule, the dominant long-range interaction is the attractive r^{-4} polarization potential considered earlier; for this case we use a (12-4) or (12-6-4) potential. We express the potential energy in terms of the depth ϵ of its minimum, the separation r_m at which this minimum energy $-\epsilon$ occurs, and a dimensionless parameter γ measuring the relative strength of the r^{-6} and r^{-4} energies:

$$\Phi(r) = \frac{1}{2}\epsilon\left[(1+\gamma)\left(\frac{r_m}{r}\right)^{12} - 4\gamma\left(\frac{r_m}{r}\right)^{6} - 3(1-\gamma)\left(\frac{r_m}{r}\right)^{4}\right] . \qquad (3\text{-}13)$$

The case of $\gamma = 1$ is the Lennard-Jones (12-6) potential, and that of $\gamma = 0$ is the (12-4) potential.

Table 3-4 shows the assumed form and the parameters of the potential for several pairs of atmospheric species. We have excluded ions in their parent gases because, at room temperature and above, charge exchange dominates; a classical calculation would be dubious and the resulting elastic momentum transfer negligible at energies above 0.03 eV. For ion-neutral interactions we choose one parameter by requiring that the r^{-4} term of Eq. 3-18 match the polarization potential, Eq. 3-14; for example, for $N^+ + O$ we use the polarizability α of O to calculate γ by

$$\gamma = 1 - \frac{e^2\alpha}{3\varepsilon r_m^4} \quad . \tag{3-19}$$

For the bottom three pairs in Table 3-4, Mason (Reference 14) has estimated ion mobilities for the temperature range $0 < kT < 0.22$ eV. The mobility K_o (cm^2/statvolt-sec) at standard density of a species of singly-charged ions in a weak electric field is related to our coupling coefficient s_{jk} for static gases ($V \approx 0$) by (Reference 12, Section 5)

$$s_{jk}(T,0) + s_k^*(T,0) = \frac{e}{n_o K_o(T)} \quad , \tag{3-20}$$

where $n_o = 2.69 \times 10^{19}$ molecules/cm^3 is the density of neutrals at standard conditions (0°C and 1 atm). For the last three systems in Table 3-4 Mason used the mobility of the $H^+ + H_2$ or $NO^+ + N_2$ system as a model and scaled it. An equivalent procedure, which we adopted, is to assume that the potential energy of the system is given by Eq. 3-18 with ε and γ being the same as for Mason's model system and r_m being determined from Eq. 3-19 and the polarizability α of the actual system. Thus, for these

Table 3-4. Characteristics of potential energy functions of pairs of atmospheric species for separations greater than 1×10^{-8} cm.

Colliding pair	Nature of interaction[a]	Form of $\Phi(r)$	ε eV	r_m 10^{-8} cm	γ
N + N	val.	12-6	9.84[c]	1.105[c]	
N + O	val.	12-6	6.64[c]	1.15[c]	
O + O	val.	12-6	5.22[c]	1.22[c]	
He + He	rep.	12-6	0.00088[f]	2.9[f]	
N_2 + N_2	rep.	12-6	0.0074[g]	4.2[g]	
O_2 + O_2	rep.	12-6	0.0086[g]	3.9[g]	
N^+ + O	val.	12-6-4	4.57[c]	1.23[c]	0.65[e]
O^+ + N	val.	12-6-4	10.97[c]	1.06[c]	0.61[e]
N^+ + N_2	val.[b]	12-6-4	~2.7[b,d]	1.83[e]	~0.72[b,d]
O^+ + O_2	val.[b]	12-6-4	~2.7[b,d]	1.79[e]	~0.72[b,d]
O_2^+ + O	rep.[b]	12-4(?)[b]	~0.11[b] 0.32[c]	2.41[e]	

[a] rep. = short-range repulsive force

val. = short-range attractive valence force

[b] Mason, 1970 (Reference 14)

[c] Gilmore, 1972 (Reference 15)

[d] Mason and Vanderslice, 1959 (Reference 16)

[e] Calculated from Eq. 3-19 by using the polarizability of the neutral species in Table 3-2 together with ε and r_m (orγ) from this table. For the (12-4) potential, γ is zero.

[f] Hirschfelder, et al., 1964 (Ref. 20). Kestin and Leidenfrost (Ref. 21) give $r_m = 2.48 \times 10^{-8}$ cm and a larger energy, $\varepsilon = 0.0060$ eV.

[g] Hilsenrath, et al, 1955 (Reference 22)

systems our coupling coefficient $s_{jk}(T_m,V)$ corresponds exactly to Mason's mobility but extends to higher temperature and to nonzero relative gas velocity $V = |\vec{V}_n - \vec{V}_i|$.

For $O_2^+ + O$, Mason made an educated guess that the short-range force is repulsive. The dissociation energy given by Gilmore (Reference 15), $O_3^+ \rightarrow O_2^+ + O - 0.32$ eV, supports this assumption. Mason also estimated the mobility of $NO^+ + O$ based on a short-range repulsive force, but this assumption appears wrong in view of Gilmore's dissociation energy, $NO_2^+ \rightarrow NO^+ + O - 2.60$ eV.

The momentum-transfer cross section for a (12-6-4) potential has been tabulated in the dimensionless form $q_D(V)/\pi r_m^2$ as a function of $\frac{1}{2}\mu V^2/\epsilon$ and the parameter γ (References 17, 18). Figures 4-2 to 4-8 show plots of the cross sections q_D that are found by interpolation from this table. In Section 5 the rate coefficients $s_{jk}(T_m,V)$ and $h_{jk}(T_m,V)$ for elastic scattering are found by integration from Eqs. 2-33 and 2-34; they are plotted in Figures 5-1 and 5-3. An alternate method, which we used as a check, is to find $s(T_m,0)$ by interpolation from the tabulated collision integral $\bar{\Omega}^{(1,1)}(T)$ in Reference 17 together with the relation (see Reference 2, p.139)

$$s_{jk}(T,0) = \frac{8}{3\sqrt{\pi}} \left(\frac{2m_j m_k kT}{(m_j+m_k)} \right)^{1/2} \bar{\Omega}^{(1,1)}(T) \quad . \tag{3-21}$$

For $O_2^+ + O$, for which the nature of the interaction is less certain, the estimated uncertainty in s (or K_o) is a factor of two (Reference 14) for temperatures up to 0.22 eV and an order of magnitude at high temperatures. For $N^+ + N_2$ and $O^+ + O_2$ we feel that the uncertainty should be a factor of two over the whole temperature range, and for the first five systems in Table 3-4 we estimate ±30% uncertainty.

(c) Scattering from 50 to 30000 eV

In ion-atom encounters at center-of-mass energies above 200 eV elastic scattering is exceeded by charge exchange (see Figures 4-1 to 4-8). These charge-exchange encounters cause very little momentum transfer between the fast particles and the slow ones. The slowing down of the fast particles is most likely brought about by atom-atom scattering. We have therefore concentrated on atom-atom scattering rather than ion-atom scattering in this energy range.

We use a two-atom Thomas-Fermi interaction potential with a scaling rule for unlike atoms (Reference 19). The range of validity of the treatment is restricted at the lower end to energies much greater than molecular binding energies, say center-of-mass kinetic energies above 50 eV. At the upper end inelastic scattering involving excitation and ionization overtakes elastic scattering at a speed around 10^8 cm/sec (see Appendix C and Figure 4-6).

The colliding pair is described simply by the atomic numbers Z_1 and Z_2. The scales for distance and energy are

$$\lambda = \frac{1}{2}\left(\frac{3\pi}{4}\right)^{2/3}\left(\frac{2}{\sqrt{Z_1}+\sqrt{Z_2}}\right)^{2/3} a_o \qquad (3\text{-}22)$$

$$= 0.469 \times 10^{-8}\left(\frac{2}{\sqrt{Z_1}+\sqrt{Z_2}}\right)^{2/3} \text{cm} \quad ,$$

and

$$\varepsilon_o = e^2 Z_1 Z_2/\lambda \qquad (3\text{-}23)$$

$$= 0.0307\ Z_1 Z_2 \left(\frac{\sqrt{Z_1}+\sqrt{Z_2}}{2}\right)^{2/3} \text{keV}.$$

The scaled center-of-mass kinetic energy of the colliding particles is denoted by

$$W = \frac{1}{2}\mu v^2/\varepsilon_o \quad , \tag{3-24}$$

and the momentum-transfer cross section is given in the dimensionless form $F(W)$ in Table 3-5, which is taken from Table 2 of Reference 19:

$$q_D(v) = \lambda^2 F(W). \tag{3-25}$$

At intermediate energies we use log-log interpolation in the table, and at the high-energy end we extrapolate by

$$F(W) = 0.066(10/W)^{3/2} \qquad \text{if} \quad W > 10. \tag{3-26}$$

These cross sections for $H_e + H_e$, N + N, O + O, and N + O are shown in Figures 4-1, 4-2, 4-3, and 4-5, respectively; these are believed to be accurate to better than a factor 2 (Reference 19). For atom-molecule collisions such as $O + O_2$ we have simply added the appropriate atom-atom scattering cross sections (Figures 4-6 to 4-8).

Collisions of singly charged ions with atoms are more complicated than atom-atom collisions because one should take into account charge exchange. This is not done in the classical scattering calculation used here for atom-atom cross sections. For a rough estimate one might take the ion-neutral scattering cross section to equal the corresponding neutral-neutral one; we do this in Section 5 in extending the rate coefficients s_{jk} and h_{jk} to temperatures above 50 eV.

Table 3-5. The function $F(W) = q_D(v)/\lambda^2$ (Reference 19, Table 2).

W	F(W)	W	F(W)
0.005	110.	0.3	5.28
0.010	70.	1.	1.46
0.025	37.	3.	0.367
0.05	22.6	10.	0.066
0.1	13.4	>10.	$0.066\times(10/W)^{3/2}$

SECTION 4
CHARGE-EXCHANGE CROSS SECTIONS FOR ATMOSPHERIC SPECIES

1.1 INTRODUCTION

We consider symmetric charge exchange of six positive ions:

$$He^+ + He \rightarrow He + He^+ , \quad (4\text{-}1)$$

$$N^+ + N \rightarrow N + N^+ , \quad (4\text{-}2)$$

$$O^+ + O \rightarrow O + O^+ , \quad (4\text{-}3)$$

$$N_2^+ + N_2 \rightarrow N_2 + N_2^+ , \quad (4\text{-}4)$$

$$NO^+ + NO \rightarrow NO + NO^+ , \quad (4\text{-}5)$$

$$O_2^+ + O_2 \rightarrow O_2 + O_2^+ , \quad (4\text{-}6)$$

and eight asymmetric charge-exchange reactions:

$$N^+ + O \rightarrow N + O^+ + 0.92 \text{ eV} , \quad (4\text{-}7)$$

$$N^+ + N_2 \rightarrow N + N_2^+ - 1.05 \text{ eV} , \quad (4\text{-}8)$$

$$N_2^+ + N \rightarrow N_2 + N^+ + 1.05 \text{ eV} , \quad (4\text{-}9)$$

$$O^+(^4S) + O_2 \rightarrow O + O_2^+ + 1.56 \text{ eV} , \quad (4\text{-}10)$$

$$O^+(^2D) + O_2 \rightarrow O + O_2^+ + 4.88 \text{ eV} , \quad (4\text{-}11)$$

$$O_2^+ + O \rightarrow O_2 + O^+ - 1.56 \text{ eV} , \quad (4\text{-}12)$$

$$N^+ + NO \rightarrow N + NO^+ + 5.27 \text{ eV} , \quad (4\text{-}13)$$

$$O^+(^4S) + NO \rightarrow O + NO^+ + 4.35 \text{ eV} , \quad (4\text{-}14)$$

$$O^+(^2D) + NO \rightarrow O + NO^+ + 7.68 \text{ eV} , \quad (4\text{-}15)$$

$$N^+ + U \rightarrow N + U^+ + 8.4 \text{ eV} , \quad (4\text{-}16)$$

$$O^+ + U \rightarrow O + U^+ + 7.5 \text{ eV} . \quad (4\text{-}17)$$

For three other asymmetric reactions we have searched the literature but found no reliable cross section:

$$O^+ + N \rightarrow O + N^+ - 0.92 \text{ eV} , \quad (4\text{-}18)$$

$$NO^+ + N \rightarrow NO + N^+ - 5.27 \text{ eV} , \quad (4\text{-}19)$$

$$NO^+ + O \rightarrow NO + O^+ - 4.35 \text{ eV} . \quad (4\text{-}20)$$

Ground-state reactants are emphasized; information on the states of the reactants is included where available. The products of the asymmetric reactions are likely to be excited, and all states are included. The energy excesses shown are only limits because they are calculated by assuming that the products as well as the reactants are in their ground states.

We have searched the literature through November 1974 for measured cross sections. Where experimental data is available we have relied on it rather than on theoretical calculations.

Tables 4-1a to 4-1k list the studies selected. The first column includes the name of the first author and the publication date. The second column gives the experimental technique and the particle detection method, where important, as follows:

- FA flowing afterglow
- SA stationary afterglow
- DT drift tube
- FDT flowing-afterglow drift tube
- ICR ion cyclotron resonance
- HPMS high-pressure mass spectrometer ion source, operated in the many-collision pressure regime
- B beam in gas cell, operated in the single-collision pressure regime
- Eq beam in gas cell, equilibrium method, fast-particle detection
- CB crossed beams
- MB merging beams, including magnetic analysis of products
- f detection of fast particles
- s detection of slow particles. If the energy of the primary ions in a beam experiment exceeds 10^5 eV, the slow product ions include many that are produced by ion-impact ionization. Also, if the energy of the primary ions is very low, the slow ions include elastically scattered primary ions.
- m product ions analyzed by a mass spectrometer
- i reactants isotopically labeled.

Another column gives the range of ion energy for which a cross section is measured. If the author used center-of-mass energy $E_{cm} = (m_1 m_2/(m_1+m_2))v^2/2$, this range is given in brackets. Where a temperature range is given, the measured quantity is indicated under Remarks; it is either the ion mobility

(see Eq. 3-20) in the case of ions in their parent gas or the rate coefficient in the case of asymmetric charge exchange.

4.2 SYMMETRIC CHARGE EXCHANGE

$He^+ + He \rightarrow He + He^+$: We selected the investigations in Table 4-1a. Reference 26 is a study of $^3He^+ + {}^4He \rightarrow {}^3He + {}^4He^+$, which is not strictly symmetric, but the difference between the ionization energies of ^3He and ^4He is assumed to be too small to affect the resonance character of the charge exchange. References 28 to 40 agree well and provide a cross section down to ion energy 4 eV, which is shown in Figure 4-1. For convenience Figures 4-1 to 4-8 are placed together at the end of Section 4, immediately preceded by the notes on these figures.

For $1.1 \times 10^5 < v < 2.3 \times 10^5$ cm/sec we use the mobility measurements of Reference 25 together with Eqs. 3-20, 2-33b, and 2-43 to obtain an empirical power-law fit to* $q_D(v) + 2\,\sigma_x(v)$:

$$q_D(v) + 2\,\sigma_x(v) = 92 \times 10^{-16}\ \text{cm}^2\ (v/1.58 \times 10^5\ \text{cm/sec})^{-0.56} \quad . \tag{4-21}$$

At these low energies there is no experimental data on how to separate this into $q_D(v)$ and $\sigma_x(v)$ individually; we separate them arbitrarily by taking the elastic scattering $q_D(v)$ to be given by its polarization limit, Eq. 3-15. For ion energies below 1 eV this charge-exchange cross section $\sigma_x(v)$ is dotted in Figure 4-1 as a reminder that it was chosen merely to make the total, $q_D(v) + 2\,\sigma_x(v)$, consistent with measurements.

---

* Strictly one obtains a fit to the quantity

$$q_D(v) + \int_{4\pi} (1 + \cos\theta)\, \frac{d\sigma_x}{d\Omega}\, d\Omega \quad ,$$

which is the $Q^{(1)}$ of Reference 2, Eq. 5-7-1.

Table 4-1a. Studies of the cross section for $He^+ + He \rightarrow He + He^+$.

Reference	Technique	Ion Energies	Remarks
23 (Heiche, 1970)	theory	$[2\times10^{-5}<E_{cm}<4$ eV]	
24 (Dickinson, 1968)	theory	$[0.0037<E_{cm}<0.13$ eV]	
25 (Orient, 1967)	DT	[190°<T<650°K]	Ion Mobility
26 (Smith, 1974)	ICR,i	$[0.1<E_{cm}<20$ eV]	Used $^3He^+ + {}^4He$
27 (Mahadevan, 1968)	B,s	1 to 75 eV	
28 (Cramer, 1957)	B,s	4 to 400 eV	
29 (Belyaev, 1968)	ME	$[7<E_{cm}<100$ eV]	
30 (Hayden, 1964)	B,s	50 to 1000 eV	
31 (Ghosh, 1957)	B,s	100 to 800 eV	
32 (Nagy, 1969)	B,s	400 to 2000 eV	
33 (Shelton, 1971)	B,s	2 to 20 keV	
34 (Stedeford, 1955)	B,s	2 to 40 keV	
35 (Barnett, 1958)	Eq	8 to 200 keV	
36 (DeHeer, 1966)	B,s	10 to 140 keV	
37 (Fedorenko, 1956)	B,s	13 to 180 keV	
38 (Jones, 1959)	B,f,m	25 to 100 keV	
39 (Allison, 1956)	B,f	100 to 450 keV	
40 (Nikolaev, 1961)	B,f,m	320 to 1300 keV	

$N^+ + N \rightarrow N + N^+$: We use the only known measurement (Reference 29) and extrapolate in both directions by following the shape of the Rapp and Francis theoretical curve (Reference 41). See Table 4-1b and Figure 4-2. Above 30 keV ion energy we estimate the cross section from measurements by Fite's group on the charge exchange of $N^+ + N_2$ and $O^+ + O_2$ (Reference 73) and of $O^+ + O$ (Reference 44); at a given speed our estimate is

$$\sigma_x(N^+ + N) \approx \sigma_x(N^+ + N_2) \frac{\sigma_x(O^+ + O)}{\sigma_x(O^+ + O_2)} \quad . \tag{4-22}$$

Table 4-1b. Studies of the cross section for $N^+ + N \rightarrow N + N^+$

Reference	Technique	Energy Range
29 (Belyaev, 1968)	MB	$7 < E_{cm} < 100$ eV
41 (Rapp, 1962)	Theory	$0.005 < E_{cm} < 35000$ eV

$O^+ + O \rightarrow O + O^+$: The agreement among the measurements in Table 4-1c is very good, and the result is shown in Figure 4-3. We have again extrapolated down to 0.3 eV ion energy by following the shape of the theoretical cross section of Reference 41.

Oxygen atoms formed by thermal dissociation of O_2 are in the ground state, while those produced by an rf discharge are likely to include excited atoms. For the resonant reaction 4-3 one would not expect the presence of excited states to influence the cross section greatly

Table 4-1c. Studies of the cross section for $O^+ + O \rightarrow O + O^+$.

Reference	Technique	Production of O atoms	Ion Energies
42 (Stebbings, 1964)	CB,s,m	rf discharge	40 to 10000 eV
43 (Rutherford, 1974)	CB,s,m	thermal dissoc.	60 to 500 eV
44 (Lo, 1969)	B,f,m	thermal dissoc.	30 to 2000 keV

$N_2^+ + N_2 \rightarrow N_2 + N_2^+$: We selected fifteen sources of experimental cross sections, as listed in Table 4-1d. Discrepancies among these cross sections are partly due to differences in the distribution of electronic and vibrational states of the primary N_2^+. In all of the beam experiments in this table except Reference 31 the primary N_2^+ ions were produced by electron impact on N_2; the electron energy is in the third column. Four investigators (References 52, 54, 57 and 58) studied the effect of changing the distribution of states of the primary N_2^+ by varying this electron energy. They find that changing the electron energy from 16 or 18 eV to high energies (25 to 90 eV) decreases the cross section somewhat. The largest decrease measured was a factor 1.35.

Maier (Reference 52) has calculated the initial distribution of electronic and vibrational states of N_2^+ for three electron-impact energies. Of the known electronic states only $N_2^+(A^2\Pi_u)$ is sufficiently populated and has a long enough lifetime to affect the measured cross sections. The cross sections for $N_2^+(A^2\Pi_u)$ ions in various vibrational levels to charge-transfer with ground-state N_2 are estimated theoretically to be significantly smaller than the cross sections for ground-state $N_2^+(^2\Sigma_g^+)$ reacting with ground-state N_2 (Reference 58, p. 5506). The lifetimes of the vibrational levels of the $A^2\Pi_u$ state (Reference 52, Table II) are comparable to the elapsed time between formation and reaction

Table 4-1d. Studies of the cross section for $N_2^+ + N_2 \rightarrow N_2 + N_2^+$.

Reference	Technique	Electron Energy	Ion Energies	Remarks
45 (Moseley, 1969)	DT,m		[T=300°K]	Ion Mobility
46 (Huntress, 1971)	ICR		[300°<T_i<500°K]	Note b
47 (Kobayashi, 1975)	DT,m		[0.05<E_{cm}<2.5 eV]	
48 (Tiernan)	B,i	not known	~0.3 eV	
49 (Nichols, 1966)	B,s	95 eV	0.5 to 17 eV	
50 (Leventhal, 1967)	B,s,m,i	50 to 70 eV	1 to 50 eV	
51 (Stebbings, 1963)	CB,s	~90 eV	15 to 5000 eV	
52 (Maier, 1974)	B,s,m,i	19.2 eV[a]	20 to 45 eV	
53 (Gustafsson, 1960)	B,s,m	high, ~70 eV	50 to 900 eV	
54 (Amme, 1964)	B,s	21.5 eV[a]	50 to 1000 eV	
31 (Ghosh, 1957)	B,s	rf discharge	100 to 800 eV	
55 (Savage, 1968)	MB	30 to 50 eV	100 to 1000 eV	
56 (Neff, 1964)	B,s	not stated	190 to 3000 eV	
57 (McGowan, 1964)	B,f	55 eV[a]	600 to 2000 eV	
58 (Flannery, 1973)	B,f	Note a	750 to 2200 eV	Note c

[a] The electron energy was varied to study the effect of changes in the distribution of states of the primary N_2^+ ions.

[b] The quantity plotted in Huntress's Figure 3 is $k = \bar{\xi}/n$, where $\bar{\xi}$ is the velocity average of the (momentum-transfer) collision frequency and n is the number density of N_2. This is related to the reduced mobility K_0 by Huntress's Eq. 24, and our Eq. 3-20 then gives $s_{jk} + s_k^* = m_k k$. The abscissa of Fig. 3 is the ion kinetic temperature T_i; the temperature of the neutrals we take to be $T_n = 293$ °K.

[c] Gives only relative cross sections as a function of electron energy.

of the N_2^+ in various beam experiments. This latter time depends on ion energy and is not stated for most of the beam experiments in Table 4-1d. Thus one can find only an upper limit to the fractional population of the $A^2\Pi_u$ state in the incident N_2^+ beam.

We have not attempted to adjust the measured cross sections to refer to a given distribution of states, such as a pure beam of ground-state N_2^+ ions. The discrepancies due to different distributions of states in the primary N_2^+ seem to be no larger than the discrepancies due to unknown other sources. For example, at an ion energy around 50 eV the cross sections from Table 4-1d differ by factors up to 2.0, and the smallest (Reference 52) and largest (Reference 54) are from experiments that used similar low electron energy.

Figure 4-4 shows our recommended cross section. The extension to ion energies above 5000 eV is an extrapolation.

For $5.9 \times 10^4 < v < 7 \times 10^7$ cm/sec we use the dc and ac mobility measurements of References 45 and 46 together with Eqs. 3-20, 2-33b, 2-21, and 2-43 to obtain an empirical power-law fit to $q_D(v) + 2\,\sigma_x(v)$:

$$q_D(v) + 2\,\sigma_x(v) = 1.6 \times 10^{-14}\ \text{cm}^2\ (v/5.97 \times 10^4\ \text{cm/sec})^{-0.1}. \tag{4-23}$$

We calculated σ_x below 1 eV by the same arbitrary separation procedure that is described above for $He^+ + He \rightarrow He + He^+$, and the same remarks apply.

$O_2^+ + O_2 \rightarrow O_2 + O_2^+$: The seven references in Table 4-1e show no serious discrepancies. The $O_2^+ + O_2$ measurements of Reference 47 were published after Figure 4-4 was completed, but only small adjustments

Table 4-1e. Studies of the cross section for $O_2^+ + O_2 \rightarrow O_2 + O_2^+$.

Reference	Technique	Ion Energies	Remarks
59 (Snuggs, 1971)	DT,m	[T = 300 °K]	Ion Mobility
47 (Kobayashi, 1975)	DT,m	[0.045 < E_{cm} < 2.8 eV]	
60 (Varney, 1970)	DT,m	~0.2 eV	
48 (Tiernan)	B,i	~0.3 eV	
51 (Stebbings, 1963)	CB,s	25 to 6500 eV	
61 (Ghosh, 1957)	B,s	100 to 800 eV	
54 (Anme, 1964)	B,s	100 to 1000 eV	

are indicated for speeds above 2×10^5 cm/sec. Below 1 eV ion energy we used the mobility measurement of Reference 59 and followed the same procedure described for $He^+ + He$ amd $N_2^+ + N_2$. The result is more uncertain in this case because the temperature dependence of the mobility was not measured and must be estimated.

Two investigators (References 62 and 54) have studied the effect of changing the distribution of states of the primary O_2^+ by varying the electron energy used in producing the O_2^+ by electron-impact ionization. Compared to the accuracy of the measurements, this effect is unimportant.

$NO^+ + NO \rightarrow NO + NO^+$: The cross sections from Table 4-1f are considerably more uncertain than for the other cases of symmetric charge exchange considered in this study. One cause is the presence of excited states in the primary NO^+ ions (References 51 and 62). For primary NO^+

Table 4-1f. Studies of the cross section for $NO^+ + NO \rightarrow NO + NO^+$.

Reference	Technique	Ion Energies	Remarks
63 (Volz, 1971)	DT,m	[T = 300 °K]	Ion Mobility
64 (Henglein, 1962)	B,s,m	5-40 eV	
51 (Stebbings, 1963)	CB,s,m	25 to 4000 eV	
61 (Ghosh, 1957)	B,s	100 to 800 eV	
62 (Moran, 1974)	B,f	400 to 1200 eV	Note a

[a] Gives only relative cross sections as a function of electron energy.

ions produced by electron-impact ionization, varying the electron energy from 9 to above 30 eV increases the cross section by a factor 1.5 at ion energy 400 eV (Reference 62); this effect is opposite to that for $N_2^+ + N_2$ mentioned above.

4.3 ASYMMETRIC CHARGE EXCHANGE

$\underline{N^+ + O \rightarrow N + O^+}$: From the sources in Table 4-1g we put together the cross section in Figure 4-5. The two arrows above this curve are measured upper limits. In References 43 and 67 the O atoms are known to be in the ground state because they are formed by thermal dissociation. The cross section for reaction with the metastable $N^+(^1D)$ ion,

$$N^+(^1D) + O \rightarrow N + O^+ \quad , \tag{4-24}$$

is reported to be not large compared to that for ground-state N^+ ions, even at ion energies as low as 5 eV (Reference 43).

Table 4-1g. Studies of the cross section for $N^+ + O \rightarrow N + O^+$.

Reference	Technique	Production of O atoms	Ion Energies	Remarks
65 (Bortner, 1973)	not stated		not stated [a]	Estimate of rate coeff.
66 (Neynaber)	MB	charge transfer	0.19 eV	Upper limit, $\sigma_x < 10^{-17} cm^2$
43 (Rutherford, 1974)	CB,s,m	thermal dissoc.	5 eV 400 eV	Upper limit
67 (Lo, 1970)	B,f,m?	thermal dissoc.	30 to 2000 keV	

[a] We have assumed that the estimate applies for $200° < T < 700$ °K.

$N^+ + U \rightarrow N + U^+$ and $O^+ + U \rightarrow O + U^+$: Also shown in Figure 4-5 are 1974 results of crossed-beam experiments of Neynaber, Rutherford, and Vroom (Reference 68).

$N^+ + N_2 \rightarrow N + N_2^+$: In the detailed low-energy study of Maier and Murad (Reference 69) the reactants were isotopically labeled and the kinetic energies of the product N_2^+ were determined. They conclude that this reaction proceeds by both atom and electron transfer. For ion energies below 16 eV the cross sections for electron and atom transfer are roughly equal, but at higher energy the cross section for electron transfer is dominant. Also the kinetic energy transferred into internal energy of the products is considerably larger than the minimum of 1.05 eV required for this reaction to occur; it increases from 3.2 to 10 eV as the center-of-mass kinetic energy increases from 4 to 50 eV.

The effect of excited states of N^+ has been studied in References 71 and 53. Neynaber et al. (Reference 71) conclude that the cross section for the reaction

$$N^+(^1D) + N_2 \rightarrow N + N_2^+ \qquad (4\text{-}25)$$

is expected to be, and is observed to be, small. (They used ion energies of ~10 to 500 eV.) McGowan and Kerwin (Reference 53) report only a small increase (~20 percent) in the cross section as the electron energy used to produce the N^+ ions is varied.

The differences among the three cross sections presented in References 69 and 70 are a factor of 2 to 4, and when those of References 51 and 53 are considered, the discrepancies are far larger. See Table 4-1h. Maier and Murad (Reference 69) discuss the differences and recommend that the cross section of Reference 70 be preferred when the primary N^+ ions are produced by electron impact on low-pressure N_2. We adopt the cross section of Reference 70 for ion energies up to 500 eV.

At high energies the agreement between References 72, 73 and 40 is good. (Note that in References 40 and 72 the cross sections are given in cm^2/atom instead of cm^2/molecule as used in Figure 4-6). For these energies the cross sections refer to the reaction

$$N^+ + N_2 \rightarrow N + \text{slow products} \quad . \qquad (4\text{-}26)$$

Figure 4-6 shows the recommended cross section, in which these high-energy results are joined to that of Reference 70 by a smooth dotted curve.

Table 4-1h. Studies of the cross section for $N^+ + N_2 \rightarrow N + N_2^+$.

Reference	Technique	Ion Energies
69 (Maier, 1971)	B,s,m,i	3 to 50 eV
	B,s,m	1.5 to 100 eV
70 (Neynaber, 1971)	CB,s,m	1.5 to 500 eV
51 (Stebbings, 1963)	CB,s	20 to 5000 eV
53 (Gustafsson, 1960)	B,s,m	25 to 900 eV
57 (McGowan, 1964)	B,f	2000 eV
72 (Ormrod, 1971)	B,f,m	15 to 70 keV
73 (Brackmann, 1968)	B,f,m	30 to 1300 keV
40 (Nikolaev, 1961)	B,f,m	500 to 2400 keV

$N_2^+ + N \rightarrow N_2 + N^+$: Kretschmer and Petersen (Reference 74) have measured the rate coefficient at 300 °K temperature by an indirect technique using Langmuir probes. Their rate coefficient, 1.4×10^{-13} cm^3/sec, is much lower than the upper limit determined by the afterglow experiments of Ferguson et al. (Reference 75). The result of Reference 74 is shown as a point on Figure 4-6.

$O^+ + O_2 \rightarrow O + O_2^+$: The cross sections for ground-state $O^+(^4S)$ and for metastable $O^+(^2D)$ have been measured separately in three beam experiments (References 48, 68, and 85; see Table 4-1i). Their results are consistent, and we have shown a separate cross section for $O^+(^2D) + O_2$ in Figure 4-7.

Table 4-li. Studies of the cross section for $O^+ + O_2 \rightarrow O + O_2^+$.

Reference	Technique	Ion Energies	Remarks
76 (Dunkin, 1968) 77 (Ferguson, 1969)	FA	[80°<T<600°K]	Rate Coefficient
78 (Smith, 1968) 79 (Copsey, 1966)	SA	[180°<T<600°K]	Rate Coefficient
80 (Lindinger, 1974)	FA	[300°<T<800°K]	Rate Coefficient
81 (Warneck, 1967)	HPMS	[700°<T_i<1100°K][a]	Rate Coefficient
82 (Pharo, 1971)	ionospheric	[T = 900°K]	Rate Coefficient
83 (Johnsen, 1973)	DT,m	300°K to 2 eV	
84 (McFarland, 1973)	FDT,m	[0.05<E_{cm}<3.2 eV]	
48 (Tiernan)	B	~ 0.3 eV	Also $O^+(^2D)+O_2$
68 (Neynaber, 1974)	CB,s,m	4 to 500 eV	Also $O^+(^2D)+O_2$
85 (Stebbings, 1966)	CB,s,m	10 to 100 eV	Also $O^{+*}+O_2$
57 (McGowan, 1964)	B,f	1.6 keV	
86 (Turner, 1969)	B	8 to 60 keV	
87 (Solov'ev, 1972)	B,f,m	28 to 180 keV	
73 (Brackmann, 1968)	B,f,m	30 to 2000 keV	

[a] To compare to other temperatures in this column one must calculate the temperature T_m (Eq. 2-21 or 2-47) characterizing the distribution of relative velocities of $O^+ - O_2$ pairs. For an O_2 temperature of 300°K the range of this temperature is 600°<T_m<800°K.

The drift-tube measurements are believed to refer to ground-state $O^+(^4S)$ ions (Reference 83), and we have assumed the same for the afterglow experiments. The temperature-dependent rate coefficients have been used to estimate charge-exchange cross sections $\sigma_x(v)$ by using Eq. B-11b to obtain an empirical power-law fit to $\sigma_x(v)$. Some of the recent measurements (References 80, 82, and 48) indicate a lower cross section at low energies than do References 76 to 79, 81, and 83; the discrepancy is nearly a factor of 2 in the range $1 \times 10^5 < v < 2 \times 10^5$ cm/sec. We choose an intermediate cross section here and indicate the conflict by a dashed line in Figure 4-7.

At intermediate energies we follow the cross section of Noynaber et al. (Reference 68). At high energies References 87 and 73 agree well and we have followed the latter. For these energies the cross sections refer to the reaction

$$O^+ + O_2 \rightarrow O + \text{slow products} \quad . \tag{4-27}$$

In Figure 4-7 this high-energy curve is connected to that of Reference 68 by a smooth dotted curve.

$O_2^+ + O \rightarrow O^+ + O_2$: The only measurement is the crossed-beams experiment of Stebbings et al. (Reference 88), covering ion energies from 70 to 6000 eV. This measurement is probably strongly affected by the presence of excited atoms and excited ions in the incident beams. To estimate the cross section for ground-state reactants we compared measurements of Reference 88 to those of Reference 43 for two similar charge-exchange reactions, those for $N_2^+ + O$ and $N^+ + O$ (reaction 4-7). In Reference 43, where the reactant O atoms are in the ground state and the ions are produced by impact of lower energy electrons, these two cross sections are smaller than those of Reference 88 by a factor of about 6. For our estimate of the cross section for $O_2^+ + O$, we divided the cross section of Reference 88 by 6 (and at 2 keV ion energy by a more conservative factor of 3). Figure 4-7 shows the result, which covers only the range $v < 2 \times 10^7$ cm/sec.

$N^+ + NO \rightarrow N + NO^+$: Rutherford (Reference 91) has extended the crossed-beams measurements of Turner (Reference 92) down to 1 eV ion energy; the cross section remains nearly constant at $\sigma_x \approx 1.5 \times 10^{-16}$ cm^2. At room temperature, however, the flowing afterglow measurement (Reference 89) indicates a cross section of about 100×10^{-16} cm^2 for $v \approx 7 \times 10^4$ cm/sec. Between room temperature and 1 eV are the measurements of References 90 and 48 at two well-placed energies. It is unfortunate that the range of ion temperature or mean ion energy used for this reaction by Warneck (Reference 90) is not stated more precisely, but his measurement is nonetheless significant. The cross sections from the four experiments mentioned so far (the first four in Table 4-1j) decrease monotonically as the energy is increased to 1 eV. Taken together, they support the steep drop in cross section shown in Figure 4-8.

It is not known whether atom transfer, as opposed to electron transfer, is important at low energies (Reference 89). The effect of excited states of N^+ was studied in Reference 92 by varying the energy of the electrons used to produce the N^+; the cross section is relatively insensitive to electron energy.

At high energies we average the charge-exchange cross sections of Reference 73 for $N^+ + N_2$ (reaction 4-8) and for $N^+ + O_2$. Figure 4-8 shows our recommended cross section, which covers the range $6 \times 10^4 < v < 5 \times 10^8$ cm/sec. (At high energies this curve is indistinguishable from that for $O^+ + NO$).

$O^+ + NO \rightarrow O + NO^+$: Both beam experiments in Table 4-1k have measured separately the cross sections for ground-state $O^+(^4S)$ and for metastable $O^+(^2D)$, and the results of Reference 48 are consistent with extrapolations of the results of Reference 68. At the lowest ion energies in these experiments (0.3 and 1.5 eV), however, even the measurements for ground-state O^+ exceed the flow-drift tube result (Reference 93) by a

Table 4-1j. Studies of the cross section for $N^+ + NO \rightarrow N + NO^+$.

Reference	Technique	Ion Energies	Remarks
89 (Goldan, 1966)	FA	[T≈300°K]	Rate Coefficient
90 (Warneck, 1967)	HPMS or LPMS	Note a	Rate Coefficient
48 (Tiernan)	B,i	~0.3 eV	
91 (Rutherford)	CB,s,m	1 to ≥5 eV	
92 (Turner, 1966)	CB,s,m	5 to 200 eV	

a
The ion temperature range for the group of rate coefficients summarized in Ref. 90 is $400°<T_i<2000°K$, but each individual reaction was studied only over part of this range. See footnote to Table 4-1i.

Table 4-1k. Studies of the cross section for $O^+ + NO \rightarrow O + NO^+$.

Reference	Technique	Ion Energies	Remarks
93 (McFarland, 1974)	FDT,m	[T=280°K] [$0.22<E_{cm}<4$ eV]	Upper limit for rate coefficient
48 (Tiernan)	B	~0.3 eV	Also $O^+(^2D)+NO$
68 (Neynaber, 1974)	CB,s,m	1.5 to 500 eV	Also $O^+(^2D)+NO$

factor of 3 or more. Being unable to resolve this discrepancy we give an intermediate cross section for $O^+(^4S) + O_2$ at these energies and indicate the decreased accuracy by a dotted line in Figure 4-8. Above 30 keV we have averaged the charge-exchange cross sections of Reference 73 for $O^+ + N_2$ and $O^+ + O_2$ (reaction 4-10).

$O^+ + N \rightarrow O + N^+$ and $NO^+ + N \rightarrow NO + N^+$: Our literature search reveals no measurement of the cross section for either of these reactions. For ground-state reactants the endothermicities are 0.92 and 5.27 eV, respectively, giving threshold speeds of 4.9×10^5 and 1.0×10^6 cm/sec.

$NO^+ + O \rightarrow NO + O^+$: For ground-state reactants this reaction has an endothermicity of 4.35 eV, giving it a threshold speed of 9.0×10^5 cm/sec. The only known measurement of the cross section (Reference 88) is probably strongly affected by the presence of excited states in the beams. Our rough estimate is that, for speeds above the threshold, the cross section equals that discussed above for $O_2^+ + O$. The measurements of Reference 88, which include both these cross sections for ion energies from 70 to 6000 eV, are consistent with our estimate within experimental uncertainty.

Notes to Figures 4-1 to 4-8: The six cross sections for symmetric charge exchange (Figures 4-1 to 4-4) and the eleven for asymmetric charge exchange (Figures 4-5 to 4-8) are described above in Section 4. These charge-exchange cross sections are recommended values based on a literature search, and they lean heavily on experimental rather than theoretical cross sections. They are plotted in the form of effective momentum-transfer cross sections, $q^*(v)$ or $q_T(v)$ (Eq. 2-43 or B-31). The cross sections are intended to refer to ground-state reactants within the stated accuracy; comments about the states of the reactants in the experiments have been included above. For symmetric charge exchange the recommended cross sections are also tabulated in Table 4-2.

Also shown on Figures 4-1 to 4-8 are momentum-transfer cross sections for elastic scattering $q_D(v)$. For center-of-mass energies below 20 eV these are calculated from Eq. 3-15 and Table 3-2 or are described in Section 3.3b. For high energies up to $v \sim 10^8$ cm/sec the cross sections are described in Section 3.3c. In Figures 4-5 to 4-7 we have interpolated a dotted line to join the low and high energy portions of $q_D(v)$. At the highest energies $q_D(v)$ is extrapolated by a straight dotted line, $q_D(v) \propto v^{-3}$.

The momentum-transfer cross sections for inelastic scattering $q_{inel}(v)$ are calculated from Eq. C-8 and Table C-1. Symbols are defined in the Glossary in Appendix A.

The weight of a line is an indication of accuracy. A solid line indicates an accuracy within ±30 percent, a dashed line has an accuracy of roughly a factor of two, and a dotted line is for order-of-magnitude accuracy. There are two kinds of dashed lines having the same meaning; both have dashes three times as long as the intervening spaces. Similarly the dotted lines and very short dashes, which are only as long as the

Table 4-2. Total cross sections for symmetric charge exchange of atmospheric species. The values are best estimates based on a review of the literature.[a]

Relative speed v, cm/sec	Charge-exchange cross section σ_x (10^{-16} cm^2)					
	$He^+ + He$	$N^+ + N$	$O^+ + O$	$N_2^+ + N_2$	$O_2^+ + O_2$	$NO^+ + NO$
2(5)		57	43			
2.5(5)		55	41	45	35	24.5
5(5)		47.5	36	39	28.5	19.7
7(5)	27	44	33	37	26	18
1(6)	24	40	30.5	34.5	23.5	16
2(6)	20.5	33	26	31	19	13.3
3(6)	18.3	29	23.5	28.5	17	12.3
6(6)	15	24	20	25.5	14.5	10.6
1(7)	12.5	20.5	17.5	23.2	14	9.6
2(7)	10	16	14.4	20.5	14	9.4
5(7)	6.8	11.5	10.8	16	13.3	
1(8)	4.7	8.5	8.0	12.5	12.5	
1.5(8)	3.2	6.4	6.3			
2(8)	2.15	4.5	4.8			
3(8)	0.93	1.78	2.65			
4(8)	0.39	0.71	1.35			
5(8)	0.17	0.31	0.7			
6(8)	0.080					
8(8)	0.017					

[a] 2(5) means 2×10^5 cm/sec. The number of digits given is not a measure of accuracy; see text and Figures 4-1 to 4-4.

intervening spaces, have the same meaning. For experimental charge-exchange cross sections, a solid line indicates that the cross section is supported by adequate experimental data; a dashed line indicates that the cross section is supported by uncertain or conflicting measurements; and a dotted line indicates that the cross section is unsupported by data.

The scale above each figure gives the ion energy of one species of ion when the neutrals are at rest. Note that Figures 4-4 to 4-8 involve more than one species of ion, and the energy scale applies to only one of these species.

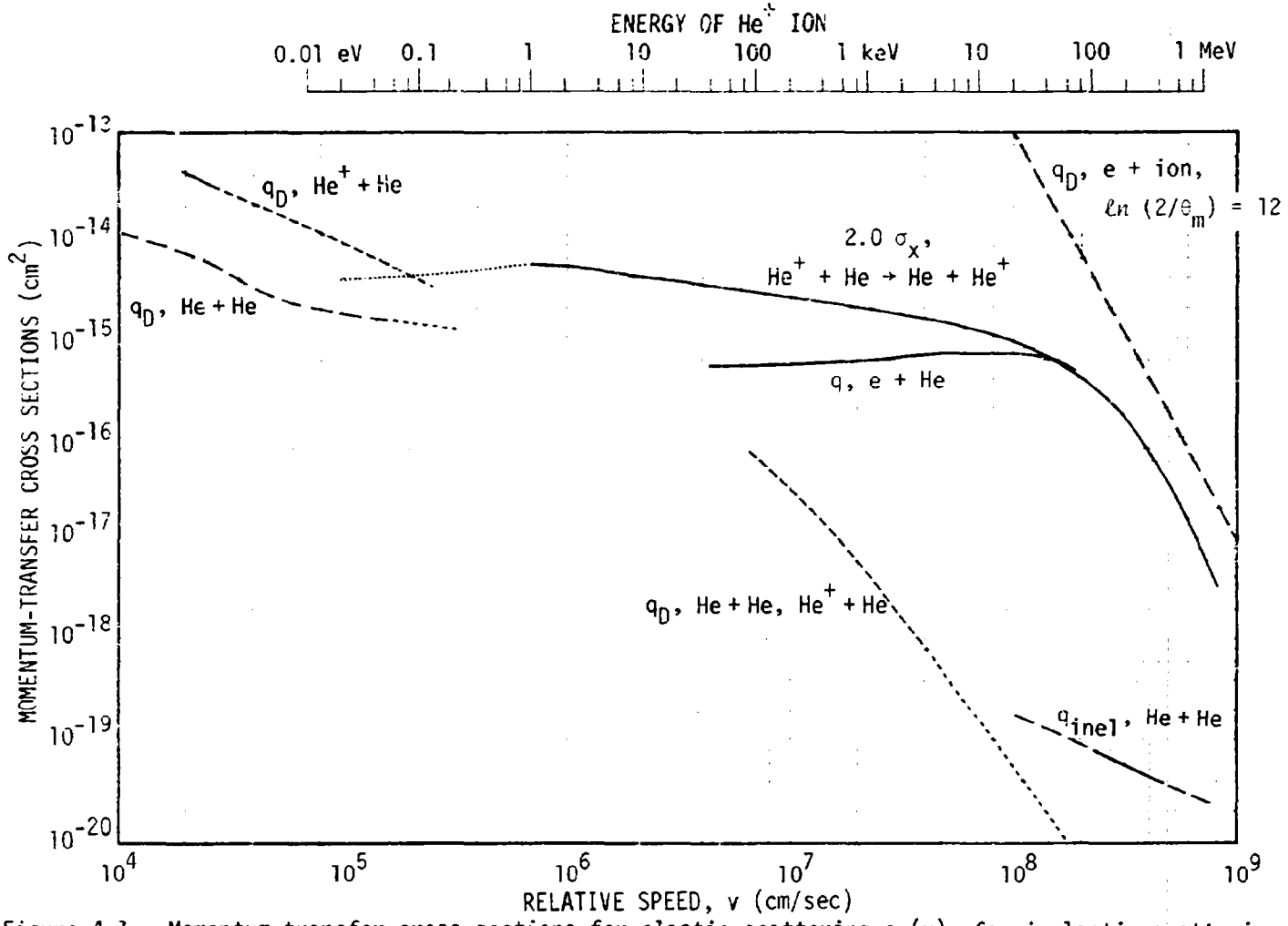

Figure 4-1. Momentum-transfer cross sections for elastic scattering $q_D(v)$, for inelastic scattering $q_{inel}(v)$, and for symmetric charge exchange $q^*(v) = 2\ \sigma_x(v)$ of He^+ + He and He + He.

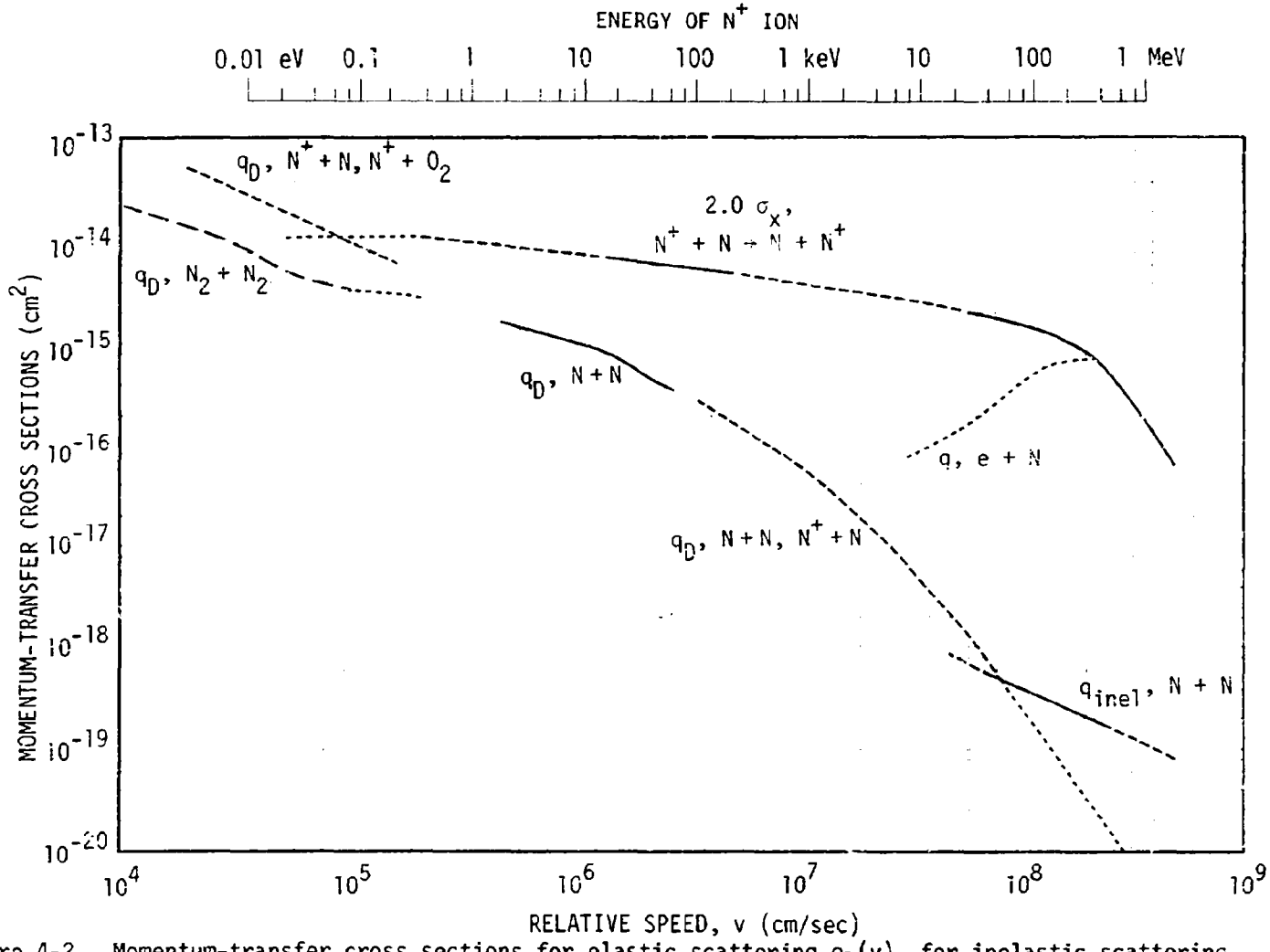

Figure 4-2. Momentum-transfer cross sections for elastic scattering $q_D(v)$, for inelastic scattering $q_{inel}(v)$, and for symmetric charge exchange $q^*(v) = 2\,\sigma_x(v)$ of $N^+ + N$, $N + N$, and $N_2 + N_2$.

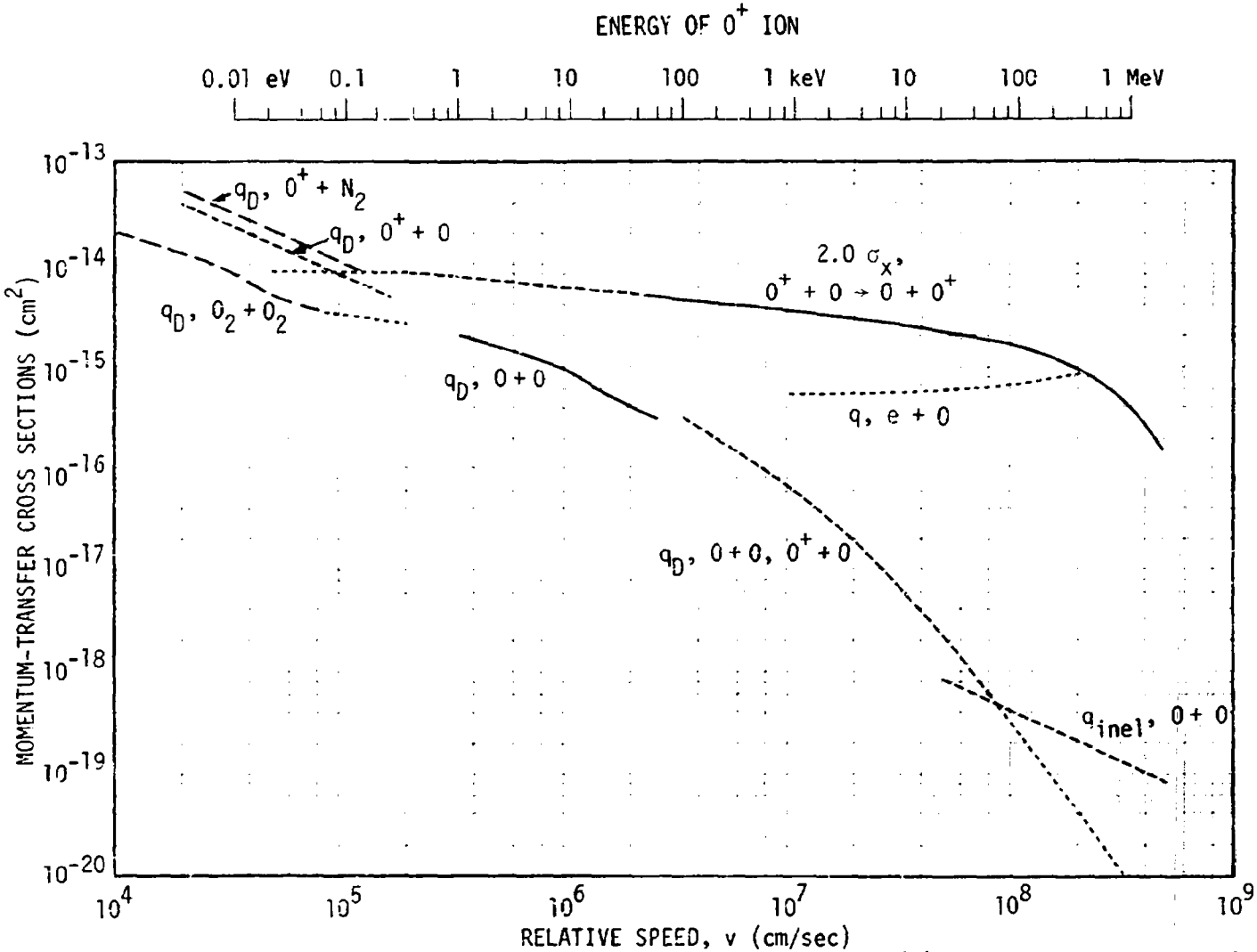

Figure 4-3. Momentum-transfer cross sections for elastic scattering $q_D(v)$, for inelastic scattering $q_{inel}(v)$, and for symmetric charge exchange $q^*(v) = 2\ \sigma_x(v)$ of $0^+ + 0$, $0 + 0$, and $O_2 + O_2$.

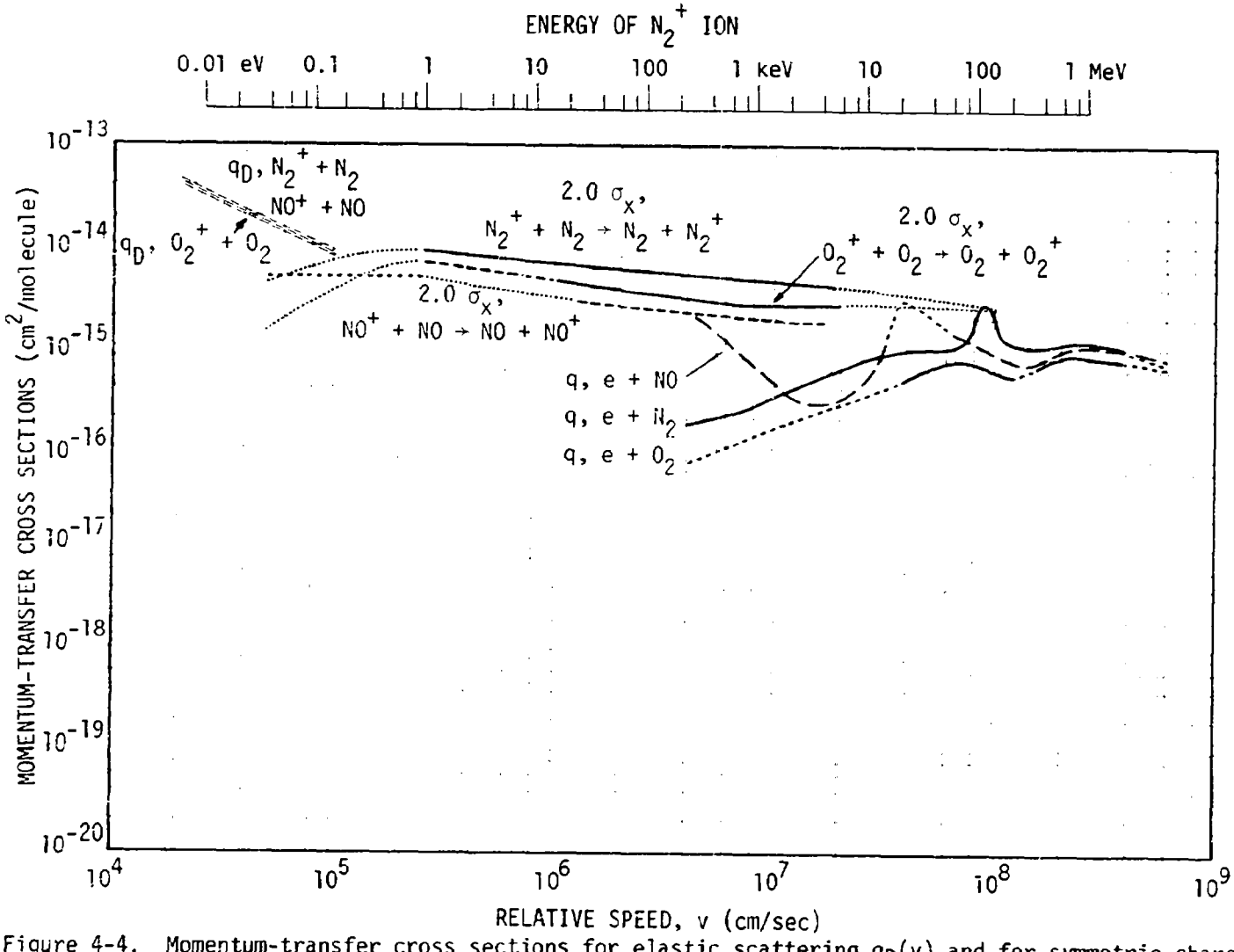

Figure 4-4. Momentum-transfer cross sections for elastic scattering $q_D(v)$ and for symmetric charge exchange $q^*(v) = 2\,\sigma_x(v)$ of $N_2^+ + N_2$, $O_2^+ + O_2$, and $NO^+ + NO$.

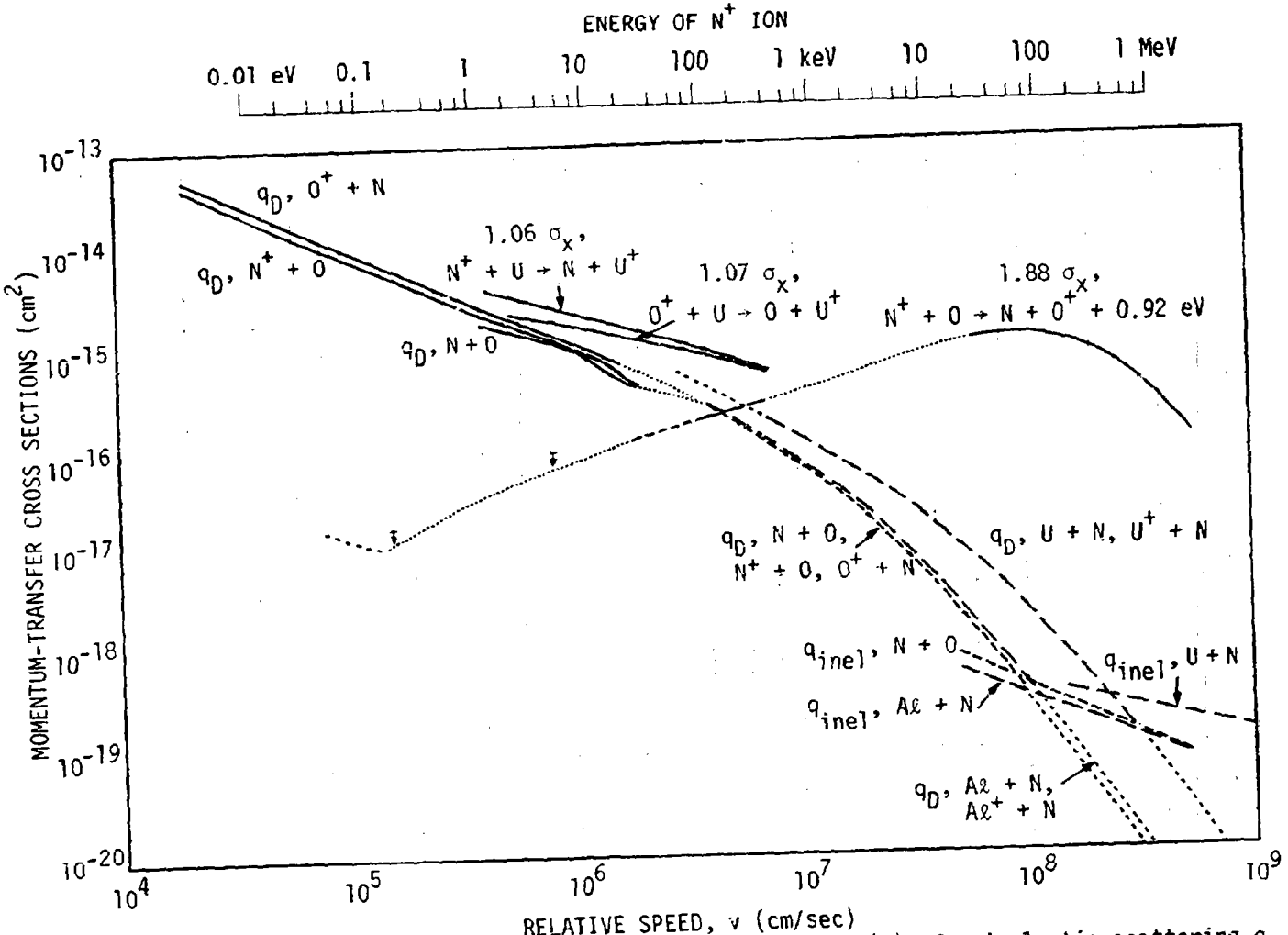

Figure 4-5. Momentum-transfer cross sections for elastic scattering $q_D(v)$, for inelastic scattering $q_{inel}(v)$, and for asymmetric charge exchange $q_T(v)$ of $N^+ + O$, $O^+ + N$, $N + O$, $N^+ + U$, and $O^+ + U$.

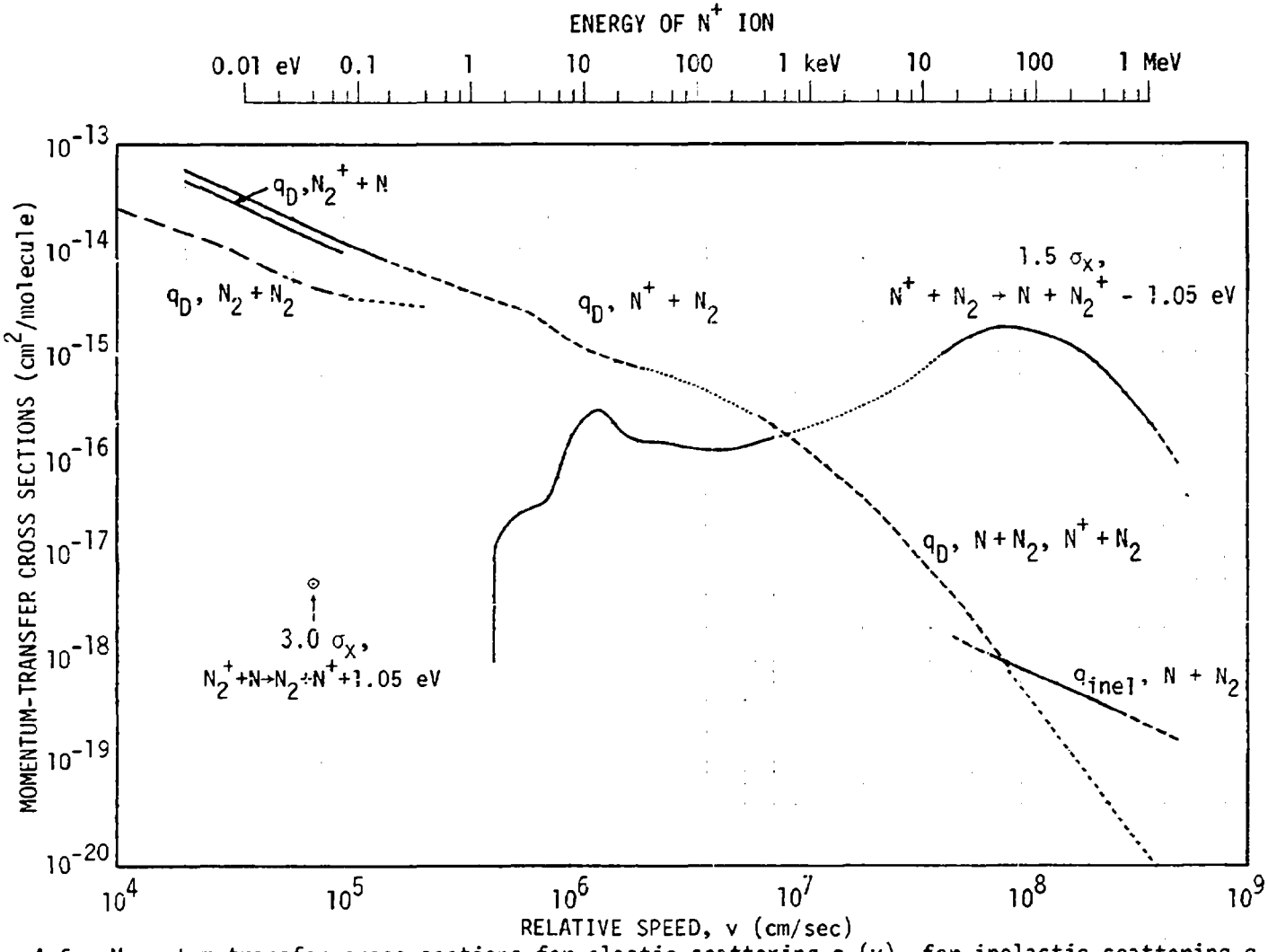

Figure 4-6. Momentum-transfer cross sections for elastic scattering $q_D(v)$, for inelastic scattering $q_{inel}(v)$, and for asymmetric charge exchange $q_T(v)$ of $N^+ + N_2$, $N_2^+ + N$, and $N_2 + N_2$.

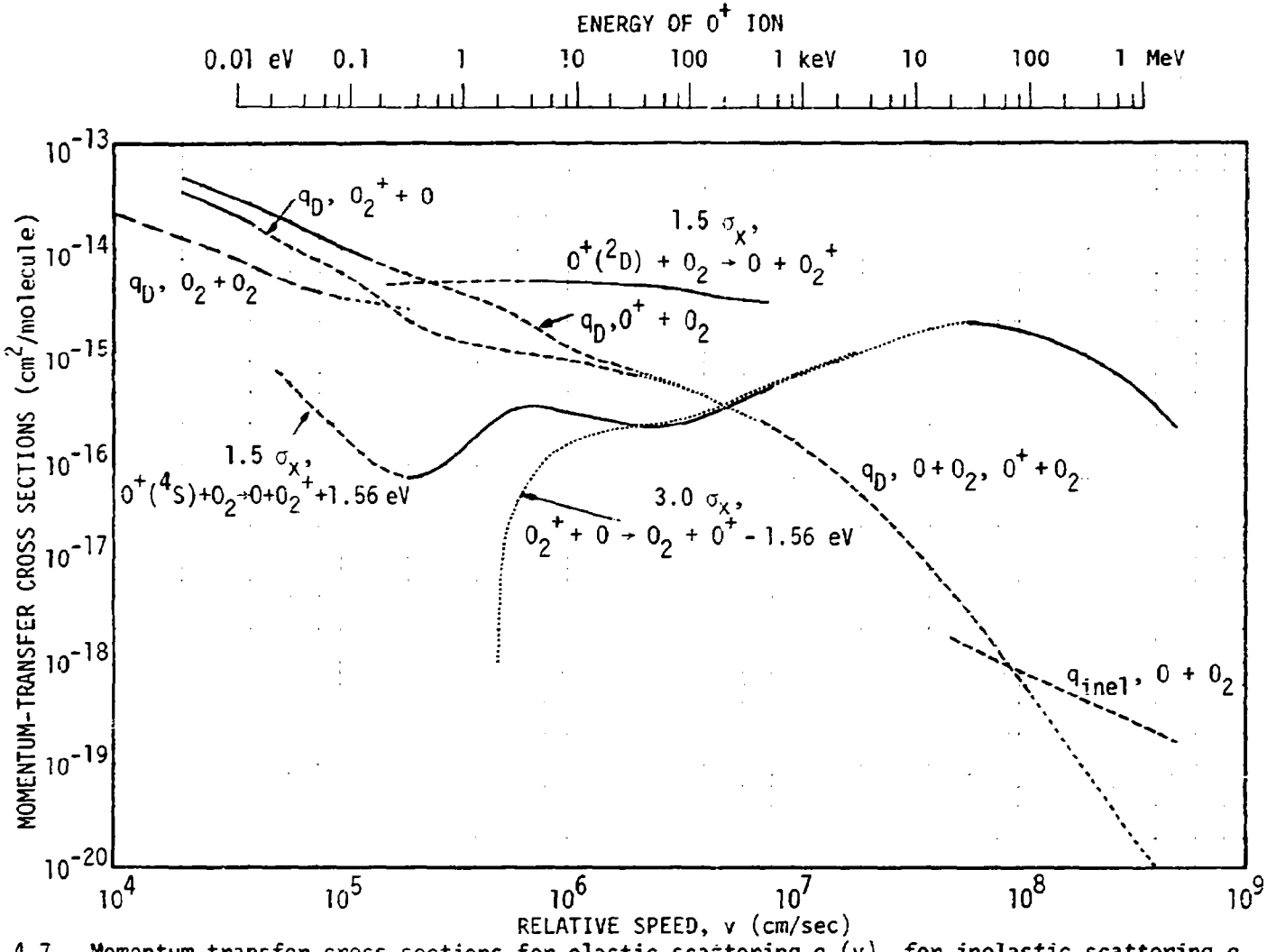

Figure 4-7. Momentum-transfer cross sections for elastic scattering $q_D(v)$, for inelastic scattering $q_{inel}(v)$, and for asymmetric charge exchange $q_T(v)$ of $O^+ + O_2$, $O_2^+ + O$, and $O_2 + O_2$.

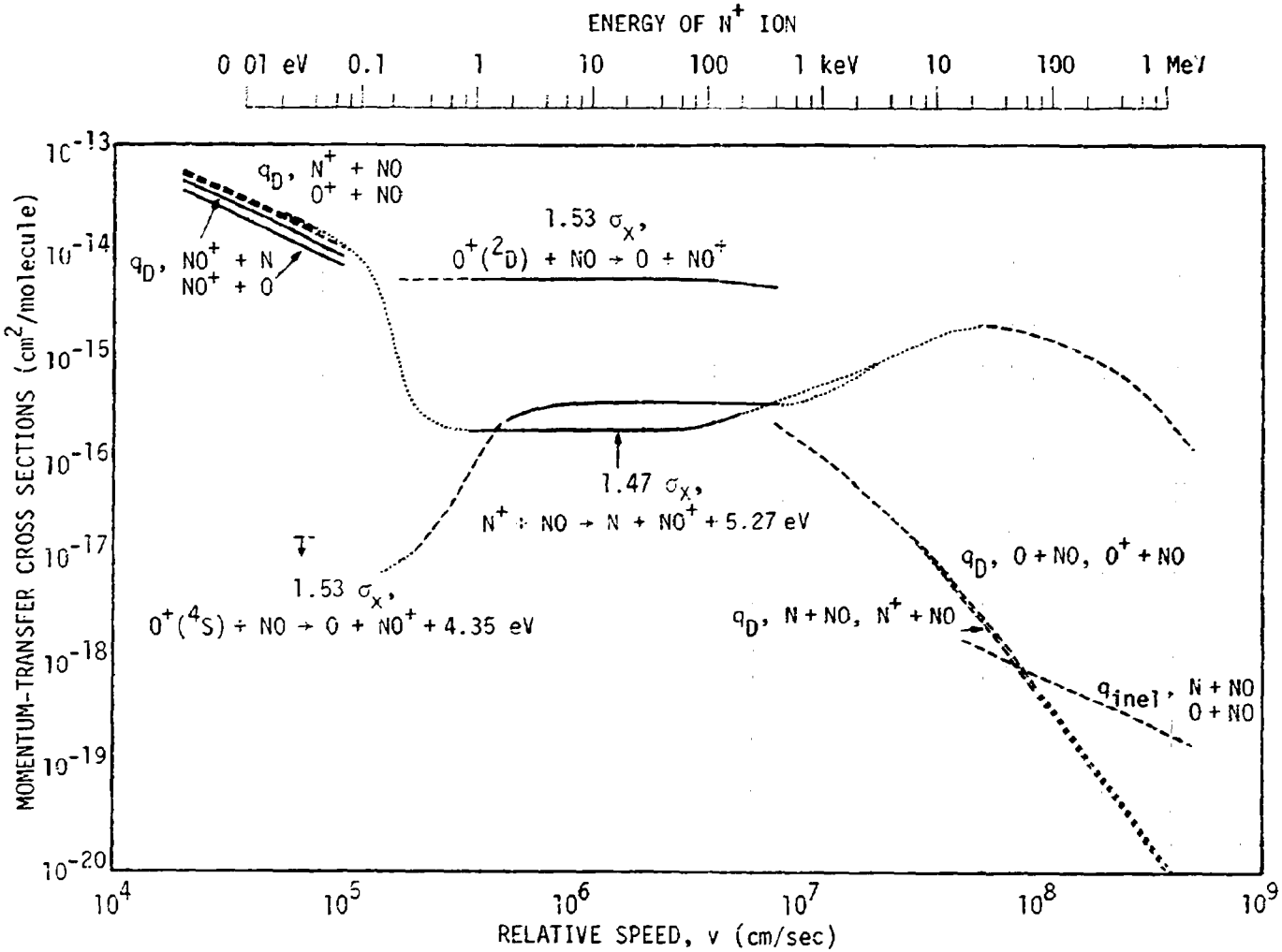

Figure 4-8. Momentum-transfer cross sections for elastic scattering $q_D(v)$, for inelastic scattering $q_{inel}(v)$, and for asymmetric charge exchange $q_T(v)$ of $N^+ + NO$, $O^+ + NO$, $NO^+ + N$, and $NO^+ + O$.

SECTION 5

COEFFICIENTS FOR COLLISIONAL MOMENTUM AND HEAT TRANSFER FOR TWO-FLUID NUCLEAR-BURST SIMULATIONS

5.1 COUPLING AND HEAT-TRANSFER COEFFICIENTS

Sections 3 and 4 give cross sections as a function of the relative speed of the pair of particles. We now integrate these over a distribution of speeds to obtain averaged quantities, the momentum-coupling coefficient and heat-transfer coefficient, as a function of the temperatures and macroscopic velocities of the two gases. These are found by using Eqs. 2-33 and 2-34 to integrate the momentum-transfer cross sections. We have already done these integrals analytically for two cases: in Section 3.2 for electron-ion elastic scattering and in Section 3.3a for ion-neutral elastic scattering by the polarization force alone. We now integrate numerically for the cases of electron-neutral scattering, ion-neutral elastic scattering, and symmetric charge exchange.

The specific cross sections treated are as follows: The coefficients s_k^* and h_k^* due to symmetric charge exchange (such as $N^+ + N \rightarrow N + N^+$) are based on the cross sections in Figures 4-1 to 4-4 (or Table 4-2). (Asymmetric charge exchange, such as $N^+ + O \rightarrow O^+ + N$ in Figure 4-5, is omitted here; this should be treated as a chemical reaction, as in Appendix B.) The coefficients s_{jk} and h_{jk} for elastic scattering of ions and neutrals are based on the cross sections in Figures 4-1 to 4-8. For pairs for which only the polarization-force cross section is shown, the coefficients s_{jk} and h_{jk} are taken from Table 3-3, while for the other five pairs (in Figures 4-5 to 4-7) they are found by numerical

integration. The coefficients s_{je} and h_{je} for electron-neutral scattering are based on the cross sections of Section 3.1. The coefficients s_{ke} and h_{ke} for electron-ion elastic scattering are given by Eqs. 3-7 to 3-9 and 3-5 with $\ell n(2/\theta_m) = 12$. Since the electron-ion coupling coefficient of Eq. 3-7 is essentially independent of ion mass, it equals the combined coupling coefficient s_{ie} of Eq. 2-50.

These coupling coefficients and heat-transfer coefficients are found by integrating Eqs. 2-33 and 2-34 analytically or numerically. The numerical integrations used Simpson's rule with a step size of $\Delta\xi = 0.05$ over the interval $0 < \xi < (V/U+4)$; the resulting integrals are accurate to three digits or more. If a cross section is known only over a range $v_\ell < v < v_u$, we calculate the coupling and heat-transfer coefficients only for temperatures such that

$$\frac{1}{2} v_\ell^2 < \frac{kT_1}{m_1} + \frac{kT_2}{m_2} < \frac{1}{2} v_u^2 \quad . \tag{5-1}$$

The coupling coefficients are first calculated for zero relative gas velocity ($\vec{V}_1 - \vec{V}_2 = 0$) as a function of the weighted mean temperature $(m_2 kT_1 + m_1 kT_2)/(m_1 + m_2)$ (Eq. 2-21) from 0.01 to 500 eV. Figure 5-1 shows the resulting ion-neutral and electron-ion coupling coefficients. The extension of these results to small nonzero relative gas velocity is discussed later in this subsection. Because of crowding Figure 5-1 does not show the (constant) coupling coefficients for $O^+ + O$, $N^+ + NO$, or $O^+ + NO$; these are given in Table 5-3.

The accuracy of a coupling coefficient is indicated roughly by the weight of the line. The solid (most accurate), dashed and dotted portions of the cross-section curves (Figures 4-1 to 4-8) have been repeated in Figure 5-1. The remarks about the three weights of curves made in Section 4 apply here.

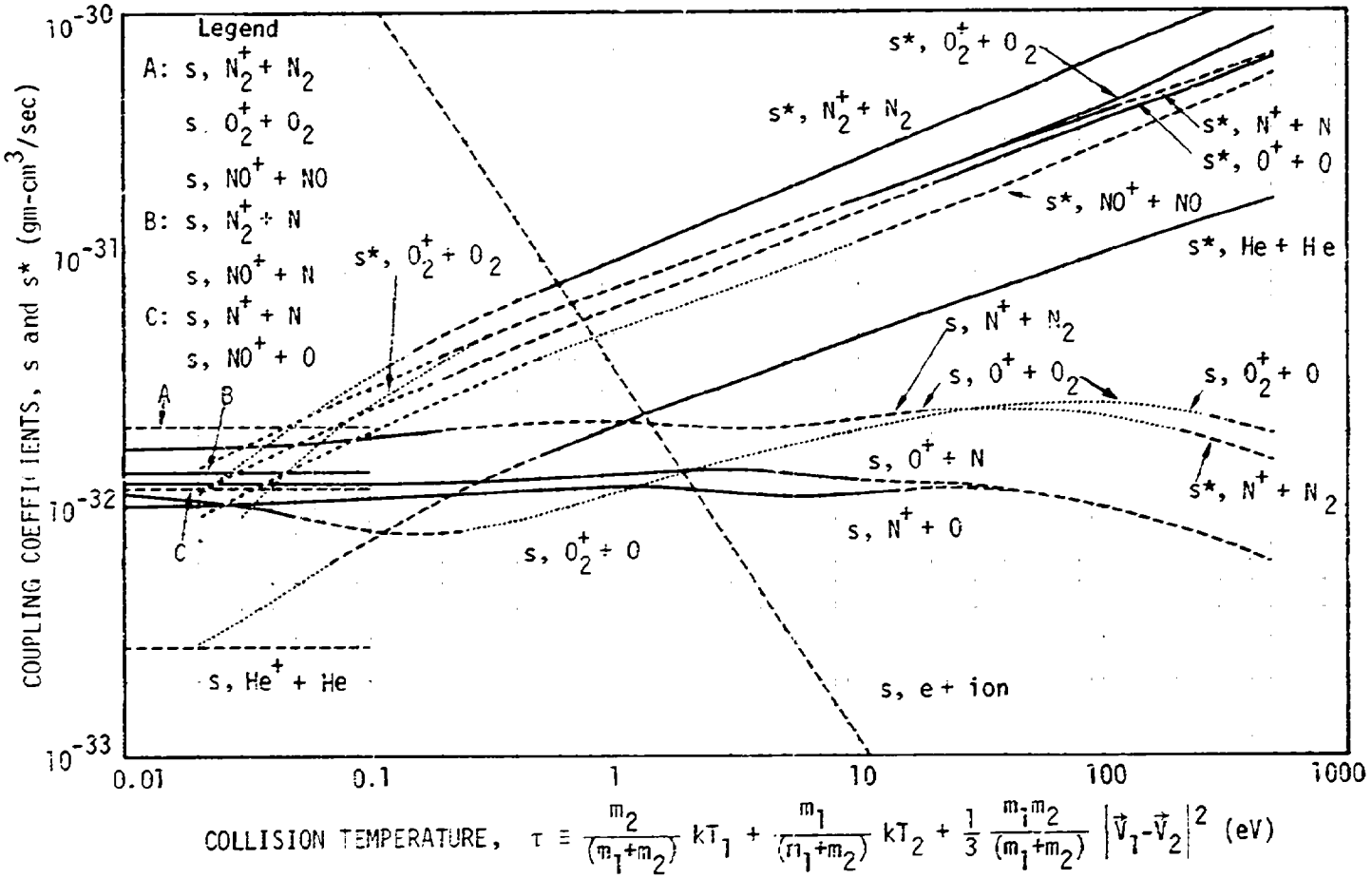

Figure 5-1. Coupling coefficients for elastic scattering s_{jk} and for symmetric charge exchange s_k^* vs. collision temperature. These are valid when $|\vec{V}_1-\vec{V}_2|^2 \lesssim kT_1/m_1 + kT_2/m_2$.

Figure 5-2 shows the electron-neutral coupling coefficients and an extension from Figure 5-1 of the electron-ion coefficient, which is independent of ion mass. Figures 5-3 and 5-4 show the heat-transfer coefficients for zero gas velocities. These are related to the coupling coefficients of Figures 5-1 and 5-2 by Eq. 2-34b. Because of crowding Figure 5-3 does not show the heat-transfer coefficient for $O^+ + N$, which is slightly greater than that for $N^+ + O$ (see Figure 5-1 or Table 3-3), or that for $NO^+ + O$, which is given in Table 3-3.

We have also computed all these coefficients for nonzero gas velocities, $|\vec{V}_1 - \vec{V}_2| > 0$. Presenting the results is simplified by using a new independent variable. We let $\overline{v^2}$ denote the mean square relative speed of pairs of particles of species 1 and 2; the new independent variable τ is then $[m_1 m_2/(m_1+m_2)]\overline{v^2}/3$, which is 2/3 of the mean kinetic energy of pairs of particles in their center-of-mass frames:

$$\tau \equiv \frac{m_2}{(m_1+m_2)} kT_1 + \frac{m_1}{(m_1+m_2)} kT_2 + \frac{1}{3}\frac{m_1 m_2}{(m_1+m_2)} |\vec{V}_1 - \vec{V}_2|^2 \quad . \qquad (5\text{-}2)$$

We call τ the "collision temperature" for collisions between species 1 and 2; when $\vec{V}_1 = \vec{V}_2$ it is simply the weighted mean temperature kT_m (Eq. 2-21). For electron-neutral and electron-ion collisions the neutral and ion temperatures are usually small compared to $(m_2/m_e)T_e$, so Eq. 5-2 reduces to

$$\tau = kT_e + \frac{1}{3} m_e |\vec{V}_e - \vec{V}_2|^2 \quad , \qquad (5\text{-}3)$$

where $\vec{V}_2$ is either the velocity of the neutrals or that of the ions.

Using τ as one of the independent variables, one finds that the coupling coefficients and heat-transfer coefficients are nearly independent of $|\vec{V}_1 - \vec{V}_2|$ when

$$|\vec{V}_1 - \vec{V}_2|^2 \ll \frac{kT_1}{m_1} + \frac{kT_2}{m_2} \quad , \qquad (5\text{-}4)$$

which is usually satisfied in late-time two-fluid simulations.

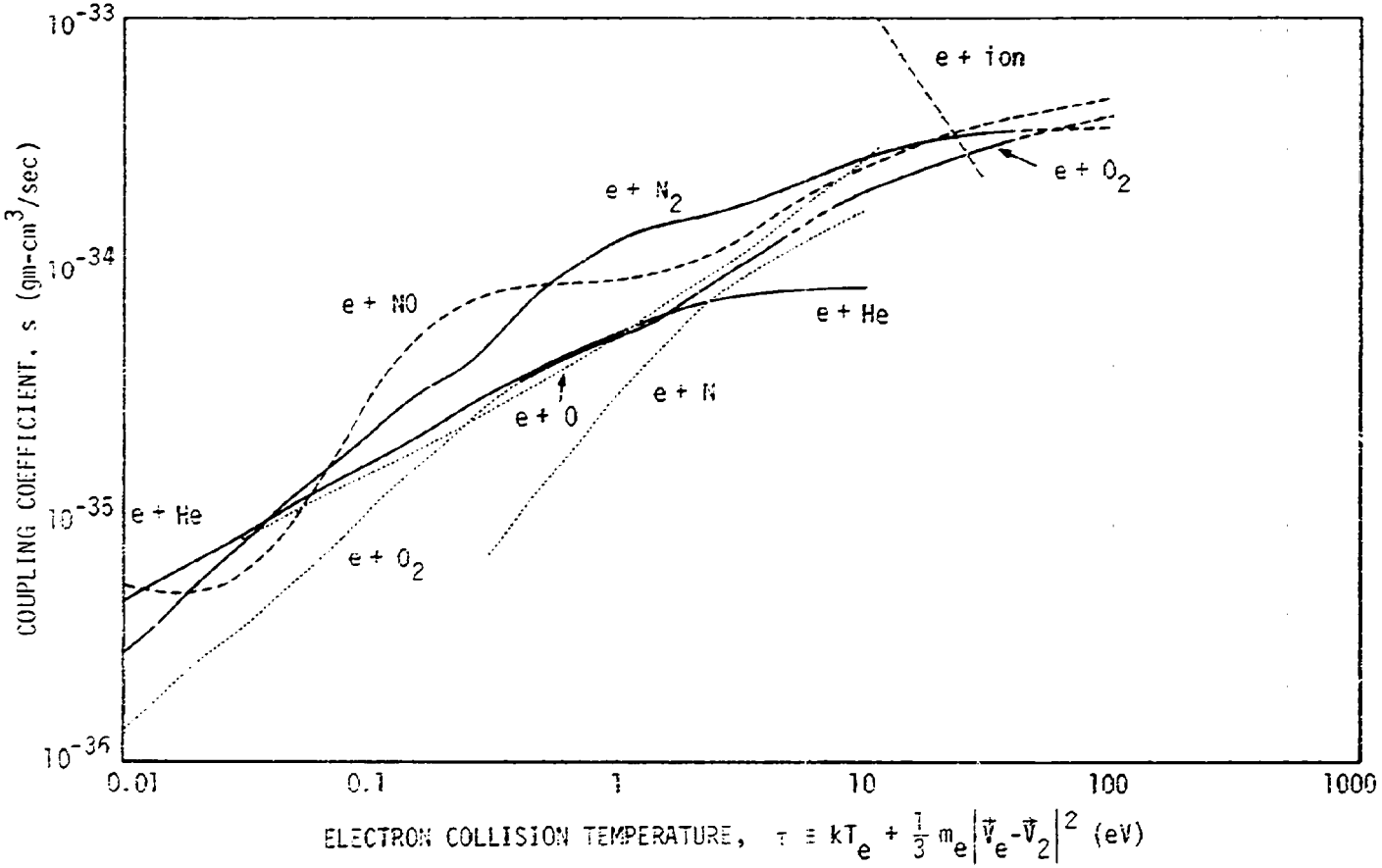

Figure 5-2. Coupling coefficients for electron-neutral scattering s_{je} and electron-ion scattering s_{ie} vs. electron collision temperature. These are valid when $m_e \left|\vec{V}_e - \vec{V}_2\right|^2 \lesssim kT_e$.

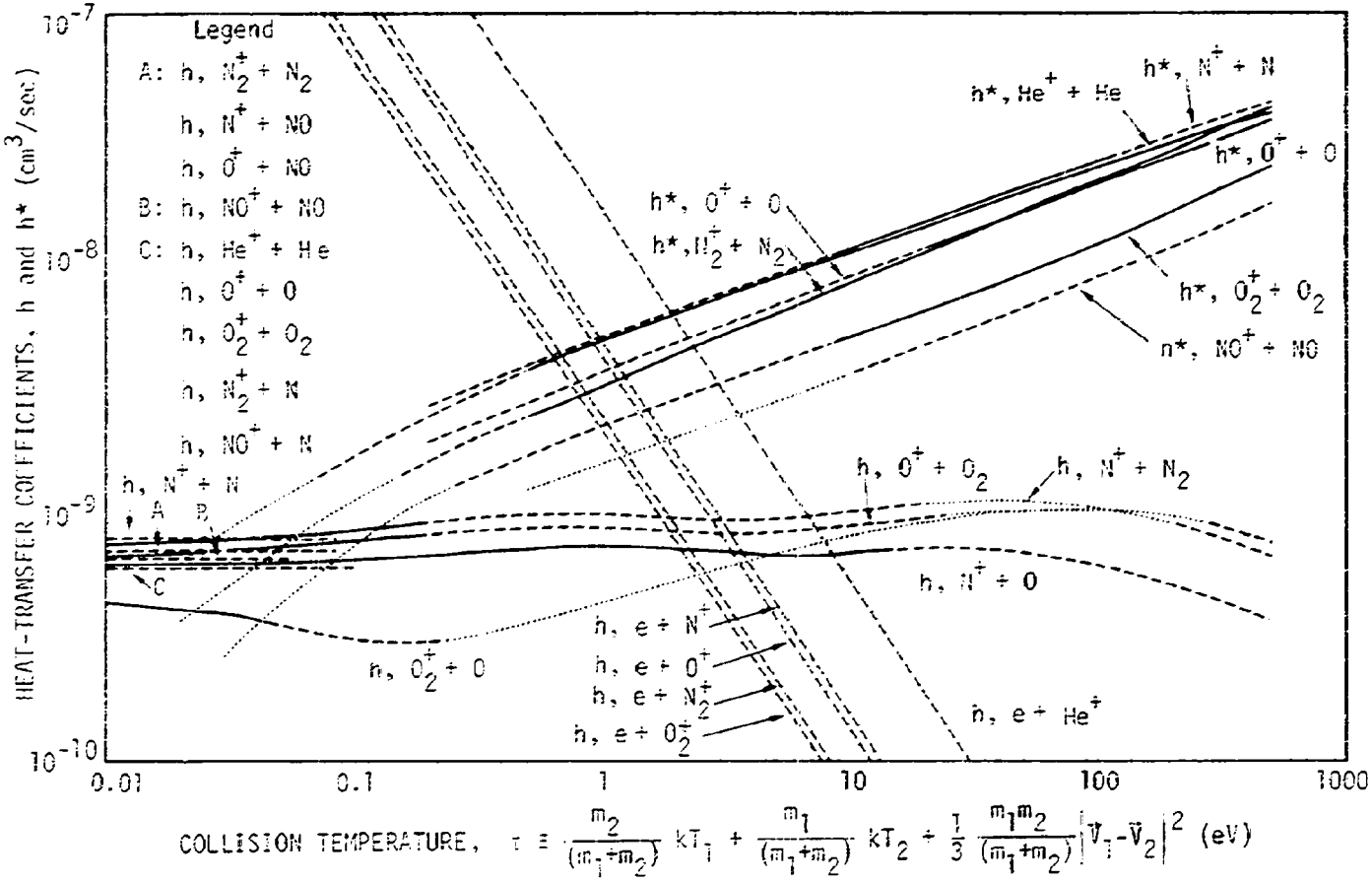

Figure 5-3. Heat-transfer coefficients for elastic scattering h_{jk} and for <u>symmetric</u> charge exchange h_k^* vs. collision temperature. These are valid when $|\bar{V}_1-\bar{V}_2|^2 \leq kT_1/m_1 + kT_2/m_2$.

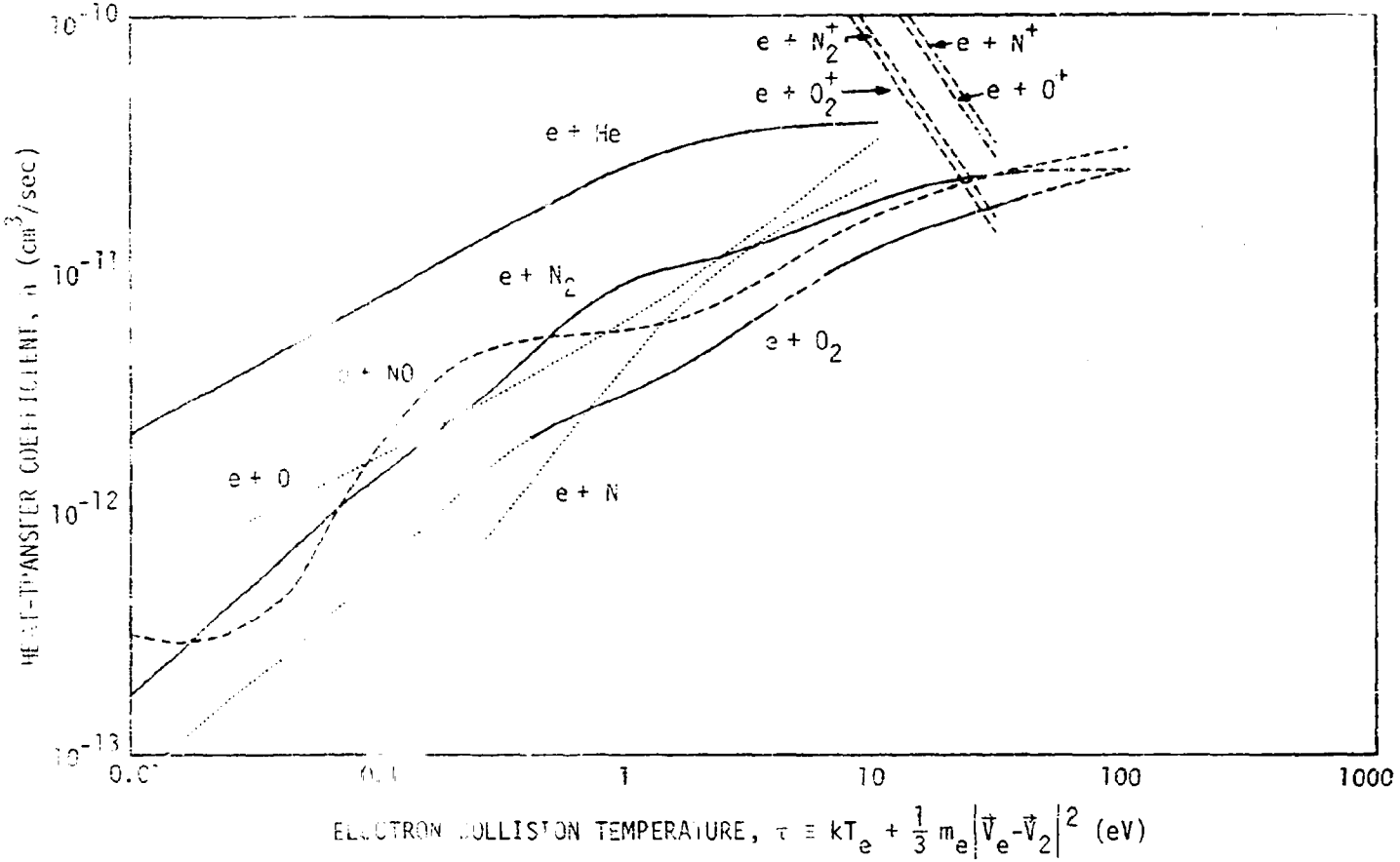

HEAT-TRANSFER COEFFICIENT, h (cm^3/sec)

ELECTRON COLLISION TEMPERATURE, $\tau \equiv kT_e + \frac{1}{3} m_e \left|\vec{V}_e - \vec{V}_2\right|^2$ (eV)

Figure 5-4. Heat-transfer coefficients for electron-neutral scattering h_{je} and electron-ion scattering h_{ji} vs. electron collision temperature. These are valid when $m_e \left|\vec{V}_e - \vec{V}_2\right|^2 \leq kT_e$.

To indicate this we have labeled the abscissas of Figures 5-1 to 5-4 as τ. For relative speeds satisfying inequality 5-4 the calculated coupling and heat-transfer coefficients are always within ±15 percent of the values given in Figures 5-1 to 5-4. Larger relative speeds make substantial changes in these coefficients, however, so these Figures and Table 5-1 should be used only for speeds that satisfy inequality 5-4.

Table 5-1 gives empirical fits to the momentum-coupling coefficients of Figures 5-1 and 5-2. Since these are valid only for low relative gas velocity, heat-transfer coefficients can be calculated from them by the relation $h = 3s/(m_1+m_2)$ (Eq. 2-34b).

5.2 HOW TO USE THE COUPLING AND HEAT-TRANSFER COEFFICIENTS IN TWO-FLUID SIMULATIONS

We have presented a method of treating the momentum and energy transfers due to elastic scattering and symmetric charge exchange in ion-neutral, electron-neutral, and electron-ion encounters. We give a brief summary for the reader who is primarily interested in results.

The neutrals are composed of several species ($j=1,2,\ldots$) having particle masses m_j, number densities n_j^o, and total number density $n_n = \Sigma_j n_j^o$. The neutrals are characterized by a mean velocity $\vec{V}_n$ and a single temperature T_n; we consider the particle velocity distribution of each neutral species to be Maxwell-Boltzmann in the frame moving at the mean velocity $\vec{V}_n$. The ions are composed of singly charged species ($k=1,2,\ldots$) having number densities n_k^+ and total number density $n_i = \Sigma_k n_k^+$. The ion and electron velocity distributions are similarly characterized by $\vec{V}_i$, $\vec{V}_e$ and T_e. The electron number density is given by $n_e = n_i$, and the mean electron velocity can be eliminated by Eq. 2-46,

$$\vec{V}_e = \vec{V}_i - \vec{J}/en \quad . \tag{5-5}$$

Table 5-1a. Parameters of the coupling coefficients due to electron-neutral scattering s_{je} and elastic electron-ion scattering s_{ie} as given by $s = B\tau^b$. The collision temperature τ (Eq. 5-3) is in eV and s is in gm-cm^3/sec.

Pair of species	$s_{je} = B\tau^b$		Range of τ, in eV
	B	b	
e + He	5.90(-35)[a]	+0.564	$0.01<\tau<0.8$
	5.52(-35)	+0.267	$0.8<\tau<4$
	8.0(-35)	0.	$4<\tau<10$
e + N	3.09(-35)	+1.258	$0.3<\tau<2$
	5.24(-35)	+0.498	$2<\tau<10$
e + O	5.0(-35)	+0.530	$0.03<\tau<1$
	5.0(-35)	+0.748	$1<\tau<10$
e + N_2	1.43(-34)	+0.846	$0.01<\tau<0.8$
	1.30(-34)	+0.436	$0.8<\tau<24$
	5.2(-34)	0.	$24<\tau<100$
e + O_2	8.30(-35)	+0.903	$0.01<\tau<0.3$
	5.42(-35)	+0.549	$0.3<\tau<18$
	1.27(-34)	+0.255	$18<\tau<100$
e + NO	5.0(-36)	0.	$0.01<\tau<0.03$
	7.27(-34)	+1.420	$0.03<\tau<0.2$
	8.72(-35)	+0.102	$0.2<\tau<1.7$
	6.70(-35)	+0.597	$1.7<\tau<13$
	1.79(-34)	+0.214	$13<\tau<100$
e + ion	3.18(-32)[e]	-1.5	Note d

a 5.90 (-35) means 5.90×10^{-35}.

d $10^{-5}\ n_e^{1/3} < \tau < 30$ eV, where n_e is in electrons/cm^3. The lower limit is from Debye theory, as mentioned in Section 3.3b.

e We used $\ell n(2/\theta_m) = 12$ in Eqs. 3-5 and 3-7. This factor is tabulated in Reference 8, Table 5.1 (called $\ell n\Lambda$) and plotted in Reference 7, Figure 8-6.

Table 5-1b. Parameters of the coupling coefficients due to ion-neutral elastic scattering s_{jk} and to symmetric charge exchange s_k^* as given by $s_{jk} \equiv B\tau^b$ and $s_k^* = B^*\tau^c$. The collision temperature τ (Eq. 5-2) is in eV and s_{jk} and s_k^* are in gm-cm^3/sec.

Pair of species	$s_{jk} = B\tau^b$		Range of τ, in eV	$s_k^* = B^*\tau^c$		Range of τ, in eV
	B	b		B^*	c	
$He^+ + He$	2.75(-33)	0.	$0.01<\tau<500$	2.94(-32)	0.600	$0.02<\tau<0.3$
				2.18(-32)	0.351	$0.3<\tau<500$
$N^+ + N$	1.21(-32)	0.	$0.01<\tau<500$	7.6(-32)	0.358	$0.02<\tau<500$
$O^+ + O$	1.07(-32)	0.	$0.01<\tau<500$	6.3(-32)	0.381	$0.02<\tau<500$
$N_2^+ + N_2$	2.13(-32)	0.	$0.01<\tau<500$	1.38(-31)	0.618	$0.02<\tau<0.2$
				9.90(-32)	0.412	$0.2<\tau<500$
$O_2^+ + O_2$	2.17(-32)	0.	$0.01<\tau<500$	1.24(-31)	0.697	$0.02<\tau<0.2$
				7.42(-32)	0.397	$0.2<\tau<500$
$NO^+ + NO$	2.17(-32)	0.	$0.01<\tau<500$	5.1(-32)	0.381	$0.02<\tau<500$
$N^+ + O$	1.1(-32)	0.	$0.01<\tau<70$			
	3.80(-32)	-0.292	$70<\tau<500$			
$O^+ + N$	1.25(-32)	0.	$0.01<\tau<40$			
	3.49(-32)	-0.278	$40<\tau<500$			
$N^+ + N_2$	2.15(-32)	+0.040	$0.01<\tau<70$			
	7.60(-32)	-0.257	$70<\tau<500$			
$N^+ + O_2$	1.70(-32)	0.	$0.01<\tau<500$			
$O^+ + N_2$	1.82(-32)	0.	$0.01<\tau<500$			
$O^+ + O_2$	2.16(-32)	+0.035	$0.01<\tau<200$			
	1.37(-31)	-0.314	$200<\tau<500$			
$O_2^+ + O$	6.62(-33)	-0.118	$0.01<\tau<0.2$			
	1.15(-32)	+0.227	$0.2<\tau<30$			
	2.5(-32)	0.	$30<\tau<500$			
$N_2^+ + N$	1.40(-32)	0.	$0.01<\tau<500$			
$NO^+ + N$	1.41(-32)	0.	$0.01<\tau<500$			
$NO^+ + O$	1.22(-32)	0.	$0.01<\tau<500$			
$NO^+ + N_2$	2.17(-32)	0.	$0.01<\tau<500$			
$NO^+ + O_2$	2.14(-32)	0.	$0.01<\tau<500$			
$N^+ + NO$	1.73(-32)	0.	$0.01<\tau<500$			
$O^+ + NO$	1.81(-32)	0.	$0.01<\tau<500$			

Section 2.3 gives the two-fluid momentum and energy balance equations in a form that includes elastic scattering and symmetric charge exchange (such as $N^+ + N \rightarrow N + N^+$). We repeat these relations here and then summarize how to calculate the nine coefficients for collisional momentum and heat transfer (Eqs. 5-12 to 5-19). Other symbols are defined in the Glossary in Appendix A. The momentum balance equations for the neutral fluid, for the ion-electron plasma, and for the electrons (Eqs. 2-51 to 2-53) are

$$\frac{\partial(\rho_n \vec{V}_n)}{\partial t} + \nabla \cdot (\rho_n \vec{V}_n \vec{V}_n) = - \nabla P_n + \rho_n \vec{g} - n_n n_i s_{ni} (\vec{V}_n - \vec{V}_i) - n_n n_e s_{ne} (\vec{V}_n - \vec{V}_e), \quad (5\text{-}6)$$

$$\frac{\partial(\rho_i \vec{V}_i)}{\partial t} + \nabla \cdot (\rho_i \vec{V}_i \vec{V}_i) = - \nabla (P_i + P_e) + \vec{J} \times \vec{B} + (\rho_i + \rho_e)\vec{g} + n_n n_i s_{ni} (\vec{V}_n - \vec{V}_i) + n_n n_e s_{ne} (\vec{V}_n - \vec{V}_e) \quad , \quad (5\text{-}7)$$

$$0 = - \nabla P_e - e n_e \left(\vec{E} + \frac{\vec{V}_e \times \vec{B}}{c} \right) + \rho_e \vec{g} + n_n n_e s_{ne} (\vec{V}_n - \vec{V}_e) + n_i n_e s_{ie} (\vec{V}_i - \vec{V}_e) \quad . \quad (5\text{-}8)$$

The internal energy balance equations for the neutral fluid, for the ions and for the electrons (Eq. 2-55 to 2-57) are

$$\frac{\partial(\rho_n I_n)}{\partial t} + \nabla \cdot (\rho_n I_n \vec{V}_n) = - P_n \nabla \cdot \vec{V}_n + n_n n_i s_{ni} d_{ni}^{(n)} \left| \vec{V}_n - \vec{V}_i \right|^2 + n_n n_e s_{ne} d_{ne}^{(n)} \left| \vec{V}_n - \vec{V}_e \right|^2 + n_n n_i h_{ni} k (T_i - T_n) + n_n n_e h_{ne} k (T_e - T_n) \quad , \quad (5\text{-}9)$$

$$\frac{\partial(\rho_i I_i)}{\partial t} + \nabla \cdot (\rho_i I_i \vec{V}_i) = - P_i \nabla \cdot \vec{V}_i + n_n n_i s_{ni} (1 - d_{ni}^{(n)}) \left| \vec{V}_n - \vec{V}_i \right|^2 + n_i n_e s_{ie} d_{ie}^{(i)} \left| \vec{V}_i - \vec{V}_e \right|^2 - n_n n_i h_{ni} k (T_i - T_n) - n_i n_e h_{ie} k (T_i - T_e) \quad , \quad (5\text{-}10)$$

$$\frac{\partial\left(\frac{3}{2}\, n_e k T_e\right)}{\partial t} + \nabla\cdot\left(\frac{3}{2}\, n_e k T_e \vec{V}_e\right) = - P_e \nabla\cdot\vec{V}_e$$

$$+ n_n n_e s_{ne}\left(1-d_{ne}^{(n)}\right)\left|\vec{V}_n-\vec{V}_e\right|^2 + n_i n_e s_{ie}\left(1-d_{ie}^{(i)}\right)\left|\vec{V}_i-\vec{V}_e\right|^2$$

$$- n_n n_e h_{ne} k(T_n - T_e) + n_i n_e h_{ie} k(T_i - T_e) \quad . \qquad (5\text{-}11)$$

These six balance relations should include additional terms to account for chemical reactions. (Asymmetric charge exchange, such as reactions 4-7 to 4-20, is classed in this work as a chemical reaction. See Appendix B and Figs. 4-5 to 4-8.) Eq. 5-11 should also include an additional term to account both for the heat transfer resulting from vibrational excitation and de-excitation of N_2 by electron impact and for the electron energy loss resulting from electronic excitation and ionization of neutrals and ions by electron impact.

The coupling and heat-transfer coefficients depend on the fluid composition. The first one, s_{ni}, is calculated from Eq. 2-48 as the weighted sum of the coupling coefficients s_{jk} for elastic scattering of pairs of species consisting of a neutral species j and an ion species k ($N^+ + N$, $N^+ + O$ $N^+ + N_2$, etc.) plus a sum of the coupling coefficients s_k^* due to symmetric charge exchange of ions with their parent atoms or molecules ($N^+ + N$, $NO^+ + NO$, etc.); the relation is

$$n_n n_i s_{ni} \equiv \sum_j \sum_k n_j^o\, n_k^+\, s_{jk} + \sum_k n_k^o\, n_k^+\, s_k^* \quad , \qquad (5\text{-}12)$$

where n_j^o is the number density of neutral species j and n_k^+ is the number density of ion species k. The coupling coefficients s_{jk} and s_k^* for individual pairs of species can be found from Table 5-1b as

a function of the collision temperature τ (Eq. 5-2) for that pair. Table 5-1b applies when the ion-neutral relative speed $\left|\vec{V}_n - \vec{V}_i\right|$ satisfies inequality 5-4.

The ion-neutral heat-transfer coefficient h_{ni} should be summed at the same time; it is given by Eq. 2-59,

$$n_n n_i h_{ni} \approx \sum_j \sum_k n_j^o n_k^+ \frac{3 s_{jk}}{(m_j + m_k)} + \sum_k n_k^o n_k^+ \frac{3 s_k^*}{2 m_k} \quad . \tag{5-13}$$

For the fractional coupling coefficient $d_{ni}^{(n)}$ one may use the approximate Eq. 2-66 rather than sum with the definition, Eq. 2-53a; these relations are

$$n_n n_i s_{ni} d_{ni}^{(n)} \equiv \sum_j \sum_k n_j^o n_k^+ \frac{m_k}{(m_j + m_k)} s_{jk} + \sum_k n_k^o n_k^+ \frac{1}{2} s_k^*$$

$$\approx 0.4 \; n_n n_i s_{ni} \quad . \tag{5-14}$$

The electron-neutral coupling coefficient s_{ne} is calculated from Eq. 2-49 as a sum over all neutral species:

$$n_n n_e s_{ne} \equiv n_e \sum_j n_j^o s_{je} \quad . \tag{5-15}$$

The individual coefficients s_{je} are found from Table 5-1a as a function of the electron-neutral collision temperature τ, which is given by Eq. 5-3. The electron-neutral heat-transfer coefficient h_{ne} is given by Eq. 2-60,

$$n_n n_e h_{ne} \approx n_e \sum_j n_j^o \, 3 s_{je} / m_j \quad , \tag{5-16}$$

which can be approximated by Eq. 2-62. The coefficient $d_{ne}^{(n)}$ is defined by Eq. 2-54, but one can usually approximate by using the mass of the N_2 molecule (Eq. 2-63); these relations are

$$n_n n_e s_{ne} d_{ne}^{(n)} \approx n_e \sum_j n_j^o \frac{m_e}{(m_j+m_e)} s_{je}$$

$$\approx 2.0 \times 10^{-5} n_n n_e s_{ne} \quad . \tag{5-17}$$

The electron-ion coupling coefficient s_{ie}, which is independent of the composition of the ion fluid, is given by the bottom line of Table 5-1a or by Eqs. 3-7, 3-5, and 3-9. It is a function of the electron-ion collision temperature T, which is given by Eq. 5-3. The heat-transfer coefficient h_{ie} is given by Eq. 2-61 and normally can be approximated by using the mass of the O^+ ion (Eq. 2-64); these relations are

$$n_i n_e h_{ie} \approx 3 n_e s_{ie} \sum_k n_k^+/m_k$$

$$\approx 3 n_i n_e s_{ie}/m(O^+) \quad . \tag{5-18}$$

The coefficient $d_{ie}^{(i)}$ involves the same sum and is given by

$$n_i n_e s_{ie} d_{ie}^{(i)} = n_e m_e s_{ie} \sum_k n_k^+/m_k$$

$$\approx 3.4 \times 10^{-5} n_i n_e s_{ie} \quad . \tag{5-19}$$

Our coupling coefficients may be more familiar if they are interpreted as collision frequencies and related to the electrical resistivity. The average momentum-loss collision frequency for electron-ion collisions is

$$\nu_{ei} = \frac{n_i}{m_e} s_{ie} \quad , \tag{5-20}$$

and that for collisions of electrons with neutrals of species j is

$$\nu_{ej} = \frac{n_j^o}{m_e} s_{je} \quad . \tag{5-21}$$

These quantities are related to the electrical resistivity η (in cm^2/sec) by

$$\eta = \frac{c^2 m_e}{e^2 n_e} \left(\nu_{ei} + \sum_j \nu_{ej} \right)$$

$$= \frac{c^2}{e^2} \left(s_{ie} + \frac{1}{n_e} \sum_j n_j^o s_{je} \right) \quad . \tag{5-22}$$

The electron momentum balance equation (Eq. 2-53 or 5-8) can be expressed in terms of the resistivity by using Eqs. 5-22, 5-5, and 2-49. If one can neglect the magnetic field, the electron pressure gradient, gravity, and the ion-neutral slip velocity $\vec{V}_n - \vec{V}_i$, the resulting relation reduces to a form of Ohm's law, $\vec{E} \approx \eta \vec{J}/c$. More generally, the resulting relation can be substituted into Faraday's law, $\partial \vec{B}/\partial t = -c \nabla \times \vec{E}$, to give

$$\frac{\partial \vec{B}}{\partial t} = \nabla \times \left[\vec{V}_i \times \vec{B} - \eta \vec{J} - \frac{c \vec{J} \times \vec{B}}{e n_i} + \frac{c \nabla p_e}{e n_e} - \frac{c}{e} n_n s_{ne} (\vec{V}_n - \vec{V}_i) \right] \quad . \tag{5-23}$$

MHD simulations usually ignore the last three terms, although the validity of this approximation is uncertain.

Simplified forms of the momentum-coupling coefficients, heat-transfer coefficients, and electrical resistivity η are useful. For the temperature ranges and species mixtures encountered after the first second of a nuclear bursts, the following forms are within a factor of two of results found by using Eqs. 5-12 to 5-22 with Table 5-1 or Figs. 5-1 to 5-4:

$$n_n n_i s_{ni} = 1.2 \times 10^{-32} \{ [N+O] + 1.6 \, [N_2+O_2+NO] \} [N^+ + O^+ + NO^+]$$
$$+ 4.8 \times 10^{-32} (kT_n + kT_i)^{0.375} \{ 1.2 [N][N^+] + [O][O^+] + 0.84 [NO][NO^+] \} \quad , \tag{5-24}$$

$$n_n n_i h_{ni} = 7.0 \times 10^{-10} n_n n_i + 27. \times 10^{-10} (kT_n + kT_i)^{0.375} \cdot$$
$$\times \{1.36[N][N^+] + [O][O^+] + 0.45[NO][NO^+]\} \quad , \qquad (5\text{-}25) \star\star\star$$

$$n_n n_e s_{ne} = 7.4 \times 10^{-35} (kT_e)^{0.64} n_n n_e, \qquad (5\text{-}26) \star\star\star$$

$$n_n n_e h_{ne} = 6.0 \times 10^{-12} (kT_e)^{0.64} n_n n_e, \qquad (5\text{-}27) \star\star\star$$

$$n_i n_e s_{ie} = 3.18 \times 10^{-32} (kT_e)^{-1.5} n_i n_e, \qquad (5\text{-}28) \star\star\star$$

$$n_i n_e h_{ie} = 3.6 \times 10^{-9} (kT_e)^{-1.5} n_i n_e, \qquad (5\text{-}29) \star\star\star$$

$$\eta = \frac{1.24 \times 10^8}{(kT_e)^{1.5}} + 2.89 \times 10^5 (kT_e)^{0.64} \; n_n/n_e \qquad (5\text{-}30) \star\star\star$$

where kT_n, kT_i, and kT_e are in eV, η is in cm^2/sec, and the other quantities are in cgs units. In Eqs. 5-28 to 5-30 we used $\ell n(2/\theta_m) = 12$; the weak dependence of this factor on n_e and T_e is given in Reference 8 Table 5.1 (where $\ell n\Lambda = \ell n(2/\theta_m)$) or in Reference 7, Figure 8-6.

Using the simplified form of the momentum-coupling coefficients, the ion-neutral collision frequency ν_{in}, the electron-neutral collision frequency ν_{en}, and the electron-ion collision frequency ν_{ei} are given by

$$\nu_{in} = n_n n_i s_{ni}/\rho_i = 1.2\times10^{-32}\{[N+O] + 1.6[N_2+O_2+NO]\}[N^+ + O^+ + NO^+]/\rho_i$$
$$+ 4.8\times10^{-32}(kT_n+kT_i)^{0.375}\{1.2[N][N^+] + [O][O^+] + 0.84[NO][NO^+]\}/\rho_i,$$

$$\nu_{en} = n_n n_e s_{ne}/\rho_e = 8.1\times10^{-8} \; (kT_e)^{0.64} n_n,$$

$$\nu_{ei} = n_i n_e s_{ie}/\rho_e = 3.5\times10^{-5} \; (kT_e)^{-1.5} n_i, \qquad (5\text{-}31) \star\star\star$$

where kT_n, kT_i, and kT_e are in eV and the other quantities are in cgs units.

REFERENCES

1. Goldstein, H., Classical Mechanics, Addison-Wesley, Reading, Mass., 1950.

2. McDaniel, E. W., and E. A. Mason, The Mobility and Diffusion of Ions in Gases, Wiley, New York, 1973.

3. Desloge, E. A., Exchange of Energy between Gases at Different Temperatures, Phys. Fluids, 5, 1223-1225 (1962).

4. Phelps, A. V., Electron Collision Frequencies and Radio-Frequency Absorption, Chapter 21 in Defense Nuclear Agency Reaction Rate Handbook, Second Edition, DNA 1948H, edited by M. H. Bortner and T. Baurer, General Electric TEMPO, Santa Barbara, 1972.

5. Itikawa, Y., Momentum-transfer Cross Sections for Electron Collisions with Atoms and Molecules, Atomic Data Nucl. Data Tables, 14, 1-10 (1974).

6. Bederson, B., and L. J. Kieffer, Total Electron-Atom Collision Cross Sections at Low Energies—a Critical Review, Rev. Mod. Phys., 43, 601-640 (1971).

7. Longmire, C. L., Elementary Plasma Physics, Interscience, New York, 1963.

8. Spitzer, L., Jr., Physics of Fully Ionized Gases, Second Edition, Interscience, New York, 1962.

9. Vogt, E., and G. H. Wannier, Scattering of Ions by Polarization Force, Phys. Rev., 95, 1190-1198 (1954).

10. McDaniel, E. W., Collision Phenomena in Ionized Gases, Wiley, New York, 1964.

11. Wannier, G. H., Statistical Physics, Wiley, New York, 1966.

12. Langevin, P., Une Formule Fondamentale de Théorie Cinétique, Annales Chim. Phys., Ser. 8, 5, 245-288 (1905), [English translation in Ref. 10, Appendix II].

13. Dalgarno, A., M.R.C. McDowell, and A. Williams, Philos. Trans. Roy. Soc. (London), A 250, 411-425 (1958).
Dalgarno, A., The Mobilities of Ions in their Parent Gases, ibid., 426-429.

14. Mason, E. A., Estimated Ion Mobilities for some Air Constituents, Planet. Space Sci., 18, 137-144 (1970).

15. Gilmore, F. R., Basic Energy-level and Equilibrium Data, Chapter 10 in Defense Nuclear Agency Reaction Rate Handbook, second edition, DNA 1948H, edited by M. H. Bortner and T. Baurer, General Electric TEMPO, Santa Barbara, 1972. See Figures 10-5 to 10-7 and Table 10-1.

16. Mason, E. A., and J. T. Vanderslice, Mobility of Hydrogen Ions (H^+, H_2^+, H_3^+) in Hydrogen, Phys. Rev., 114, 497-502 (1959).

17. Mason, E. A., and H. W. Schamp, Jr., Mobility of Gaseous Ions in Weak Electric Fields, Annals Phys. (N.Y.), 4, 233-270 (1958). The cross section and collision integral are also published in Ref. 2, Section 6-1 and Appendix I.

18. Hirschfelder, J. O., R. B. Bird, and E. L. Spotz, The Transport Properties for Non-polar Gases, J. Chem. Phys., 16, 968-981 (1948). The cross section given for the (12-6) potential completes the table in Ref. 17.

19. Kilb, R. W., Elastic Energy and Momentum Loss in Atom-atom Collisions above 50 eV, DNA 2876I, MRC-R-16, Mission Research Corporation, Santa Barbara, March 1972.

20. Hirschfelder, J. O., C. F. Curtiss, and R. B. Bird, Molecular Theory of Gases and Liquids, second printing, Wiley, New York, 1964, Appendix I-A.

21. Kestin, J., and W. Leidenfrost, The Viscosity of Helium, Physica (Utrecht), 25, 537-555 (1959).

22. Hilsenrath, J., et al., Tables of Thermal Properties of Gases, Circular 564, National Bureau of Standards, Washington, 1955, 488 pp.

23. Heiche, G., and E. A. Mason, Ion Mobilities with Charge Exchange, J. Chem. Phys., 53, 4687-4696 (1970), Figure 4.

24. Dickinson, A. S., The Mobility of He^+ Ions in He, J. Phys. B, 1, 387-394 (1968).

25. Orient, O. J., The Measurement of the Temperature Dependence of Atomic and Molecular Ion Mobilities in Helium, Can. J. Phys., 45, 3915-3922 (1967).

26. Smith, R. D., and J. H. Futrell, A Low Energy ICR Study of the Symmetric Charge Transfer Reaction $^3He^+ + {}^4He \rightarrow {}^4He^+ + {}^3He$, Chem. Phys. Lett., 27, 493-495 (1974).

27. Mahadevan, P., and G. D. Magnuson, Low-energy (1- to 100-eV) Charge-Transfer Cross-Section Measurements for Noble-gas-ion Collisions with Gases, Phys. Rev., 171, 103-106 (1968). We used the data points on Figure 4.

28. Cramer, W. H., and J. H. Simons, Elastic and Inelastic Scattering of Low-Velocity He^+ Ions in Helium, J. Chem. Phys., 26, 1272-1275 (1957).

29. Belyaev, V. A., B. G. Brezhnev, and E. M. Erastov, Resonant Charge Transfer of Low-energy Carbon and Nitrogen Ions, Zh. Eksp. Teor. Fiz., 54, 1720-1725 (1968) [Sov. Phys. - JETP, 27, 924-926 (1968)].

30. Hayden, H. C., and N. G. Utterback, Ionization of Helium, Neon, and Nitrogen by Helium Atoms, Phys. Rev., 135, A1575-A1579 (1964).

31. Ghosh, S. N., and W. F. Sheridan, Experimental Determinations of Charge Transfer Cross Sections and Secondary Electron Emission by Ion Bombardment, J. Chem. Phys., 26, 480-485 (1957).

32. Nagy, S. W., W. J. Savola, Jr., and E. Pollack, Measurement of the Total Cross Section for Symmetric Charge Exchange in Helium from 400-2000 eV, Phys. Rev., 177, 71-76 (1969).

33. Shelton, W. N., and P. A. Stoycheff, Measurement of the Total Cross Section for Single-Electron Transfer in Collisions of He^+ with He in the Energy Range 2-22 keV, Phys. Rev. A, 3, 613-619 (1971).

34. Stedeford, J. B. H., Further Investigations of Charge Exchange and Electron Detachment. I. Ion Energies 3 to 40 keV, Proc. Roy. Soc. (London), A 227, 466-485 (1955).

35. Barnett, C. F., and P. M. Stier, Charge Exchange Cross Sections for Helium Ions in Gases, Phys. Rev., 109, 385-390 (1958).

36. DeHeer, F. J., J. Schutten, and H. Moustafa, Ionization and Electron Capture for Helium Ions Incident on Noble and Diatomic Gases between 10 and 150 keV, Physica (Utrecht), 32, 1793-1807 (1966).

37. Fedorenko, N. V., V. V. Afrosimov, and D. M. Kaminker, Electron Capture and Ionization in the Interaction of Singly Charged Positive Ions with Gas Atoms, Zh. Tekh. Fiz., 26, 1929 (1956) [Sov. Phys.-Tech. Phys., 1, 1861-1871 (1957)].

38. Jones, P. R., F. P. Ziemba, H. A. Moses, and E. Everhart, Total Cross Sections for Multiple Electron Stripping in Atomic Collisions at Energies to 100 keV, Phys. Rev., 113, 182-191 (1959).

39. Allison, S. K., J. Cuevas, and P. G. Murphy, Experimental Cross Sections for Charge-changing Collisions of He^{+} and He^{++} Ions Traversing Gases, Phys. Rev., 102, 1041-1048 (1956).

40. Nikolaev, V. S., I. S. Dmitriev, L. N. Fateeva, and Ya. A. Teplova, Experimental Investigation of Electron Capture by Multiply Charged Ions, Zh. Eksp. Teor. Fiz., 40 (1961) [Sov. Phys.-JETP, 13, 695-702 (1961)].

41. Rapp, D., and W. E. Francis, Charge Exchange between Gaseous Ions and Atoms, J. Chem. Phys., 37, 2631-2645 (1962).

42. Stebbings, R. F., A. C. H. Smith, and H. Ehrhardt, Charge Transfer between Oxygen Atoms and O^{+} and H^{+} Ions, J. Geophys. Res., 69, 2349-2355 (1964).

43. Rutherford, J. A., and D. A. Vroom, The Reaction of Atomic Oxygen with Several Atmospheric Ions, J. Chem. Phys., 61, 2514-2519 (1974).

44. Lo, H. H., L. Kurzweg, R. T. Brackmann, and W. L. Fite, Charge Transfer in O^{+} + O Collisions, in Sixth International Conference on the Physics of Electronic and Atomic Collisions, Abstracts of Papers, held at Cambridge, Mass., July 1969, M.I.T. Press, Cambridge, 1969, pp. 705-706.

45. Moseley, J. T., R. M. Snuggs, D. W. Martin, and E. W. McDaniel, Mobilities, Diffusion Coefficients, and Reaction Rates of Mass-identified Nitrogen Ions in Nitrogen, Phys. Rev., 178, 240-248 (1969).

46. Huntress, W. T., Jr., Ion Cyclotron Resonance Power Absorption: Collision Frequencies for CO_2^{+}, N_2^{+}, and H_3^{+} Ions in Their Parent Gases, J. Chem. Phys., 55, 2146-2155 (1971).

47. Kobayashi, N., Low Energy Ion-Neutral Reactions. VI. Ar^{+} + Ar, N_2^{+} + N_2, O_2^{+} + O_2, and CO^{+} + CO, J. Phys. Soc. Jap., 38, 519-523 (1975).

48. Tiernan, T. O., private communication summarized in Chapter 18B of Defense Nuclear Agency Reaction Rate Handbook, second edition, DNA 1948H, edited by M. H. Bortner and T. Baurer, General Electric TEMPO, Santa Barbara, 1974.

49. Nichols, B. J., and F. C. Witteborn, Measurements of Resonant Charge Exchange Cross Sections in Nitrogen and Argon between 0.5 and 17 eV, NASA TN D-3265, National Technical Information Service, Springfield, VA, 1966.

50. Leventhal, J. J., T. F. Moran, and L. Friedman, Molecular Resonant Charge-Transfer Processes; H_2^+-H_2 and N_2^+-N_2, J. Chem. Phys., 46, 4666-4672 (1967).

51. Stebbings, R. F., B. R. Turner, and A. C. H. Smith, Charge Transfer in Oxygen, Nitrogen, and Nitric Oxide, J. Chem. Phys., 38, 2277-2279 (1963).

52. Maier, W. B. II, Reactions between Isotopically Labeled N_2^+ and N_2 for Primary Ion Energies below 45 eV, J. Chem. Phys., 61, 3459-3470, (1974).

53. Gustafsson, E., and E. Lindholm, Ionization and Dissociation of H_2, N_2, and CO in Charge Exchange Collisions with Positive Ions, Arkiv Fys., 18, 219-239 (1960).

54. Amme, R. C., and N. G. Utterback, Effects of Ion Beam Excitation on Charge Transfer Cross Section Measurements, in abstracts of papers of the 3rd International Conference on the Physics of Electronic and Atomic Collisions, held at London, July 1963 (Atomic Collision Processes), North-Holland, Amsterdam, 1964, pp. 847-853.

55. Savage, H. F., and F. C. Witteborn, Charge-exchange Cross Sections of N_2^{2+} in N_2, CO_2, and Ar and Contamination of N^+ Beams by N_2^{2+}, J. Chem. Phys., 48, 1872-1874 (1968).

56. Neff, S. H., Excitation in Atomic Collisions Related to Meteor Radiation, Astrophys. J., 140, 348-360 (1964).

57. McGowan, W., and L. Kerwin, Collisions of Long-lived Excited Ions of Oxygen and Nitrogen, Can. J. Phys., 42, 2086-2101 (1964).

58. Flannery, M. R., P. C. Cosby, and T. F. Moran, Molecular Charge Transfer: Experimental and Theoretical Investigation of the Role of Incident-ion Vibrational States in N_2^+-N_2 and CO^+-CO Collisions, J. Chem. Phys., 59, 5494-5510 (1973).

59. Snuggs, R. M., D. J. Volz, J. H. Schummers, D. W. Martin, and E. W. McDaniel, Mobilities and Longitudinal Diffusion Coefficients of Mass-Identified Potassium Ions and Positive and Negative Oxygen Ions in Oxygen, Phys. Rev. A, 3, 477-487 (1971).

60. Varney, R. N., Monatomic and Diatomic Ions in Oxygen, Phys. Rev. A, 2, 370-378 (1970).

61. Ghosh, S. N., and W. F. Sheridan, Cross Sections of Certain Charge Transfer Reactions, J. Chem. Phys., 27, 1436-1437 (1957).

62. Moran, T. F., M. R. Flannery, and P. C. Cosby, Molecular Charge Transfer. II. Experimental and Theoretical Investigation of the Role of Incident-ion Vibrational States in O_2^+-O_2 and NO^+-NO Collisions, J. Chem. Phys., 61, 1261-1273 (1974).

63. Volz, D. J., J. H. Schummers, R. D. Laser, D. W. Martin, and E. W. McDaniel, Mobilities and Longitudinal Diffusion Coefficients of Mass-identified Potassium Ions and Positive Nitric Oxide Ions in Nitric Oxide, Phys. Rev. A, 4, 1106-1109 (1971).

64. Henglein, A., and G. A. Muccini, Mass Spectrometric Observation of Electron and Proton Transfer Reactions between Postive Ions and Neutral Molecules, Z. Naturforsch., 17a, 452-460 (1962).

65. Bortner, M. H., R. H. Kummler, and T. Baurer, Summary of Suggested Rate Constants, Chapter 24 in Defense Nuclear Agency Reaction Rate Handbook, second edition, DNA 1948H, edited by M. H. Bortner and T. Baurer, General Electric TEMPO, Santa Barbara, 1972.

66. Neynaber, R. H., Intelcom Rad Tech, private communication, Jan. 1975.

67. Lo, H. H., and W. L. Fite, Electron-capture and Loss Cross Sections for Fast Heavy Particles Passing through Gases, Atomic Data, 1, 305-328 (1970). This review is also given in:
Fite, W. L., J. S. Greene, A. W. Ali, I. M. Pikus, Kinetics of High-energy Heavy-particle Collisional Processes, Chapter 15 in Defense Nuclear Agency Reaction Rate Handbook, second edition, edited by M. H. Bortner and T. Baurer, General Electric TEMPO, Santa Barbara, 1972. The reference given here to the original source of the $N^+ + O$ cross sections appears to be incorrect.

68. Neynaber, R. H., J. A. Rutherford, and D. A. Vroom, New Atomic Beam Studies at Low Energies, DNA 3384F, INTEL-RT 8100-005, Intelcom Rad Tech, San Diego, Aug. 1974. Submitted to J. Chem. Phys.

69. Maier, W. B. II, and E. Murad, Study of Collisions between Low-energy N^+ and N_2: Reaction Cross Sections, Isotopic Compositions, and Kinetic Energies of the Products, J. Chem. Phys., 55, 2307-2316 (1971).

70. Neynaber, R. H., J. A. Rutherford, and D. A. Vroom, Electronic and Ionic Reactions in Atmospheric Gases, DNA 2753F, Gulf-RT-A10767, Gulf Radiation Technology, San Diego, July 1971. This cross section is also plotted in Ref. 69.

71. Neynaber, R. H., J. A. Rutherford, and D. A. Vroom, Study of Ion-neutral Reactions of Importance in the Upper Atmosphere, DNA 3134F, INTEL-RT 8086-003, Intelcom Rad Tech, San Diego, July 1973, p. 28.

72. Ormrod, J. H., and W. L. Michel, Charge Equilibrium Fractions and Charge-exchange Cross Sections for Fast Ions in Nitrogen and Argon, Can. J. Phys., 49, 606-620 (1971).

73. Brackmann, R. T., and W. L. Fite, Experimental Research on Collisions of Heavy Particles at Energies up to 2 MeV, AFWL-TR-68-96, Air Force Weapons Laboratory, Kirtland AFB, N.M., Oct. 1968. The cross sections reported here are also published in Ref. 67.

74. Kretschmer, C. B., and H. L. Petersen, Use of Langmuir Probes to Study Ion-electron Recombination, J. Appl. Phys., 34, 3209-3217 (1963).

75. Ferguson, E. E., F. C. Fehsenfeld, P. D. Goldan, A. L. Schmeltekopf, and H. I. Schiff, Laboratory Measurement of the Rate of the Reaction $N_2^+ + O \rightarrow NO^+ + N$ at Thermal Energy, Planet. Space Sci., 13, 823-827 (1965).

76. Dunkin, D. B., F. C. Fehsenfeld, A. L. Schmeltekopf, and E. E. Ferguson, Ion-molecule Reaction Studies from 300° to 600°K in a Temperature-controlled Flowing Afterglow System, J. Chem. Phys., 49, 1365-1371 (1968).

77. Ferguson, E. E., D. K. Bohme, F. C. Fehsenfeld, and D. B. Dunkin, Temperature Dependence of Slow Ion-atom Interchange Reactions, J. Chem. Phys., 50, 5039-5040 (1969).

78. Smith, D., and R. A. Fouracre, The Temperature Dependence of the Reaction Rate Coefficients of O^+ Ions with Molecular Oxygen and Nitrogen, Planet. Space Sci., 16, 243-252 (1968).

79. Copsey, M. J., D. Smith, and J. Sayers, Laboratory Afterglow Studies of O^+ Ions in Helium-oxygen and Helium-oxygen-nitrogen Mixtures, Planet. Space Sci., 14, 1047-1055 (1966).

80. Lindinger, W., F. C. Fehsenfeld, A. L. Schmeltekopf, and E. E. Ferguson, Temperature Dependence of Some Ionospheric Ion-neutral Reactions from 300° - 900°K, J. Geophys. Res., 79, 4753-4756 (1974).

81. Warneck, P., Studies of Ion-neutral Reactions by a Photoionization-Mass Spectrometer Technique-III. Several Ionospheric Reactions, Planet. Space Sci., 15, 1349-1359 (1967).

82. Pharo, M. W. III, L. R. Scott, H. G. Mayr, L. H. Brace, and H. A. Taylor, Jr., An Experimental Study of the Ion Chemistry and Thermal Balance in the E- and F-Regions above Wallops Island, Planet. Space Sci., 19, 15-25 (1971).

83. Johnsen, R., and M. A. Biondi, Measurements of the $O^+ + N_2$ and $O^+ + O_2$ Reaction Rates from 300°K to 2 eV, J. Chem. Phys., 59, 3504-3509 (1973).

84. McFarland, M., D. L. Albritton, F. C. Fehsenfeld, E. E. Ferguson, and A. L. Schmeltekopf, Flow-drift Technique for Ion Mobility and Ion-molecule Reaction Rate Constant Measurements. II. Positive Ion Reactions of N^+, O^+, and N_2^+ with O_2 and O^+ with N_2 from Thermal to ~2 eV, J. Chem. Phys., 59, 6620-6628 (1973).

85. Stebbings, R. F., B. R. Turner, and J. A. Rutherford, Low-energy Collisions between some Atmospheric Ions and Neutral Particles, J. Geophys. Res., 71, 771-784 (1966).

86. Turner, B. R., Electronic and Ionic Reactions in Atmospheric Gases, DASA 2227, Defense Atomic Support Agency, Washington, Jan. 1969. The cross section reported here is also published in Ref. 67.

87. Solov'ev, E. S., R. N. Il'in, V. A. Oparin, I. T. Serenkov, and N. V. Fedorenko, Capture and Loss of Electrons by Fast Nitrogen and Oxygen Atoms and Ions in Air, Nitrogen and Oxygen, Zh. Tekh. Fiz., 42, 336-339 (1972) [Sov. Phys.-Tech. Phys., 17, 267-270 (1972)].

88. Stebbings, R. F., A. C. H. Smith, and H. B. Gilbody, Charge Transfer between some Atmospheric Ions and Atomic Oxygen, J. Chem. Phys., 38, 2280-2284 (1963).

89. Goldan, P. D., A. L. Schmeltekopf, F. C. Fehsenfeld, H. I. Schiff, and E. E. Ferguson, Thermal Energy Ion-neutral Reaction Rates. II. Some Reactions of Ionospheric Interest, J. Chem. Phys., 44, 4095-4103 (1966).

90. Warneck, P., Laboratory Rate Coefficients for Positive Ion-neutral Reactions in the Ionosphere, J. Geophys. Res., 72, 1651-1653 (1967).

91. Rutherford, J. A., Intelcom Rad Tech, private communication, Jan. 1975.

92. Turner, B. R., J. A. Rutherford, and R. F. Stebbings, Charge Transfer Reactions of Nitric Oxide with Atomic and Molecular Ions of Oxygen and Nitrogen, J. Geophys. Res., 71, 4521-4525 (1966).

93. McFarland, M., D. L. Albritton, F. C. Fehsenfeld, A. L. Schmeltekopf, and E. E. Ferguson, Energy Dependence of the Rate Constant for the Reaction $O^+ + NO \rightarrow NO^+ + O$, J. Geophys. Res., 79, 2005 (1974).

94. Ormrod, J. H., Low-energy Electronic Stopping Cross Sections in Nitrogen and Argon, Can. J. Phys., 46, 497-502 (1968).

95. Fastrup, B., A. Borup, and P. Hvelplund, Stopping Cross Section in Atmospheric Air of 0.2-0.5 MeV Atoms with $6 \leq Z \leq 24$, Can. J. Phys., 46, 489-495 (1968).

96. Weyl, P. K., The Energy Loss of Hydrogen, Helium, Nitrogen, and Neon Ions in Gases, Phys. Rev., 91, 289-296 (1953).

97. Teplova, Ya. A., V. S. Nikolaev, I. S. Dmitriev, and L. N. Fateeva, Slowing Down of Multicharged Ions in Solids and Gases, Zh. Eksp. Teor. Fiz., 42, 44-60 (1962) [Sov. Phys.-JETP, 15, 31-41 (1962)]. See Table III for N + air and Figure 6 for He + He.

98. Northcliffe, L. D., and R. F. Schilling, Range and Stopping-power Tables for Heavy Ions, Nucl. Data Tables, A7, 233-463 (1970).

APPENDIX A
GLOSSARY OF SYMBOLS

a_o	Bohr radius, 0.5292×10^{-8} cm.
A	Constant in electron-ion (Coulomb) scattering cross section, $8.06 \times 10^{17}\ \ell n(2/\theta_m)$ cm^6/sec^4 (Eq. 3-5).
$\vec{B}$	Magnetic field strength (gauss).
c	Speed of light, 2.998×10^{10} cm/sec.
d	Fractional coupling coefficient: $d_{ni}^{(n)}$, fraction of the ion-neutral frictional heating that goes into internal energy of neutrals, Eq. 2-53; $d_{ne}^{(n)}$, $d_{ie}^{(i)}$, fractional coupling coefficients for electron-neutral and electron-ion collisions, Eq. 2-54.
e	Proton charge, 4.803×10^{-10} statcoul.
	Base of natural logarithms.
$\vec{E}$	Electric field strength (statvolt/cm).
$f\left(\vec{v};\vec{V},\frac{T}{m}\right)$	Maxwell-Boltzmann velocity distribution function, Eq. 2-1; $\hat{f}_1(\vec{v}_1)$, abbreviated form defined by Eq. 2-16; $\hat{f}_2(\vec{v})$, distribution of relative velocities of pairs of particles of different species, Eq. 2-17 (sec^3/cm^6).
F(W)	Dimensionless momentum-transfer cross section for elastic atom-atom scattering, q_D/λ^2 (Eq. 3-25).
$\vec{g}$	Acceleration due to gravity (~980 cm/sec^2).

h	Planck's constant, 6.626×10^{-27} erg-sec.
$h(T_m,V)$	Rate coefficient for heat transfer due to scattering, Eq. 2-30 (see also Eq. 2-40); h_{jk}, heat-transfer coefficient for elastic scattering of neutrals of species j and ions of species k; h_{je}, h_{ke} (or h_{ie} in Section 3.2), heat-transfer coefficient for scattering of electrons and neutrals of species j or ions of species k; h_{je}, h_{ke}, heat-transfer coefficient for scattering of electrons and neutrals of species j or ions of species k; h_k^*, heat-transfer coefficient due to symmetric charge exchange of ions of species k with their parent atoms or molecules, Section 2.2b; h_{ni}, h_{ne}, h_{ie}, combined heat-transfer coefficient for ion-neutral, electron-neutral, or electron-ion collisions, Section 2.3b (cm^3/sec).
i	Specific internal energy of a gas, Section 2.1a. This is taken to include the translational kinetic energy of particle motion in the frame moving with the mean velocity $\vec{V}_1$ plus the energy of rotational excitation of molecules. Vibrational energy and ionization energy are excluded. (erg/gm)
j	Index of neutral species.
$\vec{J}$	Current density (abamp/cm^2).
k	Boltzmann constant, 1.381×10^{-16} erg/°K or 1.602×10^{-12} erg/eV.
k	Index of ion species.
$k(T_m,V)$	Reaction rate coefficient: k_s, rate coefficient for scattering collisions, Eq. 2-28, used only for inelastic collisions; k_x, rate coefficient for asymmetric charge exchange, Eq. B-8 (see also Eq. B-14) (cm^3/sec).
$K_o(T)$	Mobility of ions in a weak electric field, reduced to standard density (cm^2/statvolt-sec).
$\ell_x(T_m,V)$	Rate coefficient for specific internal energy change of a reactant due to asymmetric charge exchange, Eq. B-10 (see also Eq. B-20) (cm-sec).

m	Particle mass; m_e, electron mass; m_j, mass of a molecule of neutral species j; m_k or m_i, mass of an ion of species k (gm).
n	Number density of particles; n_e, n_i, n_n, number density of electrons, ions, or neutral molecules; $n(X_j^o)$ or n_j^o, number density of neutral species j; $n(X_k^+)$ or n_k^+, number density of ions of species k (cm^{-3}).
$p_x(T_m,V)$	Rate coefficient for velocity change of a reactant due to asymmetric charge exchange, Eq. B-9 (see also Eq. B-19) (cm-sec).
P	Fluid pressure; P_e, P_i, P_n, pressure of electrons, ions, or neutrals ($dyne/cm^2$).
q(v)	Momentum-transfer cross section of a pair of particles, Eq. 2-23; $q_{ij}(v)$, momentum-transfer cross section for elastic scattering; $q_{inel}(v)$, momentum-transfer cross section for inelastic scattering, Eq. C-3; q*(v), effective momentum-transfer cross section due to symmetric charge exchange, 2 $\sigma_x(v)$ (Eq. 2-43); $q_T(v_1)$, effective momentum-transfer cross section due to asymmetric charge exchange, $((m_1+m_2)/m_1)\ \sigma_x(v_1)$ (Eq. B-31) (cm^2).
r	Separation of two particles; r_m, separation at which their potential energy is a minimum (cm).
$s(T_m,V)$	Coupling coefficient due to scattering, Eq. 2-29 (see also Eq. 2-36); s_{jk}, coupling coefficient for elastic scattering of neutrals of species j and ions of species k; s_{je}, coupling coefficient for scattering of electrons and neutrals of species j; s_{ke}, coupling coefficient for elastic scattering of electrons and ions of species k; s_k^*, coupling coefficient due to symmetric charge exchange of ions of species k with their parent atoms or molecules, Section 2.2b; s_{ni}, s_{ne}, s_{ie}, combined coupling coefficient for ion-neutral, electron-neutral, or electron-ion collisions, Eqs. 2-48 to 2-50 ($gm-cm^3/sec$).

$S(v_1)$	Stopping cross section, $-n_2^{-1}dE_1/dx$ (Eq. C-1); $S_{inel}(v_1)$, stopping cross section due to inelastic scattering from atomic electrons (erg-cm^2/atom).
t	Time (sec).
T	Temperature; T_e, T_i, T_n, temperature of electrons, ions, or neutrals (°K or eV).
T_m	Temperature characterizing the distribution of relative velocities of pairs of particles, $(m_1T_2 + m_2T_1)/(m_1+m_2)$ (Eq. 2-21); T_{jk}, temperature characterizing the distribution of relative velocities of pairs consisting of a neutral atom or molecule of species j and and ion of species k (°K or eV).
U	Thermal speed parameter, $(2kT_1/m_1 + 2kT_2/m_2)^{1/2}$, characterizing the distribution of relative velocities of pairs of particles (Eq. 2-32) (cm/sec).
$\vec{v}$	Initial relative velocity of two particles, $\vec{v}_1-\vec{v}_2$ (Eq. 2-6); $\vec{v}'$, final relative velocity of two particles; v_t, typical relative speed, Eq. 3-4 (cm/sec).
$\vec{v}_1$	Initial velocity of first particle in the laboratory frame; $\vec{v}_1'$, final velocity of first particle (cm/sec).
$\vec{v}_{cm}$	Velocity of center of mass of two particles (cm/sec).
$\vec{V}$	Relative macroscopic velocity of two gases, $\vec{V}_1-\vec{V}_2$ (Eq. 2-20) (cm/sec).
$\vec{V}_1$	Macroscopic velocity of first gas in the laboratory frame; $\vec{V}_e$, $\vec{V}_i$, $\vec{V}_n$, macroscopic velocity of electrons, ions, or neutrals (cm/sec).
W	Dimensionless kinetic energy of a pair of particles in their center-of-mass frame, Eq. 3-24.
Z	Atomic number.

α	Angle-averaged dipole polarizability (cm^3).
γ	Dimensionless parameter measuring the relative strength of the r^{-6} and r^{-4} potential energies, Eq. 3-18.
$\delta(x)$	Dirac delta function.
$\Delta\vec{v}_1$	Change in velocity of first particle during a collision, $\vec{v}_1' - \vec{v}_1$ (cm/sec).
$\frac{\Delta\rho_x}{\Delta t}$	Rate of change of mass density due to asymmetric charge exchange, Eq. B-2 (gm/cm^3-sec).
$\frac{\Delta(\rho I)}{\Delta t}$	Rate of change of internal energy density due to scattering or symmetric charge exchange, Eq. 2-38; $\Delta(\rho I)_x/\Delta t$, rate due to asymmetric charge exchange (erg/cm^3-sec).
$\frac{\Delta\left(\frac{1}{2}\rho\overline{v^2}\right)}{\Delta t}$	Rate of change of total energy density due to scattering or symmetric charge exchange, Eq. 2-3; $\Delta\left(\frac{1}{2}\rho\overline{v^2}\right)_x/\Delta t$, rate due to asymmetric charge exchange, Eq. B-4 (erg/cm^3-sec).
$\frac{\Delta(\rho\vec{V})}{\Delta t}$	Rate of change of momentum density due to scattering or symmetric charge exchange, Eq. 2-2; $\Delta(\rho\vec{V})_x/\Delta t$, rate due to asymmetric charge exchange, Eq. B-3 ($dyne/cm^3$).
ε	Loss (or gain, if $\varepsilon<0$) of kinetic energy by a pair of particles in a collision; ε_ℓ, loss of kinetic energy in a collision in which the final states of the particles are specified by ℓ (erg).
ε	Depth of potential energy well of a pair of particles (erg or eV) (used in Section 3.3b).
ε_0	Scaling factor for energy, Eq. 3-23 (erg or keV).
η	Electrical resistivity, $(c^2/e^2)(s_{ie}+n_e^{-1}\sum_j n_j s_{je})$ Eq. 3-22); η_{ei}, resistivity transverse to a strong magnetic field, $(4/3)(2\pi m_e)^{1/2}e^2c^2\ln(2/\theta_m)/(kT)^{3/2}$ (cm^2/sec, emu).

θ	Zenithal scattering angle in the center-of-mass frame, defined by diagram in Section 2.1b; θ_m, minimum scattering angle, Eq. 3-2.
λ	Scaling factor for length, Eq. 3-22 (cm).
λ_D	Debye shielding distance, $(kT_e/4\pi e^2 n_e)^{1/2}$ (cm).
μ	Reduced mass of a pair of particles, $m_1 m_2/(m_1+m_2)$ (Eq. 2-4) (gm).
ν_{ei}	Average momentum-loss collision frequency for electron-ion collisions, Eq. 5-5; ν_{ej}, average momentum-loss collision frequency for collisions of electrons with neutrals of species j, Eq. 5-6 (sec^{-1}).
ξ	Dimensionless relative velocity of two particles, Eq. 2-31.
ρ	Mass density; ρ_e, ρ_i, ρ_n, mass density of electrons, ions, or neutrals (gm/cm^3).
$\sigma(v)$	Total cross section; $\sigma_t(v)$, total scattering cross section, Eq. 2-22, used only for inelastic collisions; $\sigma_x(v)$, total cross section for charge exchange (cm^2).
$\frac{d\sigma}{d\Omega}(v,\theta)$	Differential scattering cross section in the center-of-mass frame (Reference 1) (cm^2/sterad).
τ	Collision temperature for collisions between two species, Eqs. 5-2 and 5-3 (erg or eV).
ϕ	Azimuthal scattering angle in the center-of-mass frame, measured around the $\vec{v}$ axis.
$\Phi(r)$	Potential energy of a pair of particles (erg).
Ω	Solid angle (sterad).

APPENDIX B

MOMENTUM AND ENERGY TRANSFER BY CHARGE-EXCHANGE REACTIONS

(a) Statement of the Problem

Asymmetric charge-exchange reactions require a more general treatment than that given in Section 2.2(b) for symmetric ones. We consider reactions of the form

$$\underset{1}{A^+} + \underset{2}{B} \rightarrow \underset{3}{A} + \underset{4}{B^+} - \epsilon ; \qquad \text{(B-1)}$$

we will sometimes refer to the species by the numbers given underneath them. The quantity ϵ again denotes the loss (or gain) of kinetic energy of the pair of particles, which for endothermic reactions equals the ionization energy of species B less that of A (if A^+ and B^+ are in their ground states). We assume that this is negligible, that is, $|\epsilon| \ll \frac{1}{2}\mu v^2$.

We further assume that charge exchange results only in forward scattering ($\theta \ll 1$); this approximation is good at energies above 0.1 eV. While it would be easy enough to account for non-forward scattering, we have found no theoretical or experimental studies of the differential cross section for charge exchange at energies below 0.1 eV.

The total cross section for charge exchange is denoted by $\sigma_x(v)$ (analogous to $\sigma_t(v)$, Eq. 2-22). The rates of change due to charge exchange of the densities of mass, momentum, and total energy of species A^+ are

$$\frac{\partial \rho_{1x}}{\partial t} = - \int m_1 f_1(\vec{v}_1) f_2(\vec{v}_2) v \sigma_x(v) d^3v_1 d^3v_2 \quad , \qquad \text{(B-2)}$$

$$\frac{\Delta(\rho_1 \vec{V}_1)_x}{\Delta t} = - \int m_1 \vec{v}_1 f_1(\vec{v}_1) f_2(\vec{v}_2) v\sigma_x(v) d^3v_1 d^3v_2 \quad , \qquad \text{(B-3)}$$

$$\frac{\Delta\left(\frac{1}{2} \rho_1 \overline{v_1^2}\right)_x}{\Delta t} = - \int \frac{1}{2} m_1 v_1^2 f_1(\vec{v}_1) f_2(\vec{v}_2) v\sigma_x(v) d^3v_1 d^3v_2 \quad . \qquad \text{(B-4)}$$

For the product species A the corresponding rates are

$$\frac{\Delta\rho_{3x}}{\Delta t} = - \frac{\Delta\rho_{1x}}{\Delta t} \quad , \qquad \text{(B-5)}$$

$$\frac{\Delta(\rho_3 \vec{V}_3)}{\Delta t} = \int m_1 \vec{v}_1' f_1(\vec{v}_1) f_2(\vec{v}_2) v\sigma_x(v) d^3v_1 d^3v_2 \quad , \qquad \text{(B-6)}$$

$$\frac{\Delta\left(\frac{1}{2} \rho_3 v_3^2\right)_x}{\Delta t} = \int \frac{1}{2} m_1 v_1'^2 f_1(\vec{v}_1) f_2(\vec{v}_2) v\sigma_x(v) d^3v_1 d^3v_2 \quad . \qquad \text{(B-7)}$$

(b) Evaluation of Integrals

The procedure for evaluating these integrals is similar to that described in more detail in Section 2.1(c). We change integration variables from $\vec{v}_1$, $\vec{v}_2$ to $\vec{v}_1$, $\vec{v}$ and integrate over d^3v_1 in Eqs. B-2 to B-4. The integrals over d^3v are then expressed in terms of the following three rate coefficients. The rate coefficient for the charge exchange reaction is defined analogously to Eq. 2-28:

$$k_x(T_m, V) \equiv \frac{1}{n_2} \int \hat{f}_2(\vec{v}) \sigma_x(v) v d^3v \quad . \qquad \text{(B-8)}$$

We also define two related coefficients by

$$p_x(T_m, V)\ \vec{V} \equiv \frac{m_1 m_2}{k(m_1 T_2 + m_2 T_1)} \frac{1}{n_2} \int \hat{f}_2(\vec{v}) \sigma_x(v) v (\vec{v} - \vec{V}) d^3v \quad , \qquad \text{(B-9)}$$

$$\ell_x(T_m,V) \equiv \frac{m_1^2 m_2^2}{2k^2(m_1T_2+m_2T_1)^2}\,\frac{1}{n_2}\int \hat{f}_2(\vec{v})\sigma_x(v)v \times\left[(\vec{v}-\vec{V})^2 - \frac{3k(m_1T_2+m_2T_1)}{m_1m_2}\right] d^3v \quad . \qquad \text{(B-10)}$$

Note that k_x is in cm^3/sec, while p_x and ℓ_x are in cm-sec. We will show that p_x and ℓ_x can be interpreted as the rate coefficient for velocity change of a reactant and that for specific internal energy change.

We do the angular parts of these integrals as in Section 2.1(c). The integral in Eq. B-9 is parallel to the $\vec{V}$ direction. We again use the abbreviation $\vec{V} = \vec{V}_1 - \vec{V}_2$ and eliminate the mean temperature T_m in favor of the related thermal speed parameter (Eq. 2-32)

$$U = \sqrt{\frac{2kT_1}{m_1} + \frac{2kT_2}{m_2}} \quad .$$

The result for $k_x(T_m,V)$ has a form identical to that of Eq. 2-35 for $k_s(T_m,V)$:

$$k_x(T_m,V) = \begin{cases} \dfrac{1}{\sqrt{\pi}}\dfrac{U^2}{V}\displaystyle\int_0^\infty \sigma_x(U\xi)\xi^2\left[e^{-(\xi-V/U)^2} - e^{-(\xi+V/U)^2}\right]d\xi & \text{if } T_m > 0 \text{ and } V > 0, \\ \dfrac{4}{\sqrt{\pi}}U\displaystyle\int_0^\infty \sigma_x(U\xi)\xi^3 e^{-\xi^2}\,d\xi & \text{if } V = 0\ , \\ V\sigma_x(V) & \text{if } T_m = 0\ . \end{cases} \qquad \text{(B-11)}$$

The results for the other rate coefficients are

$$p_x(T_m,V) = \begin{cases} \dfrac{2}{\sqrt{\pi}} \dfrac{U^2}{V^3} \displaystyle\int_0^\infty \sigma_x(U\xi)\left[\left(\frac{V}{U}\xi^3 - \frac{V^2}{U^2}\xi^2 - \frac{1}{2}\xi^2\right) e^{-(\xi-V/U)^2}\right. \\ \qquad \left. +\left(\frac{V}{U}\xi^3 + \frac{V^2}{U^2}\xi^2 + \frac{1}{2}\xi^2\right) e^{-(\xi+V/U)^2}\right] d\xi \\ \qquad\qquad \text{if } T_m > 0 \text{ and } V > 0, \\ \dfrac{16}{3\sqrt{\pi}} \dfrac{1}{U} \displaystyle\int_0^\infty \sigma_x(U\xi)\left(\xi^5 - \frac{3}{2}\xi^3\right) e^{-\xi^2} d\xi \qquad \text{if } T_m > 0 \text{ and } V = 0, \\ \dfrac{\sigma_x(V)}{V} + \dfrac{d\sigma_x}{dv}(V) \qquad \text{if } T_m = 0 \text{ and } V > 0, \end{cases}$$

(B-12)

$$\nu_x(T_m,V) = \begin{cases} \dfrac{2}{\sqrt{\pi}} \dfrac{1}{V} \displaystyle\int_0^\infty \sigma_x(U\xi)\left[\left(\xi^4 - 2\frac{V}{U}\xi^3 + \frac{V^2}{U^2}\xi^2 - \frac{1}{2}\right) e^{-(\xi-V/U)^2}\right. \\ \qquad \left. +\left(-\xi^4 - 2\frac{V}{U}\xi^3 - \frac{V^2}{U^2}\xi^2 + \frac{1}{2}\xi^2\right) e^{-(\xi+V/U)^2}\right] d\xi \\ \qquad\qquad T_m > 0 \text{ and } V > 0, \\ \dfrac{3}{2} p_x(T_m,0) \qquad \text{if } T_m > 0 \text{ and } V = 0, \\ \dfrac{\sigma_x(V)}{V} + 2\dfrac{d\sigma_x}{dv}(V) + \dfrac{1}{2} V \dfrac{d^2\sigma_x}{dv^2}(V) \qquad \text{if } T_m = 0 \text{ and } V > 0. \end{cases}$$

(B-13)

(c) Results for Reactant Species

The time rates of change due to charge exchange of the densities of mass, momentum, and total energy of the first gas are

$$\frac{\Delta\rho_{1x}}{\Delta t} = - n_1 n_2 m_1 k_x(T_m,V) \quad , \tag{B-14}$$

$$\frac{\Delta(\rho_1\vec{V}_1)_x}{\Delta t} = - n_1 n_2 [k_x(T_m,V) m_1\vec{V}_1 + p_x(T_m,V)kT_1\vec{V}] \quad , \tag{B-15}$$

$$\frac{\Delta\left(\frac{1}{2}\rho_1\overline{v_1^2}\right)_x}{\Delta t} = - n_1 n_2 \left[\left(\frac{1}{2} m_1 V_1^2 + \frac{3}{2} kT_1\right)k_x(T_m,V) + p_x(T_m,V)kT_1\vec{V}\cdot\vec{V}_1 + \frac{(kT_1)^2}{m_1}\ell_x(T_m,V)\right] . \tag{B-16}$$

We again split the total energy into macroscopic kinetic energy and internal energy as in Eq. 2-38. The macroscopic kinetic energy is now found by

$$\begin{aligned}\frac{\Delta\left(\frac{1}{2}\rho_1 V_1^2\right)_x}{\Delta t} &= \frac{1}{2}\frac{\Delta[(\rho_1 V_1)^2/\rho_1]_x}{\Delta t} \\ &= \frac{\Delta(\rho_1\vec{V}_1)_x}{\Delta t}\cdot\vec{V}_1 - \frac{1}{2}V_1^2\frac{\Delta\rho_{1x}}{\Delta t} \\ &= - n_1 n_2 [k_x(T_m,V)\ \frac{1}{2} m_1 V_1^2 + p_x(T_m,V)kT_1\vec{V}\cdot\vec{V}_1] \quad ,\end{aligned} \tag{B-17}$$

so the rate of change due to charge exchange of the internal energy density of the first species is

$$\frac{\Delta(\rho_1 I_1)_x}{\Delta t} = - n_1 n_2 \left[\frac{3}{2} kT_1 k_x(T_m,V) + \frac{(kT_1)^2}{m_1}\ell_x(T_m,V)\right] . \tag{B-18}$$

The quantity $p_x(T_m,V)$ might be considered to be the rate coefficient for velocity change of a reactant because

$$\frac{\Delta\vec{V}_{1x}}{\Delta t} = \frac{1}{\rho_1}\left[\frac{\Delta(\rho_1\vec{V}_1)_x}{\Delta t} - \vec{V}_1\,\frac{\Delta\rho_{1x}}{\Delta t}\right]$$

$$= -\,n_2 p_x(T_m,\vec{V})\,\frac{kT_1}{m_1}\,\vec{V} \quad . \tag{B-19}$$

This rate coefficient $p_x(T_m,V)$ can be positive or negative. If $\sigma_x(v)$ is inversely proportional to v (say $\sigma_x(v) = K_o/v$), then $p_x(T_m,V)$ and $\Delta\vec{V}_{1x}/\Delta t$ are zero (see definitions B-9 and 2-17 of $p_x(T_m,V)$ and $\hat{f}_2(\vec{v})$); in this case every particle of the first species has the same probability per unit time of charge exchange (n_2K_o). In general, $p_x(T_m,V)$ is positive if $v\sigma_x(v)$ is an increasing function of v (as is usual for symmetric charge exchange, such as Figures 4-1 to 4-4) and is negative if $v\sigma_x(v)$ is a decreasing function.

Similarly we note that

$$\frac{\Delta I_{1x}}{\Delta t} = \frac{1}{\rho_1}\left[\frac{\Delta(\rho_1 I_1)_x}{\Delta t} - I_1\,\frac{\Delta\rho_{1x}}{\Delta t}\right]$$

$$= -\,n_2\,\frac{(kT_1)^2}{m_1^2}\,\ell_x(T_m,V) \quad , \tag{B-20}$$

where we have taken $I_1 = \frac{3}{2}\,kT_1/m_1$. One could call $\ell_x(T_m,V)$ a rate coefficient for specific internal energy change of a reactant. If $\sigma_x(v)$ is inversely proportional to v, then $\ell_x(T_m,V)$ and $\Delta I_{1x}/\Delta t$ are zero (see definition B-10).

(d) Results for Product Species

The relations for product species are quite similar to those for reactant species because of our assumptions mentioned earlier that charge exchange results only in direct forward scattering ($\theta << 1$) and that the energy defect is negligible ($|\varepsilon| << \frac{1}{2}\mu v^2$). In this case the rates for the product that has particle mass m_1 simplify to

$$\frac{\Delta\rho_{3x}}{\Delta t} = -\frac{\Delta\rho_{1x}}{\Delta t} \quad , \tag{B-21}$$

$$\frac{\Delta(\rho_3\vec{V}_3)_x}{\Delta t} = -\frac{\Delta(\rho_1\vec{V}_1)_x}{\Delta t} \quad , \tag{B-22}$$

$$\frac{\Delta\left(\frac{1}{2}\rho_3\overline{v_3^2}\right)_x}{\Delta t} = -\frac{\Delta\left(\frac{1}{2}\rho_1\overline{v_1^2}\right)_x}{\Delta t} + \frac{m_2}{(m_1+m_2)}\frac{\varepsilon}{m_1}\frac{\Delta\rho_{1x}}{\Delta t} \quad . \tag{B-23}$$

The last term of Eq. B-23 represents a part of the energy loss (or gain) occurring in each reaction (compare Eqs. 2-37 and 2-40); it need be included only if strict energy conservation is demanded.

We again split the total energy $\frac{1}{2}\rho_3\overline{v_3^2}$ into macroscopic kinetic energy and internal energy as in Eq. 2-38. The macroscopic kinetic energy is

$$\begin{aligned}\frac{\Delta\left(\frac{1}{2}\rho_3 V_3^2\right)_x}{\Delta t} &= \frac{1}{2}\frac{\Delta\left[(\rho_3 V_3)^2/\rho_3\right]_x}{\Delta t} \\ &= \frac{\Delta(\rho_3 V_3)_x}{\Delta t}\cdot\vec{V}_3 - \frac{1}{2}V_3^2\frac{\Delta\rho_{3x}}{\Delta t} \\ &= -\vec{V}_3\cdot\frac{\Delta(\rho_1\vec{V}_1)_x}{\Delta t} + \frac{1}{2}V_3^2\frac{\Delta\rho_{1x}}{\Delta t} \quad .\end{aligned} \tag{B-24}$$

For the internal energy of this product species the rate of change due to charge exchange is

$$\frac{\Delta(\rho_3 I_3)_x}{\Delta t} = \frac{\Delta\left(\frac{1}{2}\rho_3\overline{v_3^2}\right)_x}{\Delta t} - \frac{\Delta\frac{1}{2}\left(\rho_3 V_3^2\right)_x}{\Delta t} \quad ,$$

and after substitution of Eqs. B-23, B-24, 2-38, and B-17 this becomes

$$\frac{\Delta(\rho_3 I_3)_x}{\Delta t} = -\frac{\Delta(\rho_1 I_1)_x}{\Delta t} + (\vec{V}_3 - \vec{V}_1)\cdot\frac{\Delta(\rho_1\vec{V}_1)_x}{\Delta t} + \frac{1}{2}(V_1^2 - V_3^2)\frac{\Delta\rho_{1x}}{\Delta t} + \frac{m_2}{(m_1+m_2)}\frac{\epsilon}{m_1}\frac{\Delta\rho_{1x}}{\Delta t} \quad . \tag{B-25}$$

The total power per unit volume transferred by charge exchange from the total energy of both reacting gases to ionization energy is (compare Eq. 2-41)

$$-\frac{\Delta\left(\frac{1}{2}\rho_1\overline{v_1^2}\right)_x}{\Delta t} - \frac{\Delta\left(\frac{1}{2}\rho_2\overline{v_2^2}\right)_x}{\Delta t} - \frac{\Delta\left(\frac{1}{2}\rho_3\overline{v_3^2}\right)_x}{\Delta t} - \frac{\Delta\left(\frac{1}{2}\rho_4\overline{v_4^2}\right)}{\Delta t} = n_1 n_2 \epsilon k_x(T_m, V) \quad . \tag{B-26}$$

One hydrocode that uses a finite-difference scheme (the MICE code) uses a special technique when two fluid elements having different velocities are to be combined: it conserves kinetic energy, as well as mass, total energy, and the direction of momentum, and sacrifices conservation of the magnitude of momentum. Use of this technique modifies Eqs. B-24, B-25, and B-22.

(e) A Simpler Approximation

We present a simplified treatment that uses only the ordinary rate coefficient for a charge-exchange reaction instead of three rate coefficients.

Much simplification results if one assumes that the momentum and internal energy densities of reactant species can be approximated by

$$\frac{\Delta(\rho_1 \vec{V}_1)_x}{\Delta t} \approx V_1 \frac{\Delta \rho_{1x}}{\Delta t} \tag{B-27}$$

and

$$\frac{\Delta(\rho_1 I_1)_x}{\Delta t} \approx \frac{3}{2} \frac{kT_1}{m_1} \frac{\Delta \rho_{1x}}{\Delta t} \quad . \tag{B-28}$$

The neglect of terms $\rho_1 \Delta V_{1x}/\Delta t$ and $\rho_1 \Delta I_{1x}/\Delta t$ in these relations is equivalent to ignoring the rate coefficients $p_x(T_m,V)$ and $\ell_x(T_m,V)$, respectively (Eqs. B-19 and B-20). This fact enables one to simplify the other relations in the preceding two subsections.

This approximation is also equivalent to assuming that the particles that charge-exchange have the same mean velocity and specific internal energy as the rest of their species. The direction or sign of the neglected terms can be seen from subsection (c): for example, if $\sigma_x(v)v$ is an increasing function of v, then $\rho_1 \Delta V_{1x}/\Delta t$ is in the direction of $\vec{V}_2 - \vec{V}_1$.

(f) Comparing the Effect of Charge Exchange with that of Scattering

Finally, we ask how to compare the effects of asymmetric charge exchange with those due to scattering and symmetric charge exchange. First note that the former causes transfer of mass between ions and neutrals while the latter two do not. Then for comparing momentum transfer, consider the following experiment.

A beam of ions of one species is incident with speed V_1 on a cold stationary gas of a second species. While the first gas traverses

a distance $\Delta x = V_1 \Delta t$, charge exchange changes its momentum density at a distance rate

$$\frac{\Delta(\rho_1 V_{1x})}{\Delta x} = - n_1 m_1 V_1 n_2 \sigma_x(V_1) \; ; \qquad \text{(B-29)}$$

this can be obtained from Eqs. B-15 and B-11c with $T_1 = 0$, $T_2 = 0$, and $V_2 = 0$. For comparison scattering off the second gas changes this momentum density at a rate given by Eq. 2-36, which in this case can be rewritten as

$$q(V_1) = - \frac{(m_1+m_2)}{n_1 n_2 m_1 m_2 V_1} \frac{\Delta(\rho_1 V_1)}{\Delta x} \quad . \qquad \text{(B-30)}$$

This could be considered a definition of the momentum-transfer cross section q.

We have extended this relation to define an effective momentum-transfer cross section for charge exchange $q_T(V_1)$. Using Eq. B-29 one finds that

$$q_T(V_1) = \frac{(m_1+m_2)}{m_2} \sigma_x(V_1) \quad . \qquad \text{(B-31)}$$

This definition is consistent with that of the momentum-transfer cross section for symmetric charge exchange $q^*(v)$ (Eq. 2-43). The relative importance of scattering and charge exchange in transferring momentum is seen by comparing q_T with q_D and q_{inel} (see Figures 4-5 to 4-8). Note that this comparison applies only to the momentum change of the ions because definition B-31 is asymmetric between the two species. Also the comparison applies strictly only in this experiment, in which $T_1 = 0$, $T_2 = 0$, and $V_2 = 0$.

APPENDIX C
INELASTIC ION-NEUTRAL COLLISIONS ABOVE 10 keV

In collisions of atoms or ions, inelastic scattering involving excitation and ionization is important at relative speeds above 5×10^7 cm/sec (center-of-mass kinetic energy above 10 keV for N ions on N). After a high-altitude nuclear explosion such collisions are usually important only for the first second.

We use measurements of the energy loss rate dE/dx for beams of N and Aℓ ions in cold N_2 or air. The measurements of References 94 and 95 are stated in terms of the stopping cross section

$$S(v_1) \equiv -\frac{1}{n_2}\frac{dE_1}{dx} = -\frac{1}{n_2 v_1}\frac{\Delta\left(\frac{1}{2}m_1\overline{v_1^2}\right)}{\Delta t} \quad , \tag{C-1}$$

where the neutral density n_2 is in atoms/cm^3. The observed stopping cross section includes a contribution due to elastic scattering ("nuclear stopping"); this is calculated to be less than 10 percent of the total for speeds v_1 greater than 5×10^7 cm/sec (Reference 94). The remainder is due to inelastic scattering ("electronic stopping") and can be approximated by the empirical relation

$$S_{inel}(v_1) = k_o v_1^{\,P} \quad , \tag{C-2}$$

where the parameters k_o and P are given in Table C-1.

Table C-1. Parameters of the stopping cross section due to inelastic scattering as given by $S_{inel}(v_1) = k_0 v_1^p$. S_{inel} is in erg-cm^2/atom and v_1 is in cm/sec.

Colliding pair	Coefficient k_0	Exponent p	Speed range, cm/sec	Reference
N on air	4.9×10^{-34}	1.0	$5\times10^7<v_1<2.6\times10^8$	94 to 97
O on air	5.0×10^{-34}	1.0	$5\times10^7<v_1<2.5\times10^8$	94, 95
Ar on air	3.8×10^{-35}	1.14	$1.2\times10^8<v_1<3.7\times10^8$	95,97
He on He	6.1×10^{-35}	1.00	$2.7\times10^8<v_1<4.4\times10^8$	96, 97
U on N	1.8×10^{-37}	1.47	$1.5\times10^8<v_1<1.0\times10^9$	98

How is $S_{inel}(v_1)$ related to the momentum-transfer cross section $q(v,\epsilon)$? We first note that inelastic collisions involve many different kinetic energy losses ϵ, depending on the final states of the colliding particles. We denote the pair of final states by ℓ and treat the energy losses as discrete: ϵ_ℓ, $\ell = 1,2,\ldots$. The rates of energy and momentum transfer depend on two sums of cross sections:

$$q_{inel}(v) \equiv \sum_{\epsilon_\ell>0} q(v,\epsilon_\ell) \tag{C-3}$$

and the quantity $\sum_\ell \epsilon_\ell \sigma_t(v,\epsilon_\ell)$. The electronic stopping cross section $S_{inel}(v_1)$ can be related to these by Eq. 2-37 with $T_1 = 0$, $T_2 = 0$, and $\vec{V}_2 = 0$ and Eqs. 2-33c and 2-35c:

$$S_{inel}(v_1) = \frac{m_1^2 m_2}{(m_1+m_2)^2} v_1^2 q_{inel}(v_1) + \frac{m_2}{(m_1+m_2)} \sum_\ell \epsilon_\ell \sigma_t(v_1,\epsilon_\ell). \tag{C-4}$$

To evaluate $q_{inel}(v)$ we make two assumptions. At these high speeds the kinetic energy tends to dissipate in many collisions with small losses rather than in a few with big losses, so we can assume that

$$|\varepsilon_\ell| \ll \frac{1}{2} \frac{m_1 m_2}{(m_1+m_2)} v^2 \qquad \text{(C-5)}$$

whenever $\varepsilon_\ell \sigma_t(v,\varepsilon_\ell)$ is important. We further assume that scattering in these inelastic collisions is in the forward direction,

$$\theta \ll 1. \qquad \text{(C-6)}$$

From the definitions of $q_{inel}(v)$ and $\sigma_t(v,\varepsilon_\ell)$ (Eqs. C-3, 2-23, and 2-22) one then finds that

$$\sum_\ell \varepsilon_\ell \sigma_t(v,\varepsilon_\ell) = \frac{m_1 m_2}{(m_1+m_2)} v^2 q_{inel}(v) - \ldots \quad ; \qquad \text{(C-7)}$$

Approximations C-5 and C-6 imply that the correction term (indicated by dots) is small because it involves higher orders of the small quantities $2\varepsilon_\ell/\mu v^2$ and θ. It can be shown independently of approximations C-5 and C-6 that this correction term is negative, as indicated.

Combining this result with Eqs. C-4 and C-2 one finds that

$$q_{inel}(v) = \frac{(m_1+m_2)}{m_1 m_2} \frac{S_{inel}(v)}{v^2} + \ldots$$

$$\approx \frac{(m_1+m_2)}{m_1 m_2} \frac{k_o v^p}{v^2} \quad , \qquad \text{(C-8)}$$

$$\sum_\ell \varepsilon_\ell \sigma_t(v,\varepsilon_\ell) = S_{inel}(v) - \ldots$$

$$\approx k_o v^p \quad , \qquad \text{(C-9)}$$

where the neglected terms have the signs indicated.

Figures 4-2, 4-3 and 4-5 show $q_{inel}(v)$ for N, O, Aℓ, and U ions on N calculated using Eq. C-8 and Table C-1. For ion-molecule collisions we have added the appropriate ion-atom cross sections (Figures 4-6 to 4-8).

DISTRIBUTION LIST

DEPARTMENT OF DEFENSE

Director
Defense Advanced Research Projects Agency
ATTN: Strategic Tech. Office

Defense Documentation Center
12 cy ATTN: TC

Director
Defense Nuclear Agency
ATTN: STSI, Archives
ATTN: RAAE
ATTN: DDST
2 cy ATTN: STTL, Tech Lib

Commander
Field Command
Defense Nuclear Agency
ATTN: FCPR

Director
Interservice Nuclear Weapons School
ATTN: Doc Con

Chief
Livermore Division, Field Command, DNA
Lawrence Livermore Laboratory
ATTN: FCPRL

OJCS/J-3
ATTN: J-3, Ops. Anal. Br., Mr Toma

Weapons Systems Evaluation Group
ATTN: Doc. Con

DEPARTMENT OF THE ARMY

Manager
Ballistic Missile Defense Program Office
ATTN: Plans Division
ATTN: DACS-BMM

Commander
Harry Diamond Laboratories
2 cy ATTN: AMXDO-NP

Commander
TRASANA
ATTN: R. E. DeKinder, Jr.

Commander
U.S. Army Materiel Dev. & Readiness Command
ATTN: Director of Development

Commander
U.S. Army Nuclear Agency
ATTN: USANUA-W, J. Berberet

Director
Ballistic Missile Defense Advanced Tech. Center
ATTN: Mel Capps

DEPARTMENT OF THE NAVY

Chief of Naval Research
ATTN: Code 418

DEPARTMENT OF THE NAVY (Continued)

Director
Naval Research Laboratory
ATTN: Code 7700, Timothy P. Coffey

Commander
Naval Surface Weapons Center
ATTN: Code WX-21, Tech Lib

DEPARTMENT OF THE AIR FORCE

AF Cambridge Research Laboratories, AFSC
ATTN: OPR, Alva T. Stair

AF Weapons Laboratory, AFSC
ATTN: DYT, Lt Mark A. Fry
ATTN: DYT, Capt T. Johnson
ATTN: SUL

AFTAC
ATTN: TF, Maj Wiley

SAMSO/SZ
ATTN: SZJ, Maj Lawrence Doan

ENERGY RESEARCH & DEVELOPMENT ADMINISTRATION

Los Alamos Scientific Laboratory
ATTN: Doc. Con for John Zinn

DEPARTMENT OF DEFENSE CONTRACTORS

ESL, Inc.
ATTN: James Marshall

General Electric Company
Space Division
ATTN: M. H. Bortner, Space Sci. Lab.

General Electric Company
TEMPO-Center for Advanced Studies
ATTN: Tom Barrett
ATTN: DASIAC
ATTN: Warren S. Knapp

General Research Corporation
ATTN: John Ise, Jr.

M.I.T. Lincoln Laboratory
ATTN: Library A-082 for David M. Towle

Mission Research Corporation
ATTN: Ralph Kilb
ATTN: M. Scheibe
ATTN: Dave Sowle
ATTN: D. Sappenfield
ATTN: Conrad L. Longmire
ATTN: Robert E. Stoeckly
ATTN: Robert W. Stargr
10 cy ATTN: Tech. Lib.

Physical Dynamics, Inc.
ATTN: Joseph B. Workman

DEPARTMENT OF DEFENSE CONTRACTORS (Continued)

R & D Associates
ATTN: Robert L. Lelevier

Science Applications, Inc.
ATTN: D. Sachs
ATTN: Daniel A. Hamlin

Stanford Research Institute
ATTN: Walter G. Chesnut

DEPARTMENT OF DEFENSE CONTRACTORS (Continued)

Science Applications, Inc.
Huntsville Division
ATTN: Dale H. Davis

Visidyne, Inc.
ATTN: Oscar Manley